DEMONSTRATION OF A FAST RESPONSE ON-BOARD NO_X SENSOR FOR HEAVY-DUTY DIESEL VEHICLES

FINAL REPORT

SwRI Project No. 03-02256
Contract No. 98-302

Prepared for:
State of California Air Resources Board and the
California Environmental Protection Agency
Research Division
P.O. Box 2815
Sacramento, California 95812

South Coast Air Quality Management District
Technology Advancement
21865 E. Copley Drive
Diamond Bar, California 91765-4182

Principal Investigator:
Jack A. Smith

Prepared by:
Southwest Research Institute
Engine and Vehicle Research Division
P.O. Box 28510
San Antonio, Texas 78228-0510

July 14, 2000

Approved:

Daniel W. Dickey, Director
Engine and Vehicle Research Division

DISCLAIMER

The statements and conclusions in this report are those of the contractor and not necessarily those of the California Air Resources Board or the South Coast Air Quality Management District. The mention of commercial products, their source, or their use in connection with material reported herein is not to be construed as actual or implied endorsement of such products.

ACKNOWLEDGEMENTS

Southwest Research Institute would like to extend sincere thanks to the California Air Resources Board (CARB) and the South Coast Air Quality Management District (SCAQMD) for funding this work. In addition, special thanks should be given to Steve Church for his gracious understanding and assistance working through the various hurdles during this program. SwRI also extends its' best regards to the NGK Insulators, Ltd. company for providing the prototype NO_x sensors via NGK-Locke. Furthermore, SwRI would like to acknowledge Dr. James Patten of the Cummins Engine Company for providing the Cummins M11 diesel test engine.

SwRI would also like to thank Mr. Bob Davis and Bus Manufacturing USA for their efforts during the field demonstration portion of this project. Mr. Davis and his crew were instrumental in procuring demonstration vehicles and installing and maintaining the dataloggers. SwRI would also like to recognize Raley's Grocery Corporation, Ms. Kathleen Tschogl and Mr. Stan Sasaski of Raley's Grocery Corporation, and Mr. Ed Gamache of Ozark Trucking for providing the two demonstration vehicles and allowing the vehicles to be modified and monitored. Finally, SwRI would like to acknowledge Mr. Butch Quipp and Mr. Steve Schneider, both of SwRI, for their endless dedication to completing the datalogger development and test programs.

This report was submitted in fulfillment of ARB contract number 98-302 entitled, "Demonstration of a Fast Response On-board NO_x Sensor for Heavy-Duty Diesel Vehicles", by Southwest Research Institute under the sponsorship of the California Air Resources Board and the co-sponsorship (30 percent) of the South Coast Air Quality Air Management District. Work was completed as of July 14, 2000.

TABLE OF CONTENTS

Page

TABLE OF CONTENTS – cont'd

Page

LIST OF ILLUSTRATIONS

LIST OF ILLUSTRATIONS – cont'd

LIST OF ILLUSTRATIONS – cont'd

LIST OF ILLUSTRATIONS – cont'd

LIST OF TABLES

ABSTRACT

A literature search, laboratory testing, and a field demonstration were conducted to determine the suitability and performance characteristics of fast response NO_x sensors designed for use on heavy-duty diesel vehicles. Results of the literature search indicated that only the NGK Insulators, Ltd. combined NO_x/O_2 sensor was available and prepared to be evaluated in this program. Four NGK Insulators, Ltd. combined NO_x/O_2 sensors were tested under steady-state conditions, transient conditions, under the influence of interference gas, and during real world driving conditions in diesel engine exhaust. Results from the diesel engine steady-state tests showed that the sensors were accurate to ±10 percent of reading from 0-2000 ppm. In addition, the transient characteristics are such that the NO_x component of the sensor responds on average 100 to 200 msec after the O_2 component of the sensor (which takes approximately 50 msec) responds due to its design. Carbon dioxide, oxygen, and propylene interference gases all have an effect of decreasing the NO_x sensor output as the interference gas concentration is increased at a constant exhaust gas NO_x level. A steady-state natural gas engine test was also conducted on two of the sensors. The two sensors performed well and can be used in either diesel or natural gas engine exhaust in a research and development program. However, further investigation is required to fully quantify reliability issues and their impact on a production engine control system in long term, heavy-duty, diesel engine emissions control applications. In the present prototype form, the sensors are not suitable for implementation into heavy-duty, diesel engine emissions control systems.

EXECUTIVE SUMMARY

Background

The California State Implementation Plan for Ozone calls for significant reductions in the oxides of nitrogen (NO_x) emissions generated by on-road, heavy-duty vehicles. The primary means of achieving these reductions will be through new and optimizing technologies being incorporated on diesel engines. One component under development is a real-time NO_x sensor, with a response time and accuracy conducive for implementation into an engine control system for direct closed loop NO_x feedback. For a diesel engine, feedback from such a device could be used for manipulation of control variables such as fuel injection timing and rate, exhaust gas recirculation rate, water injection rate, reductant delivery rate to the after-treatment device, or others. This work was conducted to determine the suitability and performance characteristics of fast response NO_x sensors designed for use on heavy-duty diesel vehicles.

Methods

As an initial step in this project, a literature search was conducted to determine and contact the sensor manufacturers that were developing NO_x sensors and determine the current stage of development. The objective was to acquire at least two sensors developed under two different technologies. Only one sensor technology was available. Four, 5^{th} generation, prototype, NGK Insulators, Ltd. sensors were acquired and tested at Southwest Research Institute (SwRI) in the exhaust of a Cummins M11 330 horsepower diesel engine. The sensors were subjected to several steady-state tests, transient tests, interference gas tests, and a limited field demonstration. The field demonstration required six months to complete (48,188 miles and 35,277 miles), and was conducted in Sacramento, California on two Class 8 line haul trucks powered by Cummins M11 engines. The sensors were re-tested at SwRI after the field demonstration to determine the effects real world use had on sensory accuracy and response. Engine speeds from idle to rated speed and loads from 0 percent to 100 percent of maximum torque were encountered during steady-state testing, to determine sensor measurement error and linearity when compared to measurements made by the SwRI Milton-Roy emissions bench.

Carbon dioxide (CO_2), oxygen (O_2), and propylene (C_3H_6) interference gases were admitted into the exhaust downstream of the turbocharger and upstream of the sensors while the engine generated 50 percent of rated torque (essentially constant NO_x). These tests were conducted to determine if the presence of additional exhaust gas constituents had an effect on NO_x sensor output. Transient tests were conducted at various engine speeds and NO_x levels to determine the response of the sensors. A rapid change in pedal position was commanded from one known NO_x level to another known NO_x level while maintaining engine speed nearly constant. The sensors were also briefly tested under a 9 point steady-state test matrix, in the exhaust of a John Deere 8.1 liter natural gas engine, prior to any diesel testing to determine the applicability to natural gas engines.

Results

The prototype sensors functioned well throughout the program whether in a diesel or natural gas exhaust environment. The factory calibrations supplied by NGK Insulators, Ltd. needed refinement for both the NO_x and O_2 components of the sensors. However, the factory calibrations were developed on a synthetic gas exhaust test bench and not in actual exhaust gas. Moreover, the calibration for O_2 component of the sensor is fuel specific. Therefore, the target fuel must be known prior to sensor calibration and implementation.

The sensors exhibited strong linearity during steady-state testing in both the NO_x and O_2 components, with correlation coefficients typically greater than 99 percent regardless of fuel type (diesel or natural gas). All sensors exhibited greater than -10 percent measurement error at the idle speed, 100 percent load condition where carbon monoxide (CO) emissions approached the 1.0 percent level by volume. For the most part, however, the accuracy of all sensors was within ±10 percent of reading over a 0 to 2000 parts per million (ppm) NO_x scale during the pre-field demonstration diesel engine testing. Two sensors exhibited an increase in measurement error beyond ±10 percent at high gas flow conditions after the field demonstration. Both of these sensors were installed vertically in the exhaust pipe on different trucks. Hence, the installation orientation of the sensors may play a role in the reliability of the sensor.

Laboratory exposure to CO_2 and O_2 interference gases decreased the NO_x sensor output when the sensor was exposed to a constant NO_x level. The sensor's NO_x output decreased by nearly 7 percent when the CO_2 mole fraction was increased from 8 percent to 14 percent. However, only a 4 percent decrease was observed after the field demonstration for the same conditions. Hence, the effect of CO_2 interference gas appears to decrease with age. In contrast, the effect of interference O_2 increases with age. A maximum of –7.5 percent change in output was observed for one of the sensors after the post field demonstration compared to only –3.9 percent prior to the field demonstration. Unburned hydrocarbons, or the C_3H_6 interference gas, had less than a 1.0 percent effect on sensor output when the unburned hydrocarbon levels were increased from a nominal 103 ppm up to 1500 ppm.

Conclusion

In general, the NGK Insulators, Ltd. combined NO_x/O_2 sensors functioned within the NGK Insulators, Ltd. published accuracy limits of ± 10 percent of reading. The interference gas effects are presently of little concern since the exhaust gas species distribution changes proportionately. However, there may be advanced control algorithms that could suffer from the interference gas effects; for example, selective catalytic reduction systems. In the current form, the sensors and power electronics (controllers) can not be powered by a vehicle battery due to a strict 14.0 ±0.5 dc volt requirement. However, NGK Insulators, Ltd. is currently developing the power electronics for use with conventional battery systems. Further investigation is required to fully quantify reliability issues and their impact on a production engine control system in long term, heavy-duty, diesel engine emissions control applications. In the present prototype form, the sensors are not suitable for implementation into heavy-duty, diesel engine emissions control systems.

An extended test is recommended to further evaluate the sensor and to evaluate the durability of the sensors on a longer-term field demonstration (e.g., 1 year). A modified sensor may be in order for such an evaluation. In addition, the sensor needs to be evaluated within the context of an engine control system. In this context, closed loop NO_x control algorithms can be developed and tested to determine the NO_x sensor's place in the air to fuel ratio control loop. The effect of sensor installation orientation should also be investigated.

It should be reiterated that the sensors tested in this project were prototype sensors and controllers. These were the ONLY sensors at a level of development suitable for testing.

1.0 INTRODUCTION

The California State Implementation Plan for Ozone calls for significant reductions in NO_x emissions from on-road, heavy-duty vehicles. More stringent emissions standards will likely be adopted in the future. The primary means of achieving these reductions will be through new and optimizing technologies being incorporated on diesel engines.

One component, under development by some sensor manufacturers, is a NO_x sensor with a response time and accuracy conducive for implementation into an engine control system for direct closed loop control of the primary response variable of interest from the system, namely the exhaust NO_x concentration from the engine and/or after-treatment device. For a diesel engine, feedback from such a device could be used for manipulation of control variables such as fuel injection timing and rate, exhaust gas recirculation rate, water injection rate, reductant delivery rate to the after-treatment device, or others. Access to direct measurement of the parameter of interest has definite advantages to the engine control system developer in the design of the best performing and most robust control system, and would also provide a key on-board diagnostic capability. The net result of this would be engines that could achieve significantly lower NO_x emissions and maintain these lower emissions throughout their useful product life.

As a first step towards accomplishing this goal, NO_x sensors, of the type described above must be developed. In recent years, sensor manufacturers have made significant progress towards the development of such NO_x sensors. In fact, manufacturers such as NGK currently have working sensor samples exhibiting most of the characteristics necessary for the sensors to be used in a successful implementation of a closed-loop NO_x engine control system. However, field experience with these sensors is limited or nonexistent. In order for an engine manufacturer to include such a sensor into the design of an engine control system in a current or near-future product development program, more data regarding the in-service durability, reliability, required maintenance, and accuracy must be gathered. The intent of this project was to take a significant step toward filling this void.

The objectives of this project were to acquire much needed data and evaluate the performance on two sets of four NO_x sensors (8 total) of differing sensor technologies developed for on-road, heavy-duty diesel engines. Unfortunately, only one NO_x sensor technology was mature enough to be included in this project. However, very important data were gathered from each sensor by subjecting them to a battery of steady-state tests, interference gas tests, and transient tests in a laboratory setting. In addition, a six-month field demonstration and subsequent laboratory tests were conducted to determine the repeatability, linearity, accuracy, and durability of the sensor technology. Additional insight was gained regarding potential pitfalls of the sensor technology evaluated.

2.0 MATERIALS AND METHODS

2.1 Literature Search and Procurement of Test Sensors

SwRI conducted a literature search for potential NO_x measuring techniques and sensors. The fourteen literature databases listed below were searched for potential sources of information and contacts. In addition to the literature search, direct communication via phone calls and email was conducted with known sensor manufacturers. The titles of technical papers published by the American Chemical Society revealed that significant emphasis is presently being placed on the development of fast response NO_x sensors for vehicular applications. Abstracts from a number of sources were gathered for review. Several titles listed by the Chemical Abstracts Service appeared to be applicable to the project. Unfortunately, some of the papers were published in Japanese and German and were not acquired for translation. Patents were also found and reviewed. Most of the patents reviewed were simply detailed versions of published technical papers.

- INSPEC
- Ei Compendex
- SciSearch
- Transport Res
- Conference Papers Index
- Mechanical Engineering Abs
- CA Search
- NTIS
- Pollution Abs
- Environmental Bib.
- Enviroline
- Energyline
- Energy SciTec
- Global Mobility Database

A total of twenty-five sensor manufacturers/research entities were contacted to determine their current development efforts and potential for participating in this program. A questionnaire was forwarded to each company. A copy of the questionnaire is shown in Figure 2-1. The sensor specifications were provided as guidelines and not requirements of the sensor. The sensors tested during this program did deviate from the guidelines. All but four manufacturers/research entities responded by either supplying detailed information in the form of technical papers, brochures, or a statement regarding their current development efforts.

Dear Sir,

I am sending you this letter per our telephone conversation today. Southwest Research Institute (SwRI) is conducting a program for the California Air Resources Board (ARB) entitled "Demonstration of a Fast Response On-board NO_x Sensor for Heavy-Duty Diesel Vehicles". The first phase of this program involves a study of the available NO_x sensors and sensors currently under development. The focus of this study will be to identify sensors suitable for use on heavy-duty diesel engine applications. Information is currently being gathered from a survey of potential sensor manufacturers/developers and through a literature research. This information will be used to obtain details regarding the status of the sensor development, description of the technology, applicability of the technology for use on the project, and actual or anticipated high-volume production cost for the sensor. The results of the study will be summarized in a report by SwRI, for the ARB, at the end of March. Once the information has been reviewed, several NO_x sensors will be selected for evaluation in laboratory engine tests and on-vehicle field tests for the following phase of the program.

The purpose of this letter is to determine if "Company" has a NO_x sensor available, or currently under developing, that would meet the criteria for this program? If yes, who is the appropriate contact person at "Company" for obtaining further technical information/data? Also, would "Company" be interested in participating in the program described above? Below is a preliminary set of operating conditions the NO_x sensor should be able to function under and some desired sensor specifications. The sensor specifications should be considered as guidelines and may not necessarily eliminate the sensor technology from further consideration.

Sensor Operating Conditions:

1. *Four-stroke cycle, on-road HD Diesel engine exhaust gas-temperature ranging from 100 to 700 degrees C.*
2. *Exhaust gas-oxygen content between 0 and 21 percent by volume (dry basis).*
3. *Exhaust gas-water-vapor content between 0 and 15 percent by volume (wet basis).*
4. *Use in heavy-duty engines. Use in vehicles operating in either long distance line-haul or in intra-urban stop-and-go operations.*
5. *Variable diesel fuel quality and composition.*

Sensor Specifications (guidelines):

1. *Five years or 500,000-miles life, with no maintenance other than simple cleaning at an interval of 1 year or 100,000 miles.*
2. *Combined NO + NO2 range: 0 to 2,000 ppm (wet basis).*
3. *Accuracy within 1 percent of full scale (i.e. +/- 20 ppm).*
4. *Repeatability within 1 percent of full scale.*
5. *Linearity within of 1 percent of full scale. Minimal interference effects from other commonly found compounds in diesel exhaust including CH_4, NH_4, and H_2O.*
6. *Minimal contamination due to any component in diesel exhaust.*
7. *90 to 10 percent of full scale step response time of 30 milliseconds or less.*
8. *High volume production price of $100 or less per unit. Output signal compatibility with current and anticipated OEM engine control systems.*

Please review the conditions and specifications listed above and provide SwRI with any technical information or data and any technical papers describing your NO_x sensor. All information must be received at SwRI by March 12, 1999 to provide adequate time for review. This information will allow SwRI to appropriately and fairly rank your NO_x sensor among others for consideration in the laboratory and field testing phases of this program. SwRI looks forward to evaluating your NO_x sensor, whether it is production ready or under development.

Sincerely,

SwRI

Figure 2-1. Example Letter Sent to Prospective NO_x Sensor Manufacturers

2.1.1 Desired NO_x Sensor Characteristics

The desired sensor characteristics for NO_x sensors for over the road applications are listed below. The sensor manufacturers were provided with this information in the questionnaire as a definition of the operating environment and desired operating characteristics. The sensor operating conditions define the environment and application in which the sensor is expected to function. The sensor specifications were developed as guidelines and failure to meet any specification did not necessarily eliminate any sensor technology from consideration in this program.

Sensor Operating Conditions:

- Four-stroke cycle, on road heavy-duty diesel engine exhaust gas temperature range from 100°C to 700°C
- Exhaust gas oxygen content between 0 and 21 percent by volume (dry basis)
- Exhaust gas water vapor content between 0 and 15 percent by volume (wet basis)
- Use in heavy-duty engines
- Use in vehicles operated in either long distance line haul operations or intra-urban stop and go operations
- Variable diesel fuel quality and composition

Sensor Specifications (guidelines):

- Five years or 500,000 mile life, with no maintenance other than simple cleaning at intervals of one year or 100,000 miles
- Combined NO + NO_2 range of 0 to 5,000 ppm (wet basis)
- Accuracy within 1 percent of full scale (i.e. +/-50 ppm)
- Repeatability within 1 percent of full scale
- Linearity within 1 percent of full scale
- Minimal interference effects from other commonly found compounds in diesel exhaust
- Minimal contamination due to any component in diesel exhaust
- 90 to 10 percent of full scale step response time of 30 milliseconds or less
- High volume production price of $100 or less per sensor
- Output signal compatibility with current and anticipated OEM engine control systems

2.1.2 Sensor Ranking Methodology

Each sensor technology was quantitatively ranked to determine the most and least appropriate technologies for this project. Table 2-1 lists the ranking criteria, merit point range, and weighting factors that were used to provide a means of evaluating critical sensor characteristics from one sensor technology to another. The weighting factors in each category were multiplied by the associated prescribed merit points to determine a categorical score. The summation of all individual categorical scores yielded the sensor's overall ranking/score. High scores are better than low scores.

Table 2-1. Sensor Ranking Criteria

Sensor Attribute	Description	Merit Point Range	Weighting Factor
Accuracy	Self explanatory	0 to 10	5
Repeatability	Self explanatory	0 to 10	5
Linearity	Self explanatory	0 to 10	2
Response time	Self explanatory	0 to 10	4
Range	Usable NO_x concentration range as compared to specified sensor requirements	0 to 10	3
Temperature range	Range of exhaust gas temperatures which can be accommodated	0 to 10	5
Pressure/Temperature sensitivity	Sensitivity of sensor accuracy to exhaust pressure and temperature changes	0 to 10	3
Interference effects	Sensitivity of sensor accuracy to other exhaust gas compounds such as O_2, HC, CO, CO_2, and H_2O	0 to 10	4
NO vs NO_2 selectivity	Ability of the sensor to accurately measure both NO as well as NO_2	0 to 10	4
Stage of development	How near is the manufacturer to the production of the sensor	0 to 10	5
Expected high volume production cost	Self explanatory	0 to 10	4
Availability of technical information/data	Willingness and availability of technical data from which to evaluate the sensor technology	0 to 10	5
Company history/experience in this area	Manufacturer's experience in producing chemical sensing product technology for the automotive or heavy duty markets	0 to 10	4
Signal output (compatibility with ECM)	Signal output from the sensor (i.e. range, signal type), and complexity and availability of sensor control/conditioning electronics	0 to 10	3
Applicability to on-road heavy-duty diesel engines	Applicability of the sensor technology to the vibration, temperature, and EMI environment of a heavy-duty diesel vehicle application	0 to 10	5
Need for periodic replacement/maintenance	Does the sensor technology involve periodic replacement of sensing elements or periodic sensor maintenance	0 to 10	4

2.2 Laboratory Hardware and Setup

Cummins Engine Company provided, on loan, a new 1995 model M11 diesel engine for this project. This engine was the primary test bed for all diesel engine tests conducted at SwRI and was required to meet the main objectives of the project. The engine was installed in Test Cell 05 of the Engine & Vehicle Research Division, Engine Research Department Laboratory (in building 151) at SwRI, and coupled to an eddy-current dynamometer. A photograph of the engine in Cell 05 is shown in Figure 2-2. The exhaust system was fabricated to accommodate four NO_x sensors, a pressure sensor, a temperature sensor, and an emissions probe for the Milton-Roy emissions bench. The NO_x sensors were installed approximately 1.52 meters (5 feet) downstream from the turbo outlet. The Milton-Roy emissions bench measures steady-state concentrations of dry NO_x, dry oxygen (O_2), dry carbon monoxide (CO), dry carbon dioxide (CO_2), and wet unburned HCs. NO_x is measured with a chemiluminescent analyzer, O_2 with a paramagnetic analyzer, CO and CO_2 with a non-dispersive infrared analyzer, and HCs are measured with a flame ionization detector. Phillips 66 diesel fuel was blended to CARB certification and used in all diesel engine tests.

Figure 2-2. 1995 Cummins M11 Diesel Engine Installed in Test Cell 05 at SwRI

A special perforated probe was also installed between the turbo outlet and the four NO_x sensors to allow admission of interference gas into the exhaust gas upstream of the NO_x sensors as shown in Figure 2-3. One A-size bottle of polymer grade propylene (C_3H_6), three A-size bottles of instrument grade CO_2, and six A-size bottles of zero-gas O_2 were ordered and received from Scott Specialty Gases, for use as interference gases.

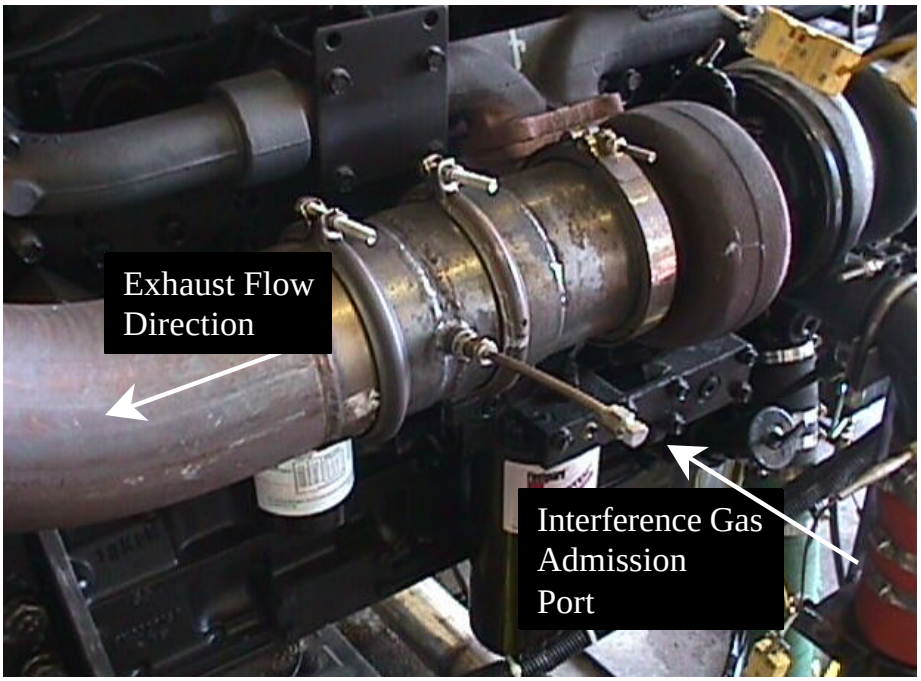

Figure 2-3. Picture of Exhaust Pipe with Interference Gas Admission Port

A Hewlett-Packard 1000 data acquisition system was employed to log all pertinent engine operating variables such as fuel flow, air flow, engine speed, torque, manifold air pressure, manifold air temperature, NO_x sensor output voltages, etc. A SwRI custom Win98 data acquisition and control system was used to interface with the Cummins CELECT engine control module (ECM) for pedal position commands. Additionally, the Win98 system supplied the dynamometer controller with speed set points in the form of analog voltages, providing a means to program transients at/to various speeds and loads. The Win98 system was used to log transient engine and NO_x sensor data at 20 Hz during two sets of tests and later at 200 Hz during a final set of transient tests to improve resolution.

SwRI is ISO 9001 compliant and maintains calibration histories of each sensor used in every test cell. All SwRI owned sensors are calibrated every six months to maintain acceptable levels of measurement accuracy; torque and pressure: ± 1% of full scale, fuel flow: ±0.5% of reading from 50% to 100% of flow and ± 2.0% below 50% flow (Micro-Motion D series units), temperature: ± 2.14 degrees F data acquisition error, thermocouples: ± 2 degrees F below 1000 degrees F, ± 20 degrees F above 1000 degrees F, and speed: ± 0.1% of full scale (2000 rpm).

2.3 Testing in Diesel Engine Exhaust

The Cummins M11 diesel engine was operated over a series of tests to evaluate the steady-state performance, transient performance, and interference effects other common exhaust gas constituents might have on sensor accuracy. Each test is described below in detail.

2.3.1 Steady-State Testing

Steady-state tests were conducted to generate various levels of NO_x emissions to adequately exercise the full range (0-2,000 ppm NO_x) of the sensors. The 19-point steady-state test matrix in Table 2-2 lists the engine speeds and loads tested. Engine speeds from idle to the maximum governed engine speed were tested over the full range of torque the engine could generate at the associated engine speed. These tests were conducted to determine the sensors' repeatability, linearity, and accuracy.

Table 2-2. 19-Point Steady-State Test Matrix

Engine Speed (rpm)	Comments	Percent Load (By Torque)
700	Idle Speed	0, 50, 100
1200	Peak Torque Speed	0, 50, 100
1400	Intermediate Speed	0, 50, 100
1600	Peak Power Speed	0, 25, 50, 75, 100
1800	Max Governed Loaded Speed	0, 25, 50, 75, 100

2.3.2 Interference Test Description

Interference gas tests were conducted to determine if the sensors would properly report NO_x values, based on suitable steady-state calibrations, when the exhaust gas was diluted with the addition of a common exhaust gas constituent. In other words, could the sensor properly measure the NO_x concentration in the exhaust gas if diluted with an interference gas? The interference effects tests were conducted by holding the NO_x level essentially constant by maintaining a constant engine speed and load. The interference gases tested in this project were CO_2, O_2, and propylene (C_3H_6). Propylene was chosen as the unburned hydrocarbon test gas, since it could be metered in a gaseous state and it possesses a hydrogen-to-carbon ratio roughly equivalent to CARB certified diesel fuel.

All interference gas tests were conducted at steady-state at 1200 rpm and 50 percent of peak torque (660 lbf-ft). At this condition, controlled amounts of CO_2, O_2, and C_3H_6 were individually admitted into the exhaust stream, approximately ten inches downstream of the turbocharger turbine outlet and upstream of a 90-degree bend in the exhaust piping (90-degree elbows promote mixing between gases). The addition of interference gas altered the concentration of all exhaust gas constituents on a molar basis. Only one interference gas was admitted during a single test point. Controlled amounts of each interference test gas were admitted into the exhaust stream to reach nominal molar concentrations of 10, 12, and 14 percent for the CO_2 and O_2 interference gas tests, and 500 ppm, 1000 ppm, and 1500 ppm for the C_3H_6 interference gas tests. Steady-state emissions (no interference gases), generated by the Cummins

M11 engine, were nominally 103 ppm HC, 116 ppm CO, 8.72 percent CO_2, 1491 ppm NO_x, and 8.69 percent O_2 at 1200 rpm and 50 percent of peak torque. The effect of the interference gas was quantified by computing the percent difference in NO_x values (based on appropriate calibrations) between those reported by the sensors and the NO_x measured by the Milton-Roy emissions bench.

2.3.3 Transient Response Testing

Sensor response time characteristics were quantified via engine transient response testing. The objective of these tests is to achieve controlled, repeatable step changes in NO_x concentration levels and measure the signal response from each NO_x sensor. Commanding step changes in pedal command (load change) at essentially constant engine speed generated the desired transients in NO_x concentration levels. Table 2-3 lists the engine speeds and NO_x conditions used for testing. Each transient test consisted of three pedal positions or test conditions.

Transients were achieved by commanding pedal position changes ("snaps") while holding engine speed constant. The pedal "snaps" occurred in 100 msec. The engine was operated at the first test condition for 30 seconds, followed by a 100 msec step change in pedal position to the second test condition. The second test condition was held for 70 seconds, before the third test condition was commanded by another 100 msec pedal position step change. The second test condition (pedal position command) was maintained for 70 seconds to provide adequate time for the Milton-Roy emissions bench to capture the NO_x emissions trace as a result of transport delay and slower responding instruments. The Milton-Roy emissions bench was only used as a verification mechanism for these tests. The pedal position commands ranged from pre-selected minimum and maximum positions that generated the desired change in NO_x emissions.

Table 2-3. Transient Response Test Conditions

Test Number	Engine Speed (rpm)	Change NO_x Conditions at Selected Engine Speed
1	Idle (700)	25% of Max-to-Max-to 25% of Max
2	Idle (700)	25% of Max-to-50% of Max-to 25% of Max
3	Idle (700)	50% of Max-to-Max-to 50% of Max
4	1200 (peak torque)	Min-to-Max-to-Min
5	1200 (peak torque)	Min-to-50% of Max-to-Min
6	1200 (peak torque)	Min-to-25% of Max-to-Min
7	1200 (peak torque)	50% of Max-to-Max-to 50% of Max
8	1800 (rated power)	Min-to-Max-to-Min
9	1800 (rated power)	Min-to-50% of Max-to-Min
10	1800 (rated power)	Min-to-25% of Max-to-Min
11	1800 (rated power)	50% of Max-to-Max-to 50% of Max

2.3.4 History Accumulation Testing

History accumulation testing was performed to accumulate operational time on each sensor between sets of steady-state, interference, and transient tests. History accumulation tests were performed at SwRI prior to the field demonstration to "age" each sensor in the lab. These tests consisted of operating the engine repetitively over a 4-minute cycle that included idle, high idle at light load, peak torque speed at approximately 63 percent of peak torque, and rated power at 1800 rpm. Three sets of history accumulation tests were conducted. The number of history accumulation hours increased from test to test. The first history accumulation test consisted of operating the engine over the 4-minute cycle for ten hours, the second for 20 hours, and the third for 40 hours. Approximately ten hours of operation were accumulated per day of testing. Figure 2-4 is a time history plot taken at the end of the 10^{th} hour of the first history accumulation test shown to provide the reader with a visual representation of the cycle. It shows the test cycle. Data were acquired for one 4-minute cycle at a sample rate of 20 Hz for the 0^{th} hour, and once every hour thereafter until the test was completed. No detailed analysis of these data was conducted. The data were taken in case an evaluation of a particular sensor's time history was warranted.

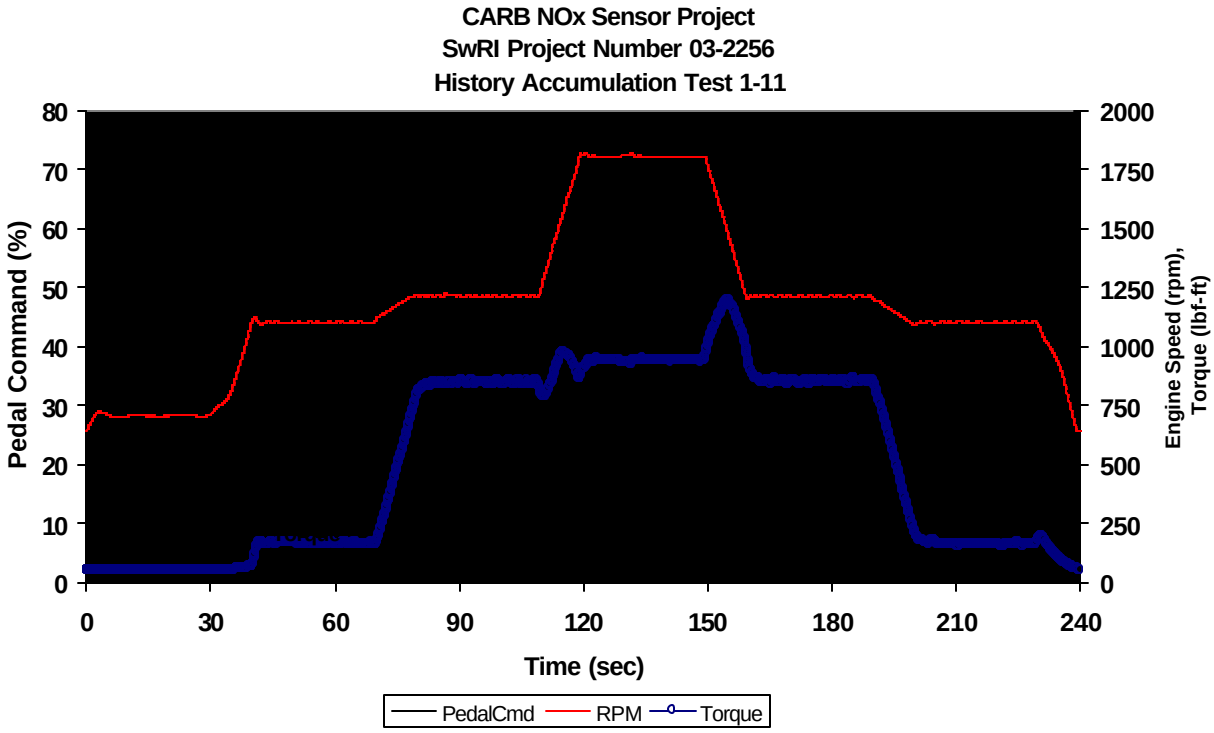

Figure 2-4. History Accumulation Test Cycle

2.3.5 Field Demonstration Testing

Field demonstration tests were conducted with all NO_x sensors tested in this program. The field demonstration tests were conducted to obtain in-service data (via a SwRI datalogger) in normal field use for 50,000 miles or six months, whichever came first. Two NO_x sensors were installed on two late model class 8 diesel powered trucks operated by the Raley's Grocery Corporation in Sacramento, California. The first truck operated over a long-haul application

logging 510 miles while traveling from Sacramento to Yreka and back to Sacramento, three times per week. This truck was powered by a 1999, 370 horsepower Cummins M11 diesel engine and is listed as truck number 1513. The second truck, operated over a short haul, intra-urban route in the Sacramento-Antioch area and switched trailers nine times per day. This truck was powered by a 1995, 330 horsepower Cummins M11 diesel engine and is listed as truck number 1585. Pictures of both trucks are shown in Figure 2-5.

Figure 2-5. Photographs of Long Haul (#1513) and Short Haul (#1585) Raley's Trucks

Both trucks were fitted with additional pressure and temperature sensors coupled to custom SwRI dataloggers. The additional sensors included an intake manifold absolute pressure, an intake manifold air temperature K-type thermocouple, an exhaust gas pressure sensor located near the NO_x sensors, and an exhaust gas temperature K-type thermocouple located near the NO_x sensors. The factory vehicle speed, engine speed, and pedal position sensors were also tapped into to log their values. Figure 2-6 shows the location of two NO_x sensors (NGK2 and NGK4), the exhaust gas thermocouple, and the exhaust gas pressure transfer tube, as well as the direction of exhaust gas flow on the short haul truck. The long haul truck was equipped in a like manner with a sensor named NGK3 installed in the same location as NGK2, and a sensor named NGK1 installed in the same location as NGK4.

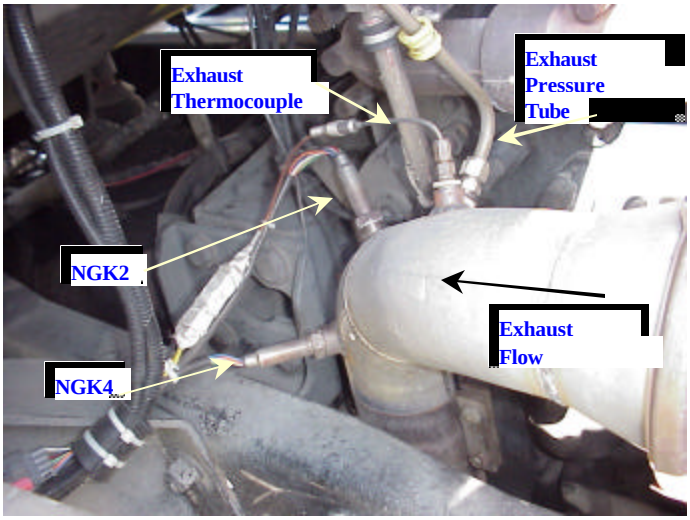

Figure 2-6. Sensor Installation Locations on Short Haul Truck (#1585)

The dataloggers were implemented to record engine operating data and NO_x sensor output during truck operation at 40 Hz. The dataloggers were based on an industrial grade 450 MHz Diversified Technologies Pentium computer with 144 Mbytes of random access memory. The computer was housed in a "shoe box" style enclosure with an ISA back plane. A Keithley-Metrabyte DAS-20 data acquisition card and two Keithley-Metrabyte EXP-20 multiplexer cards handled data acquisition duties. One EXP-20 card was utilized for standard 0-5 volt analog signals, while the other was used for low voltage thermocouples. Each datalogger was also equipped with a modem and cellular telephone to provide a means for downloading files to SwRI while the trucks were in service. The "shoe box" computer was protectively sealed from natural elements in a waterproof NEMA 7 enclosure and installed behind the cab of the truck on a perforated aluminum rack. Figure 2-7 shows two views of one of the dataloggers. Figure 2-8 shows a datalogger installed on the long haul truck number 1513. Both dataloggers were installed at the same location on each truck.

Figure 2-7. SwRI Dataloggers Installed on Raley's Trucks

Figure 2-8. Datalogger Installed on Rear of Long Haul Truck Number 1513

Time domain data was stored to the hard drive at one of two frequencies depending on the driving condition. Data were stored at 1 Hz during steady-state driving and at 10 Hz during transient conditions. Histogram data were stored at constant rate of 40 Hz. Steady-state and transient conditions were determined by computing a transient index value and comparing it to a threshold value prescribed for each truck. The transient index is a function of the first derivatives of pedal position, engine speed, and manifold absolute pressure as shown below in Equation 1. The coefficients a, b, and c are calibration constants that scale the time derivatives of pedal position, engine speed, and manifold absolute pressure to increase or decrease their influence on the function. The time derivatives of pedal position, engine speed, and manifold absolute pressure were computed from the three-point finite divided difference shown in Equation 2. During a transient, the data store rate of 10 Hz was maintained for 15 seconds to ensure that the resultant engine speed or MAP transients were captured following a pedal "snap", or rapid change in pedal position.

$$T.I. = a \cdot \frac{d(PedalPosition)}{dt} + b \cdot \frac{d(RPM)}{dt} + c \cdot \frac{d(MAP)}{dt} \tag{1}$$

$$\frac{dx_i}{dt} = \frac{(3 \cdot f(x_i) - 4 \cdot f(x_{i-1}) + f(x_{i-2}))}{2 \cdot \Delta t} \tag{2}$$

2.3.5.1 NO_x Model

Both dataloggers included NO_x models to assist SwRI in determining the functionality of the NO_x sensors throughout the demonstration phase. The predicted NO_x from the model was based on the adiabatic flame temperature of stoichiometric diesel combustion. The model takes as inputs the air-to-fuel ratio, manifold air temperature, exhaust stack temperature, ratio of specific heats of the intake charge, and the engine's compression ratio. The constants A and B shown in Equation 3 were derived from engine test data acquired during the laboratory tests. The form of Equation 3 is modeled after the emissions index function for diesel engines described John B. Heywood's "Internal Combustion Engine Fundamentals" text (p. 591). The calculation for the variable X is shown in Equation 4 and is a function of the manifold air temperature (MAT) and the exhaust stack temperature (EST).

$$Predicted\_NOx = A \cdot \exp(B \cdot X) \tag{3}$$

$$X = AFRatio \cdot \frac{((MAT) + 459.67)}{((EST) + 459.67)} \cdot \frac{10^4}{T_{f,ad}} \tag{4}$$

The adiabatic flame temperature, $T_{f,ad}$, in Equation 4 was computed from an enthalpy balance given by the first law of thermodynamics assuming adiabatic conditions and no work generated during an instantaneous combustion phase. The computation is iterative and accounts for major exhaust species that would be present during theoretical, complete, stoichiometric combustion of diesel fuel. The reactants considered for the enthalpy balance are shown in the hydrocarbon reaction equation below, Equation 5, where the H/C ratio is 2.25 for the CARB diesel fuel.

$$C_aH_b + (a + \frac{b}{4})(O_2 + 3.77N_2) \longrightarrow aCO_2 + \frac{b}{2}H_2O + 3.77(a + \frac{b}{4})N_2 \tag{5}$$

2.4 Testing in Natural Gas Engine Exhaust

In addition to the diesel engine testing, natural gas engine testing was also conducted. The natural gas engine testing was conducted to determine how well the sensors would function in a natural gas engine exhaust environment. Two NO_x sensors were installed in the exhaust system of a state-of-the-art, 280 horsepower, 8.1 liter, turbocharged, and aftercooled inline six-cylinder natural gas fueled engine. The test engine was previously set up in a SwRI test cell and available to serve as the test bed. Typical applications for this type of engine are the primary power source for school buses and metro-transit vehicles/buses. Only two sensors were available at the time of this testing. A photograph of the John Deere engine is shown in Figure 2-9. The engine was fueled with high-grade (methane concentration greater than 92 percent) natural gas supplied by the city of San Antonio. The natural gas fuel composition possessed a hydrogen to carbon ratio of 3.865, an oxygen to carbon ratio of 0.045, and a nitrogen to carbon ratio of 0.013. The natural gas lower heating value was 19,971 Btu/lbm. The nine point steady-state test matrix, shown in Table 2-4, was executed one time prior to any tests on a diesel engine. Engine emissions were measured by a SwRI Milton-Roy emissions bench. The HP1000 data acquisition system was used to acquire engine operating data and sensor output.

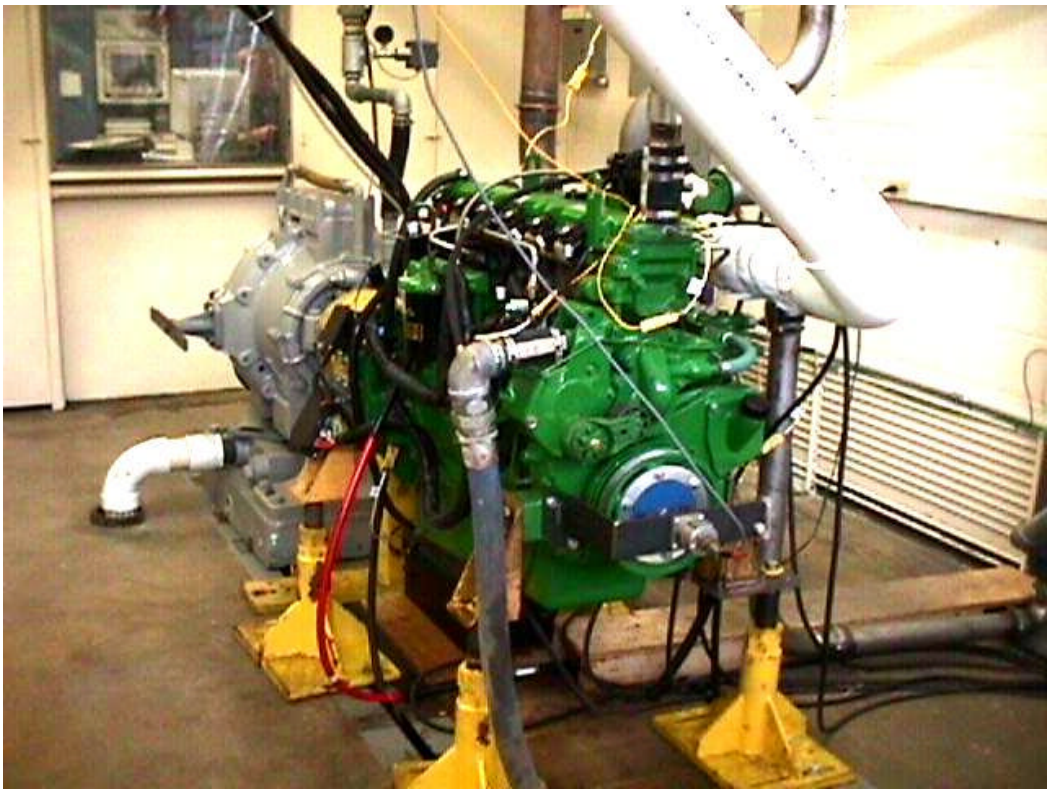

Figure 2-9. 8.1 Liter John Deere Natural Gas Engine

Table 2-4. Nine Point Natural Gas Engine Steady-State Test Matrix

Engine Speed	Percent Load (By Torque)
Idle	Curb idle torque
Peak Torque Speed	15, 50, 75, 100
Peak Power Speed	15, 50, 75, 100

2.5 Sequence of Gas and Diesel Engine Testing at SwRI

Due to the number and repetitive nature of the tests conducted during this project, the sequence of testing is presented here to provide the reader with a solid map to assist in interpreting the test results. Table 2-5 lists a test sequence number, the test name, an abbreviation that denotes the test data found on some graphs, and the engine the tests were conducted on. Only two NO_x sensors were tested during the natural gas engine testing. Four NO_x sensors were tested in all other tests with data from each being simultaneously acquired.

Table 2-5. Sequence of Gas and Diesel Engine Tests

Test Sequence No.	Test Name	Test Abbreviation	Test Engine
1	Natural Gas Testing	None	JD 8.1 L
2	19-Point Steady-State	SS1	Cummins M11
3	Interference Gas Tests	IGE1	Cummins M11
4	Transient Response Tests	Trans1	Cummins M11
5	10 Hour History Accumulation	Hist1	Cummins M11
6	19-Point Steady-State	SS2	Cummins M11
7	20 Hour History Accumulation	Hist2	Cummins M11
8	19-Point Steady-State	SS3	Cummins M11
9	40 Hour History Accumulation	Hist3	Cummins M11
10	19-Point Steady-State	SS4	Cummins M11
11	Interference Gas Tests	IGE2	Cummins M11
12	Transient Response Tests	Trans2	Cummins M11
13	Field Demonstration	None	Raley's Trucks equipped with Cummins M11s
14	19-Point Steady-State	SS5	Cummins M11
15	Interference Gas Tests	IGE3	Cummins M11
16	Transient Response Tests	Trans3	Cummins M11

3.0 RESULTS

3.1 Results of the Literature Search and Procurement of Test Sensors

Table 3-1 lists in order the sensor manufacturers that were contacted, the sensor's score, and stage of development. High-ranking scores are better than low ranking scores. The ranking is purely subjective since none of the sensors that could have been selected for this project were actually previously tested by SwRI. As a result, data given to SwRI by each sensor manufacturer was taken as received. Figure 3-1 is a bar chart illustrating scores of the sensors that were ranked.

Sensor manufacturers that did not or could not respond are also listed in Table 3-1. The NGK Insulators, Ltd. sensor scored the highest of all sensors ranked and was the only sensor available for testing during this project. All other sensors were at various stages of development and not ready for real world testing. Note, however, that the NGK Insulators, Ltd. sensor is not commercially available at this time. Only the portable NO_x analyzers from ECOM and Enerac are *commercially* available at this time. No fast response NO_x sensor for vehicular applications is commercially available. A brief discussion on selected sensors most applicable to this project is given below.

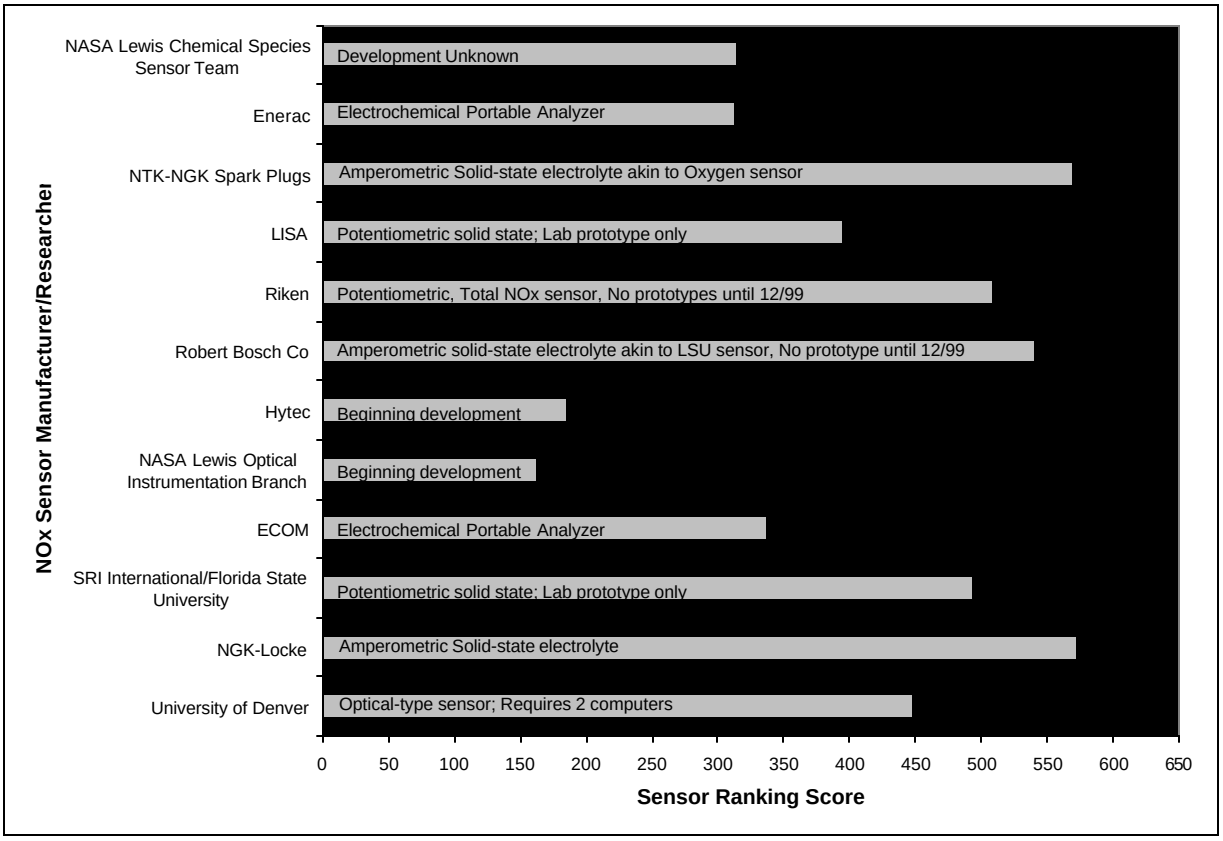

Figure 3-1. NO_x Sensor Rankings

Table 3-1. NO_x Sensor Manufacturers Contacted and Associated Rankings

Sensor Manufacturer	Ranking Score	Stage of Development	Willing to Participate?
NGK Insulators, Ltd./Siemens	572	5th Iteration	Yes
NTK-NGK Spark Plug and ECM	569	9th Iteration	No
Robert Bosch Co.	540	Prototype available 12/99	Yes
Riken	509	Prototype available 12/99	Yes
SRI International	493	Lab Prototype Only	Yes
Univ. of Denver	448	Lab Prototype Only	Yes
Canadian LISA Lab	395	Lab Prototype Only	Yes
ECOM	338	Portable Analyzer Only	Yes
NASA Lewis Chemical Species Sensor Team	314	Early	Yes
Enerac	313	Portable Analyzer Only	Yes
Hytec Electronics	185	Beginning Development	Yes
NASA Lewis Optical Instrumentation Technology Branch	162	Fundamental Materials Research Underway	Yes
Engelhard Corp.	Not Ranked	Applied Research Conducted at SwRI	Yes
Hitachi	Not Ranked	Beginning Development	Yes
Denso	Not Ranked	Cannot Disclose	Probably in Future
Figaro Engineering	Not Ranked	Not Developing Sensor	
Osaka Gas Research and Development	Not Ranked	Cannot Disclose	Probably in Future
University of Wales Swansea	Not Ranked	Worked Stopped 3 years ago	Probably in Future
Cambustion Ltd.	Not Ranked	Not Developing Sensor	
Texas Instruments	Not Ranked	Not Developing Sensor	
University of Brescia (Italy)	No Response		
Delft University of Technology (The Netherlands)	No Response		
Kyushu University (Japan)	No Response		
Siemens Automotive	No Response		

3.1.1 NGK Insulators, Ltd. NO_x Sensor

The NGK Insulators, Ltd. sensor scored the highest and appears to be well suited for the heavy-duty diesel engine environment. It has been designed for both gasoline and diesel engines. The sensor is a solid-state, thick film, amperometric, electrolyte type containing multiple diffusion cells and a temperature controlled sensing element. [1, 2, 3, 4] The design of this sensor is very similar to the widely used Universal Exhaust Gas Oxygen (UEGO) sensor manufactured by a sister company of NTK (NGK Spark Plug).

The sensor is stated as having a ±10% accuracy of reading at below 100 ppm and ±7% accuracy of reading at 300 ppm NO_x after 1000 hours of aging. [4] The current accuracy target is 5%. Much like the UEGO sensor, this sensor is slightly affected by variations in exhaust back pressure and will likely require control system software compensation. The sensor is listed as not being affected by variations in oxygen (O_2) concentration, but is known to be affected to some degree by carbon monoxide (CO), hydrocarbon (HC), and sulfur dioxide (SO_2). In addition, ammonia (NH_3), the main reagent in selective catalytic reduction (SCR) systems, is presently interpreted by the sensor as NO_x. [5] NGK Insulators, Ltd. is currently addressing this phenomenon. The output of this sensor is in the form of a 0-5 volt signal and compatible with present day engine control management (ECM) systems. The combined NO_x range of this sensor can easily accommodate the 0-2000 parts per million (ppm) NO_x requirement and has a published response time of 260 msec for a 33% to 66% step change in NO_x. [2] This sensor catalytically converts NO_2 to NO to determine total NO_x. [3] As an added application benefit, the sensor outputs a voltage that is proportional to the exhaust gas O_2 level. Hence, both NO_x and O_2 can be determined from a single sensor. Although Siemens did not respond to the questionnaire, it has been published that Siemens will be supplying a smart "chip-in-connector" wiring harness for the NGK Insulators, Ltd. Sensor. [4]

3.1.2 NTK (NGK Spark Plug) NO_x Sensor and ECM

The NTK Company manufactures the UEGO sensor used in several closed-loop, lean burn engine control systems. NTK is presently developing a NO_x sensor of the solid-state, thick film, amperometric, electrolyte type containing multiple diffusion cells with a temperature controlled sensing element. [6, 7, 8, 9] The NTK NO_x sensor is very similar to the NGK Insulators, Ltd. sensor in function and appearance.

NTK did not directly respond to requests for this project. However, a California firm named ECM provided SwRI with a brochure of the not-yet commercially available NO_x sensor. ECM designs and/or manufactures control boxes for the NTK UEGO sensor and will do the same for the NO_x sensor. [10] The sensor is entering its ninth revision according to ECM. The NTK sensor can measure up to 9999 ppm with a stated accuracy of ±20 ppm and a response time of 180 msec. [11] Sensor output can be a 0-5 volt signal, programmable, or embedded in a RS-232 protocol. Information acquired for this sensor indicates that NO and NO_2 are measured and an output signal representative of the O_2 concentration is provided. ECM stated that NTK was very cautious in terms of providing technical data and samples to uncontracted sources, and hence, would probably not participate. NTK did not respond to SwRI's requests for participation.

3.1.3 Bosch Co. NO_x Sensor

Bosch is developing a thick film, solid-state, multi-layered electrolyte NO_x sensor that functions on the same principle as the NGK Insulators, Ltd. and NTK sensors. [12]. The sensor is stated as meeting the accuracy, repeatability, and linearity guidelines of this project. The response time is unknown, but likely on the order of 200 msec. The sensor is currently affected by O_2 and NH_3 such that measures are being taken to reduce the effect. [12] Back pressure is assumed to affect the sensor as well, due to the multiple diffusion cells and operating principle. Based on current information, the sensor measures only NO and provides an additional output of the O_2 concentration. [12] The output of the sensor can be easily interfaced with an ECM in voltage form or broadcast over a control area network (CAN) link. Bosch was very receptive to the CARB project, but stated that prototypes would not be available until three months after the start of the field demonstration.

3.1.4 Riken Inc. NO_x Sensor

Riken is developing a "total" NO_x sensor using a mixed potential arrangement. [13] The sensor is a solid-state, multi-layered, potentiometric, electrolytic device that appears to be targeted for the stoichiometric and/or lean burn gasoline engine market. The sensing element is temperature controlled to provide a measuring accuracy of ±1% from 0 to 500 ppm NO_x and can measured down to 10 ppm NO_x. Accuracy decreases to ±10% at exhaust temperatures greater than 650°C, while sensitivity increases at exhaust gas temperatures below 650°C. [14]

This sensor measures NO_x by oxidizing NO into NO_2, [13] and is said to not be affected by CO, HC, or O_2 gases. [13, 14] The sensor has been tested with up to 21% O_2, but only 7% water (H_2O). The response time of the sensor has not been specifically tested, but is likely on the order of 500 msec or less. Riken was also very receptive to the CARB project, but did not have any prototypes available for testing.

3.1.5 SRI International NO_x Sensor

SRI has been working with the University of Florida in the development of a solid state, potentiometric type NO_x sensor targeted for heavy-duty diesel engine applications. [15] SRI is presently seeking additional funding to complete the development. A laboratory prototype has been tested up to 2000 ppm NO at 700°C. SRI stated that the accuracy and repeatability were within the CARB project guidelines. Sensor output is non-linear and dependent on the NO range. [15] Oxygen and H_2O are known to affect the sensor's output. [15] The response time is assumed to be within 30 msec by SRI. The sensor operates in a fashion similar to conventional exhaust gas oxygen (EGO) sensors used on many stoichiometric gasoline automobiles.

3.1.6 University of Denver NO_x Sensor

The University of Denver has been working on optical exhaust gas measurement techniques for remote roadside exhaust gas analysis. [16] The University of Denver has developed a laboratory prototype that requires multiple commercially available off-the-shelf components to generate and measure ultraviolet and infrared light. Two personal computers, monochromators, beam splitters, fiber optics, quartz windows, and spinning mirrors are required.

Of all the systems evaluated, this system appears to require the most package volume in its current form.

The system responds the fastest of all sensors considered at 10 msec. [17] Accuracy and repeatability are stated to be better than ±1% at 2000 ppm NO_x. [17] The sensor calibration is highly non-linear and changes as a function of exhaust gas temperature. Only NO is measured in the current measuring package. [17] Sensor output is not affected by O_2, H_2O, HC, or NH_3. [17] This type of sensor can also simultaneously measure CO, CO_2, and HCs. [16] Major concerns with optical sensors is the potential of soot contamination and sensor implementation in the exhaust system. The University of Denver states that the windows clean themselves at 650°C.

3.1.7 LISA Laboratory NO_x Sensor

The LISA laboratory in Canada is developing a solid-state potentiometric NO_x sensor that can measure up to 10,000 ppm NO_2 at up to 250°C. [18] The resolution of the sensor is stated as ±5 ppm and highly repeatable over several hours of operation, although the number of hours was not given. [18] The output is linear and has a 0 intercept/offset. [18] The output signal was stated as a measurable voltage that can likely be amplified to interface with an ECM. The response time was not directly tested but known to be less than one second. [18] The LISA laboratory was very interested in the CARB project. However, a vehicle-ready prototype was not currently available. They are seeking collaboration to bring the sensor to market.

3.1.8 ECOM America and Enerac NO and NO_2 Analyzers

ECOM and Enerac both manufacture and sell NO and NO_2 analyzers that are typically found in laboratory environments for measuring diesel engine NO_x. The NO and NO_2 analyzers are of the electrochemical type. [19, 20] The analyzers can meet many of the sensor guidelines in terms of accuracy, repeatability, minimal interference effects, etc. However, they are not well suited for on-vehicle measurements due to their long response times and required sample conditioning devices. In addition, the analyzers typically contain water traps that must be manually drained.

3.1.9 Engelhard Corporation NO_x Sensor

The Engelhard Corporation, with consultation from Dr. Jacob Wong, was developing a Non-Dispersive Infrared Radiation (NDIR) On-board Diagnostic Exhaust Gas Analyzer (ODEGA) for measuring NO_x and H_2O. The sensor can be easily configured to measure HCs, CO, CO_2, and potentially particulate matter. SwRI had the opportunity to conduct applied research on an early prototype. [21] The sensor was tuned to measure NO, but not collectively NO_x. The sensor was able to resolve changes in NO concentration in the range from 1844.1 ppm down to 466.7 ppm in steps of ±100 ppm. In addition, the ODEGA resolved changes in dried and cooled diesel engine exhaust in the range from 619.9 ppm down to 258.5 ppm in steps of ±50 ppm. Variations in exhaust gas thermodynamic quantities, such as temperature and water vapor concentration, currently have large effects on the ODEGA's performance. Engelhard is moving forward with detailed thermal management system analysis and plans to revise the prototype tested at SwRI. Engelhard was aware of the CARB program and willing to participate

when a suitable analyzer/sensor was developed. However, no sensor was available during the current project.

3.1.10 Procurement of NGK Insulators, Ltd. NO_x Sensors

SwRI received two of four NGK Insulators, Ltd. 5th generation, prototype, combined NO_x/O_2 sensors in June of 1999. These sensors are referred to as NGK1 (serial number 9E10B-1038) and NGK2 (serial number 9E10B-1044). These sensors were the only two sensors tested on the John Deere natural gas engine. SwRI received the final two of the four NGK Insulators, Ltd. 5th generation NO_x sensors in August of 1999. The two sensors are referred to as NGK3 (serial number 9F14A-1018) and NGK4 (serial number 9F14A-1022). All four sensors were of model type TNS-1010-3Z and were received with factory calibrations from a 0 to 2000 ppm NO_x range and paired with specific controllers prescribed by NGK Insulators, Ltd.. A photograph of a NGK Insulators, Ltd. 5th generation sensor and conditioning/controller box is show in Figure 3-2.

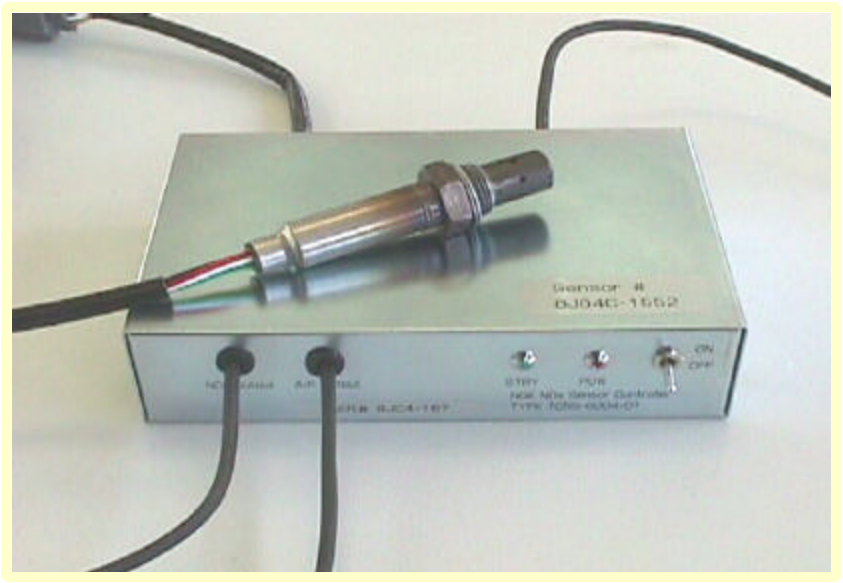

Figure 3-2. Photograph of NGK Insulators, Ltd. 5th Generation Combined NO_x and O_2 Sensor

The NGK Insulators, Ltd. sensor is comprised of an internal heater, and two internal cavities that house three oxygen pump cells and two oxygen sense cells that are all embedded in six superimposed layers of oxygen ion conductive ZrO_2. [1, 2] These features are shown in the cutaway schematic in Appendix A. The first internal cavity includes one oxygen pump cell and one oxygen sense cell. Exhaust gas enters the first internal cavity via a diffusion path under a predetermined diffusion resistance. In the first internal cavity, the oxygen pump cell lowers the exhaust gas oxygen concentration to a predetermined level utilizing feedback from the oxygen sense cell. The oxygen sense cell consists of the first pump cell's negative platinum/gold electrode and a platinum reference electrode located in an air duct that communicates with the ambient air. The sense cell provides feedback to control the oxygen concentration in the first

internal cavity via the first oxygen pump cell. Nitrogen dioxide (NO_2) is decomposed to NO and O_2 in this first internal cavity under Equation 6.

$$NO_2 \longrightarrow NO + \frac{1}{2}O_2 \tag{6}$$

Low oxygen exhaust enters the second internal cavity from the first internal cavity via another diffusion path at a designed diffusion rate. Two oxygen pump cells and one oxygen sense cell comprise the second internal cavity. The first of the two oxygen pump cells in the second internal cavity lowers the exhaust gas oxygen concentration further. The oxygen sense cell in this second internal cavity monitors the oxygen level of the oxygen reduced gas and provides feedback to the first of the two oxygen pump cells to maintain the desired oxygen concentration.

The second of the two oxygen pump cells is really a NO_x *sense* cell. This is the location where NO_x is inferred from the oxygen concentration. This pump cell utilizes a rhodium, rather than platinum, electrode that has NO_x reduction catalytic activity. Here, the NO_x decomposes on the measuring electrode by way of Equation 7. The oxygen generated reduction chemistry is detected as an oxygen pumping current in the NO_x sense cell, and hence, the NO_x is determined.

$$NO \longrightarrow \frac{1}{2}O_2 + \frac{1}{2}N_2 \tag{7}$$

The sensor supply voltage was increased from 12.0 ±0.5 volts in earlier prototypes to 14.0 ±0.5 volts in the 5th generation sensors to maintain a near constant tip measuring temperature of 850°C to minimize the effects of carbon build up. The sensors were *not* to be powered by a vehicle battery since voltage spikes could damage the sensors and control/conditioning electronics. Therefore, a variable power supply was used to power the sensors in tests conducted at SwRI. A DC-to-DC voltage converter was used to power the sensors on the Raley's trucks during the field demonstration. The prototype electronic control and conditioning box for each sensor could not be grounded and was, therefore, placed on non-conducting material during tests at SwRI, and suspended on rubber vibration dampening grommets during the field demonstration. NGK Insulators, Ltd. will be developing circuitry to maintain 9.0 to 16.0 volts when powered by a conventional automobile battery in future versions of the sensor.

No other sensor manufacturer was prepared to provide sensors for evaluation in this project prior to the first set of steady-state testing at SwRI. Therefore, all references to NGK-Insulators, Ltd. or NGK-Locke will be made as NGK in the following text. NGK-Locke acted as the conduit for providing the NGK-Insulators, Ltd. sensors for this program.

3.2 Results of Natural Gas Engine Testing

Figure 3-3 shows the dry NO_x mole fraction in the natural gas engine exhaust as a function of torque for each of the three (3) engine speeds tested. The NO_x shown in the graph is that measured by the SwRI Milton-Roy emissions bench. Note that the engine was fitted with development components. Therefore, the torque output and exhaust emissions do not necessarily

reflect John Deere production values. Figure 3-3, along with Table 3-2, shows that NGK1 and NGK2 were exposed to NO_x emissions ranging from 27.9 ppm to 722.9 ppm (approximately 37 percent of the maximum range of the sensors). Actual numeric values of the data are presented in Table 3-2.

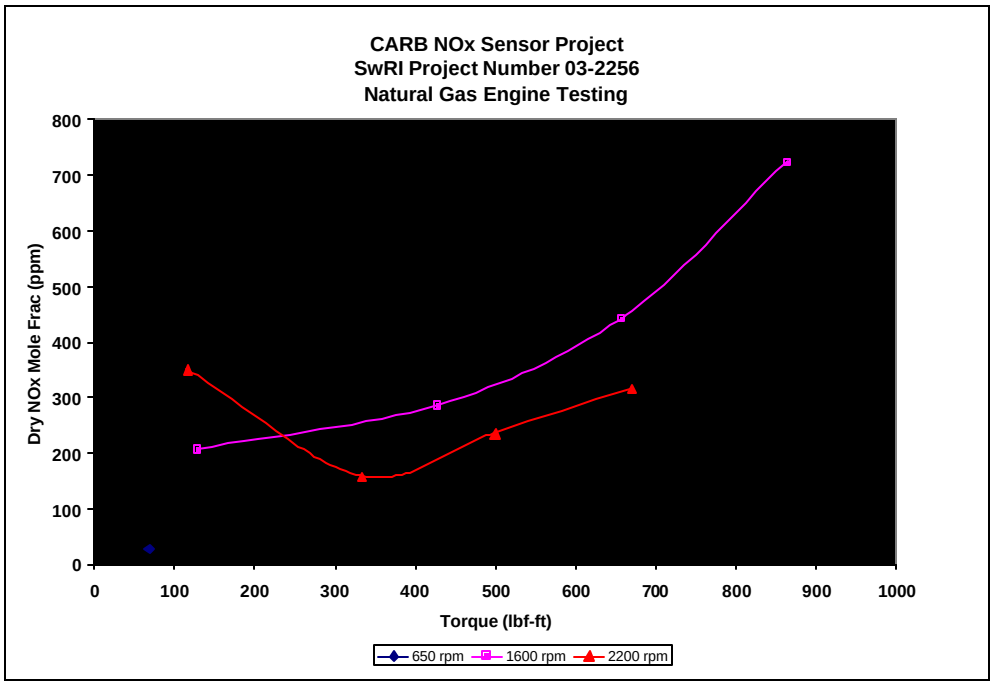

Figure 3-3. NO_x Mole Fraction as a Function of John Deere Natural Gas Engine Torque

Table 3-2. Selected Low-Speed Data Acquired During Natural Gas Engine Testing of 2 NGK Insulators, Ltd. NO_x Sensors

Run No	Speed (RPM)	Torque (lbf-ft)	BSNO$_x$ (g/bhp-hr)	Dry NO$_x$ Mole Fraction (ppm)	NGK1 NO$_x$ Output Volts	NGK2 NO$_x$ Output Volts
1083	657	68.5	0.280	27.9	0.375	0.370
1084	1610	864.7	3.948	722.9	2.192	2.096
1085	1609	658.2	2.492	441	1.359	1.355
1086	1608	428.9	1.710	285	0.993	0.983
1087	1609	129.8	1.537	205.9	0.781	0.797
1088	2209	669.2	1.853	314.7	1.053	1.069
1089	2210	499.4	1.423	234.6	0.878	0.884
1090	2208	333.3	1.032	157.4	0.686	0.689
1091	2201	116.8	2.951	350.2	1.127	1.114

Figure 3-4 shows each sensor's NO_x output voltage as a function of NO_x mole fraction along with the NGK supplied calibration data. Triangles denote NGK1 while the squares on the dashed line represent NGK2. Actual values from the plot are shown in Table 3-3. The NGK supplied data are based on a model gas apparatus (synthetic gas) and not actual engine exhaust.

The model gas apparatus test gas concentrations were 0-2000 ppm NO_x, 3 percent H_2O, and N_2 making up the remainder. Linear functions were fit to each of the four sets of data (two sets of measured data, two sets supplied by NGK). Each of the four linear functions had correlation coefficients greater than 99 percent. However, the SwRI measured data have an increased slope and reduced offset relative to the respective NGK supplied data. The slope differed by 13.6 percent and the offset by –19.6 percent for sensor NGK1 relative to the NGK supplied data. The slope differed by 18.2 percent and the offset by –30.7 percent for sensor NGK2 relative to the NGK supplied data. These differences amount to -13.3 percent in NO_x between the SwRI and NGK curve fits for NGK1 at 4.5 volts, and –10.2 percent in NO_x at 4.5 volts for NGK2 based on the curve fits. In other words, if one solves for NO_x at 4.5 volts from the curve fits shown in Figure 3-4, the difference between the computed NO_x between the SwRI curve and the NGK curve is –13.3 percent for NGK1 and –10.2 for NGK2. Hence, the calibrations developed from SwRI measured data would under-predict the NO_x mole fraction assuming the NGK supplied data are accurate for natural gas. In any event, the percent differences are good considering that NGK has published data from diesel emissions stating that the sensor is +/-10 percent accurate at and below 300 ppm NO_x.

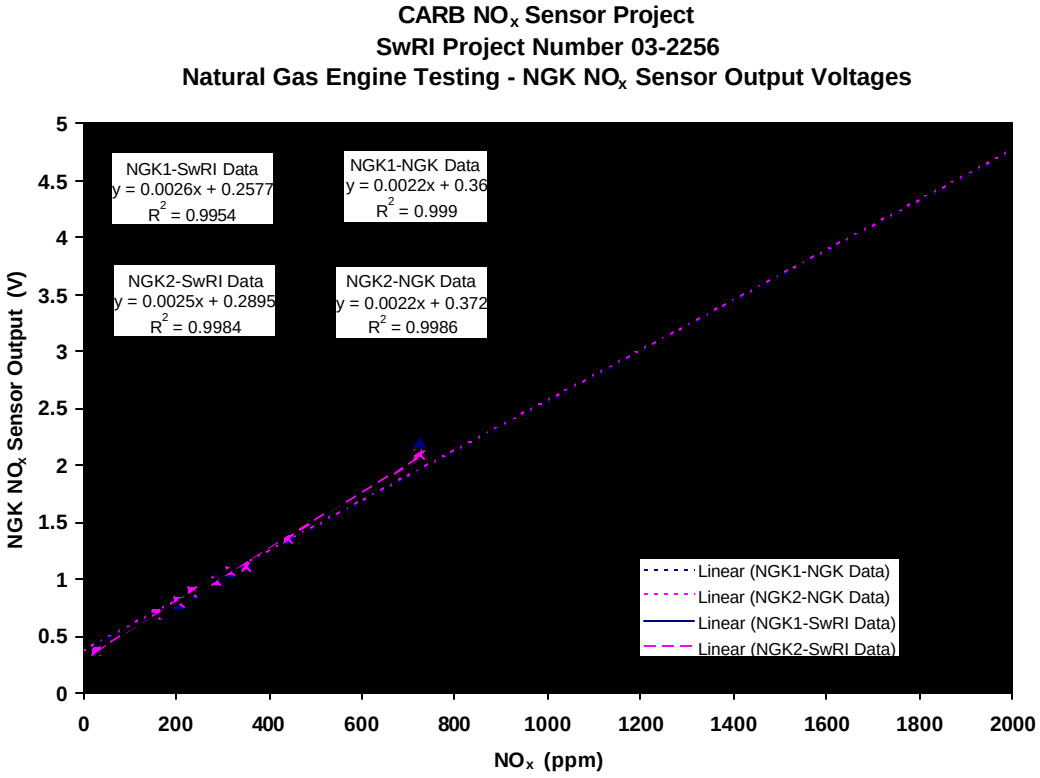

Figure 3-4. NGK Insulators, Ltd. NO_x Sensor Output Voltage as a Function of Measured NO_x Mole Fraction on Natural Gas Engine

The oxygen sensor output of the NGK NO_x sensors is shown in Figure 3-5 as function of the measured exhaust gas oxygen concentration. NGK supplied calibration data are also shown in the figure. The NGK supplied data are based on calibrations taken from a model gas apparatus. The model gas apparatus test gas concentrations were 0-18 percent O_2, 3 percent H_2O, and N_2 making up the remainder. The figure shows a significant offset shift in the calibration. A similar shift is present when wide range universal exhaust gas oxygen (UEGO) NTK sensors are re-calibrated for natural gas use. The slope differed by 1.2 percent for sensor NGK1 relative to the NGK supplied data while the slope differed by 0.6 percent for sensor NGK2. The shift in offsets was –0.1796 volts for sensor NGK1 and –0.1854 volts for sensor NGK2. These shifts in offsets are roughly 1.5 O_2 percent (e.g. 5% O_2 versus 6.5% O_2).

Table 3-3. Selected Low-Speed Data Acquired During Natural Gas Engine Testing of 2 NGK Insulators, Ltd. NO_x Sensors

Run No	Speed (RPM)	Torque (lbf-ft)	Dry O_2 Mole Fraction (%)	NGK1 O_2 Output Volts	NGK2 O_2 Output Volts
1083	657	68.5	5.65	2.960	2.971
1084	1610	864.7	8.16	3.237	3.255
1085	1609	658.2	8.36	3.254	3.271
1086	1608	428.9	8.33	3.245	3.262
1087	1609	129.8	7.10	3.106	3.188
1088	2209	669.2	8.25	3.263	3.282
1089	2210	499.4	8.23	3.247	3.263
1090	2208	333.3	8.20	3.228	3.243
1091	2201	116.8	7.13	3.108	3.120

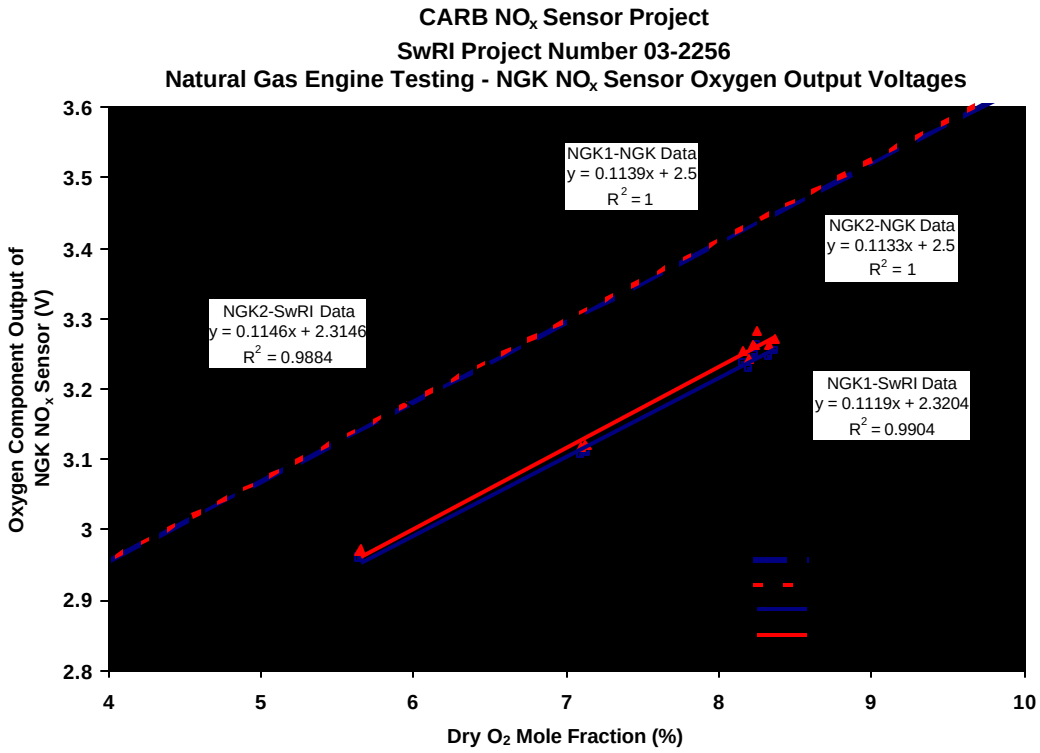

Figure 3-5. NGK Insulators, Ltd. Oxygen Component of NO_x Sensor Output as a Function of Measured O_2 Mole Fraction on Natural Gas Engine

3.3 Results of Testing in Diesel Engine Exhaust

The diesel engine test results for a given type of test will be presented together. For example, the results of all five 19-point, steady-state tests will be presented and discussed at the same time. This will allow the reader to observe how the sensors operated before and after the field demonstration (refer to Table 2-5 for a listing of the test sequence). Data from the field demonstration will be presented after all laboratory test results on the Cummins M11 diesel engine, to provide the reader with a feel for how the sensors operated during in-service use. However, it is the laboratory test data that characterizes the functionality, accuracy, repeatability, and linearity of the NO_x sensors; the primary objective of this project.

3.3.1 19-Point Steady-State Test Results for NO_x Component of the NGK Insulators, Ltd. Sensors

The engine was operated at the 19 steady-state test points shown in Table 2-2. The test matrix comprises the full range of loaded engine speeds from idle to the maximum governed loaded speed. Figures 3-6, 3-7, 3-8, and 3-9 are plots of the NO_x output voltage from a given sensor as a function of the NO_x concentration measured by the Milton-Roy emissions bench at each steady-state test condition. Each sensor is represented by a single plot, while the data from each steady-state test (19 points) are represented by a single symbol. The phrase "SS" followed by a number of one through five in the legend indicates the steady-state test. Steady-state test 4 (SS4) and 5 (SS5) are the pre- and post-field demonstration data, respectively.

Linear regression curves and the respective functions are also shown in Figures 3-6 to 3-9. In general, seven points in each plot fall outside the trend created by surrounding data. All seven of these points occurred at idle speed. The group of data created by five of the points between 1000 ppm and 1400 ppm NO_x were at maximum load. The idle speed 100 percent load condition was characteristic of CO emissions nearing the 10,000 ppm, or 1 percent level, while CO emissions was on average 125 ppm across all steady-state data. Hence, high CO concentrations appear to shift sensor output in a manner that is inversely proportional to CO emissions. In other words, increases in CO emissions decrease sensor sensitivity. This phenomenon may likely be the result of NO decomposing in the first internal cavity with the high concentration CO rather than in the second internal cavity. The net effect is the sensor outputs a voltage that is too low for the given NO_x concentration. Note, however, that it is unlikely that this engine operating point will be regularly encountered, if at all, since engine speed in most transit vehicles increases as load is commanded.

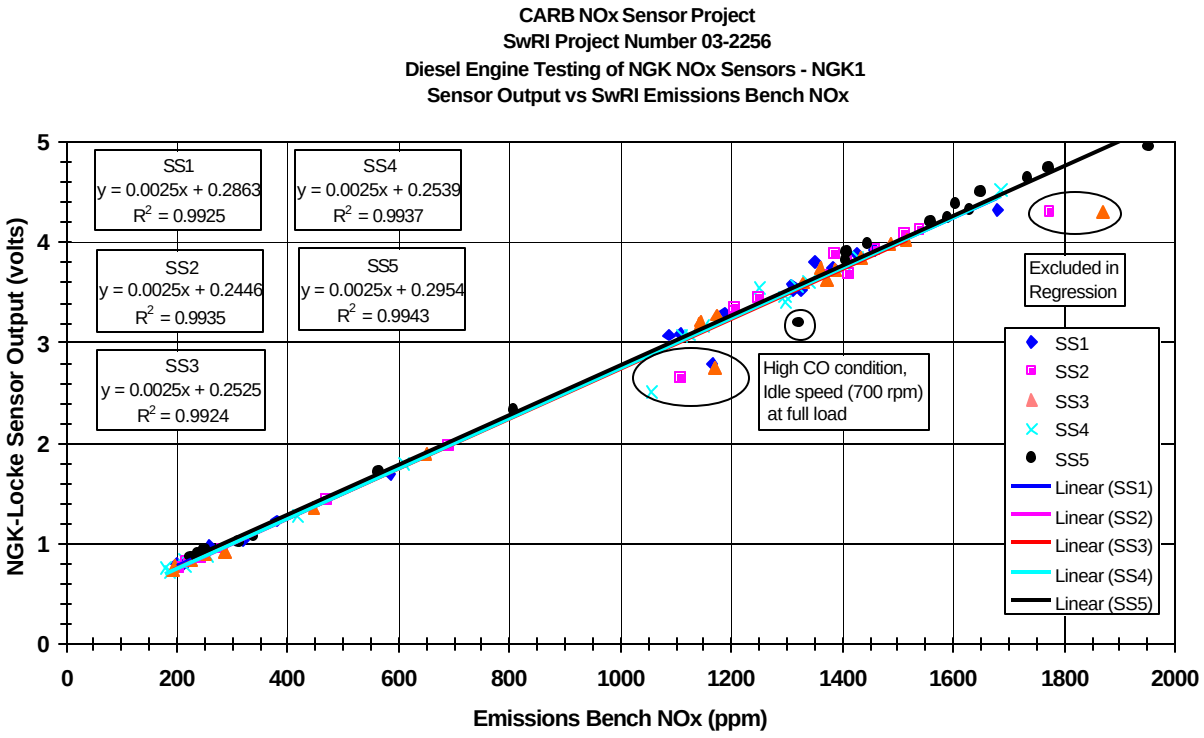

Figure 3-6. NGK1 NO_x Sensor Output Voltage as a Function of Measured NO_x Emissions

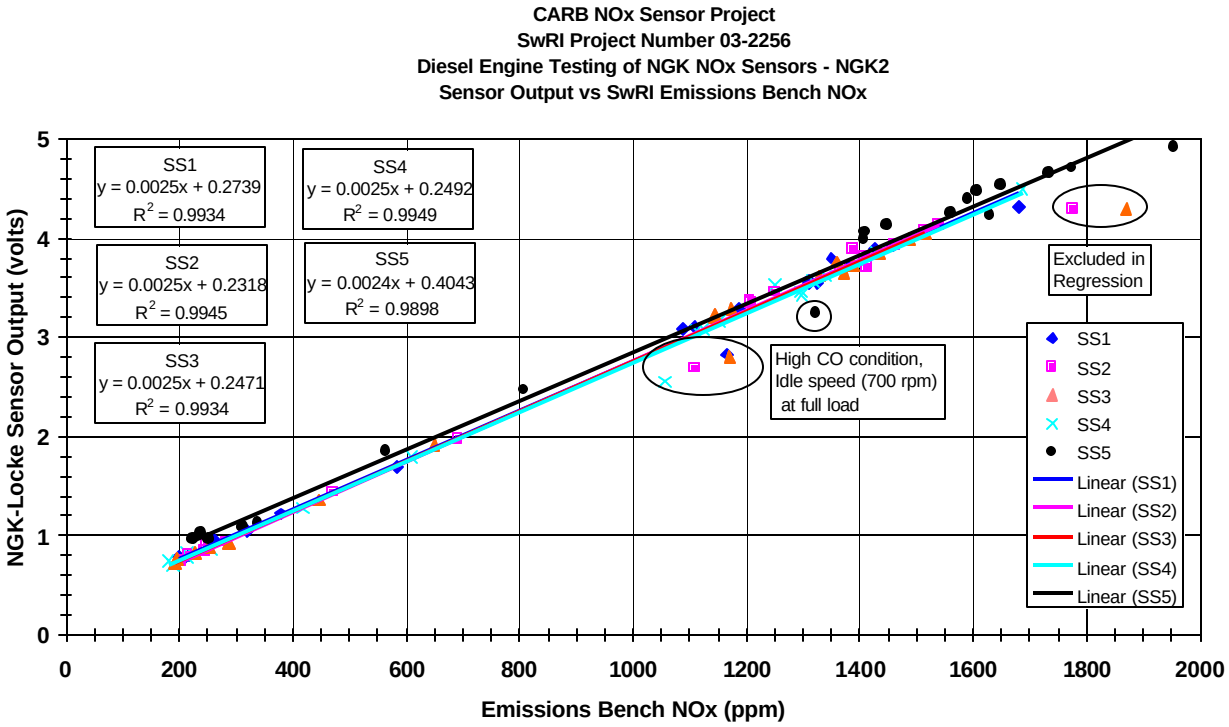

Figure 3-7. NGK2 NO_x Sensor Output Voltage as a Function of Measured NO_x Emissions

The remaining two of the seven data points are highlighted by an ellipse and lie between 1775 and 1870 ppm NO_x. These two points occurred during the second and third set of steady-state tests at idle speed and 50 percent load. They are considered outliers because engine speed and load could not be maintained at a suitable level for the Milton-Roy emissions bench to report a true steady-state value. Therefore, they are not included in the linear regressions. Engine speed was controlled to 710 rpm (as opposed to 690-700 rpm) during SS5 testing to obtain a solid steady-state value. Idle speed data is sometimes difficult to acquire due to the delicate balance required between the ECM and the dynamometer controllers. One controller typically "fights" the other, resulting in oscillations in engine speed and load.

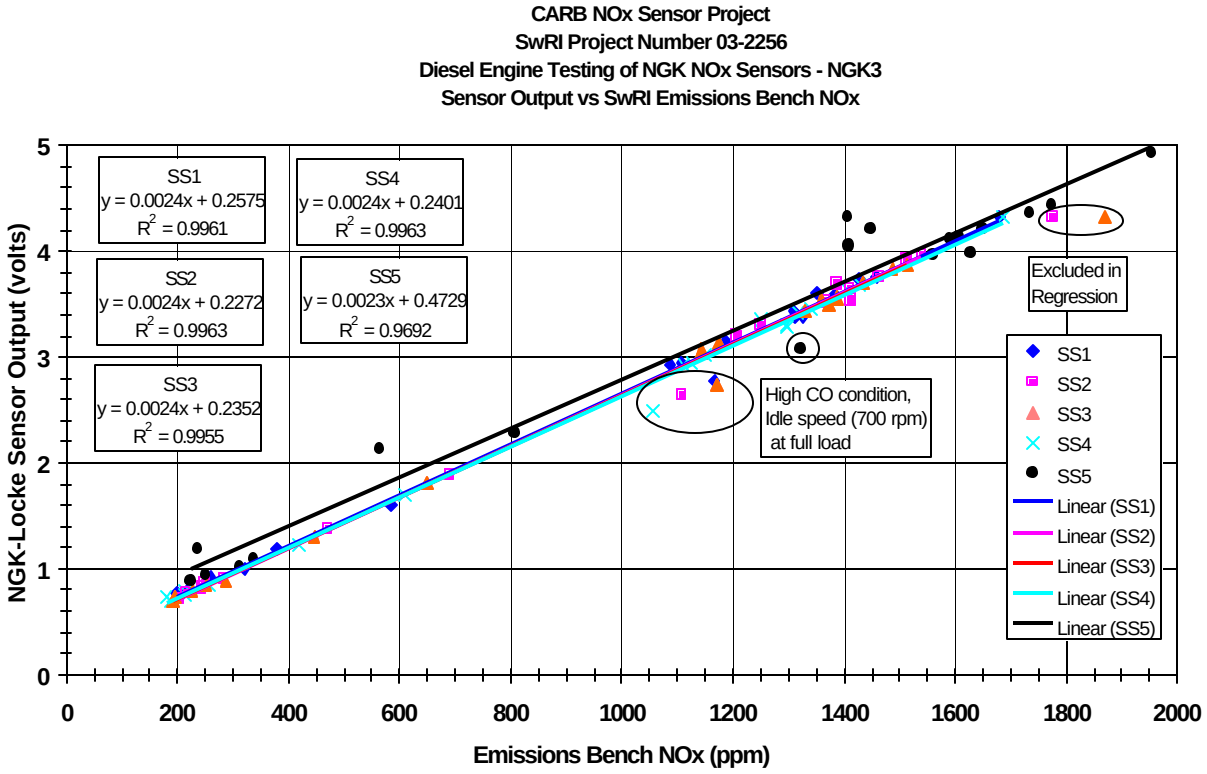

Figure 3-8. NGK3 NO_x Sensor Output Voltage as a Function of Measured NO_x Emissions

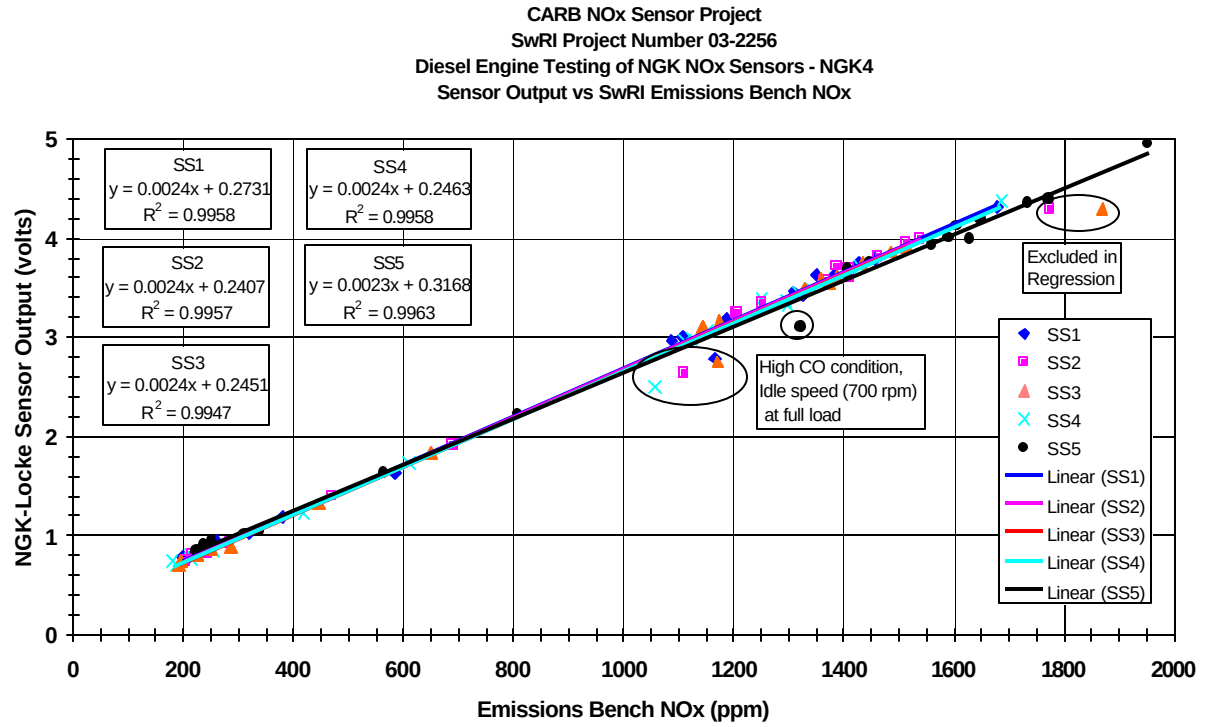

Figure 3-9. NGK4 NO_x Sensor Output Voltage as a Function of Measured NO_x Emissions

The reader will notice that there is more scatter in the SS5 (post field demo) data for sensors NGK2 (Figure 3-7) and NGK3 (Figure 3-8). These two sensors were on different trucks but arranged the same in the exhaust system. Therefore, sensor orientation or an internal anomaly could have played a role in the data scatter; for example, a slightly blocked sample port or oscillatory heater control. Four of the five outliers in the SS5 data for NGK3 occurred at 1800 rpm, with the fifth occurring at 1600 rpm; all representative of high gas flow conditions.

The slope and offset for each sensor for a given steady-state test is shown, along with the offset representation in ppm NO_x, and correlation coefficient (R^2) in Tables 3-4, 3-5, 3-6, and 3-7. The variation in each sensor's slope and offset across steady-state tests relative to the slope and offset generated from the respective sensor's first set of steady-state data (SS1) is shown. Reference was made to the SS1 data since, in typical application cases, a sensor would be initially calibrated and placed in service for some period of time and later checked relative to the initial calibration. The variation in offset between steady-state tests for a given sensor is also shown in the tables.

The slopes ranged from 0.002307 volts/ppm NO_x (NGK3, SS5), or 433.5 ppm NO_x/volt to 0.002532 volts/ppm NO_x (NGK2, SS2), or 394.9 ppm NO_x/volt. The variation in calibration slope from steady-state test to steady-state test relative to SS1 data decreased from test to test, indicating reduced sensitivity with age. The decrease in sensitivity, or sensor calibration slope (volts per ppm NO_x), ranged from 1.456 percent to 0.262 percent for NGK1, 1.622 percent to –1.687 percent for NGK2, 0.157 percent to –4.009 percent for NGK3, and 1.020 percent to –3.681 percent for NGK4.

Across all sensors and steady-state tests, the calibration offsets ranged from 0.2318 volts (NGK2, SS2), or 91.5 ppm NO_x, to 0.4729 volts (NGK3, SS5), or 205.0 ppm NO_x. The variation in offset decreased from test to test relative to the SS1 offset for a given sensor. For example, the offset variation was –14.553 percent between the SS2 and SS1 data, -11.818 percent between the SS3 and SS1 data, -11.308 percent between the SS4 and SS1 data, and 3.171 percent between the SS5 and SS1 data. All four sensors exhibited this trend. The largest changes in offset occurred between the SS1 and SS2 tests and the SS4 and SS5 tests when evaluating the change in offset relative to the offset of the previous test (e.g. comparing the SS3 offset to the SS2 offset). Recall that SS4 is the pre-field demo data and that SS5 is the post-field demo data. A change in offset after extended use is a phenomenon that is also observed in universal exhaust gas oxygen sensors and could be the result of obstructed diffusion passage ways in the sensor or reduced sensor catalytic activity. However, note that the direction (increasing or decreasing) of variation in slope from test to test for a given sensor is opposite the direction of variation in offset for the same sensor. This trend has a balancing effect, showing that the sensors are within the published accuracy limits when the SS5 sensor outputs voltages are processed with the SS1 calibrations. This point will be shown later in Figures 3-32, 3-33, 3-34, and 3-35.

The correlation coefficient for all sensors in all tests was greater than 99 percent, except for the SS5 data for the NGK2 and NGK3 sensors. Sensors NGK1 and NGK4 showed the greatest linearity after the field demonstration (SS5 data) with correlation coefficients of 99.43 percent and 99.63 percent, respectively. Hence, the sensor output as a function of NO_x is very linear. All in all, the slopes of the sensors were fairly constant across all tests conducted before and after the field demonstration. Sensor NGK3 appeared to be the most affected by the field demonstration.

Table 3-4. NGK1 NO_x Sensor Calibrations and Variations

Steady-State Test	Slope (volts/ppm NO_x)	Offset (volts)	Offset (ppm NO_x)	Linear Correlation Coef, R^2 (%)	Slope Variation Relative to SS1 (%)	Offset Variation Relative to SS1 (%)	Offset Variation Between Tests (%)
1	0.002478	0.2863	115.5	99.25	-	-	-
2	0.002514	0.2446	97.3	99.35	1.456	-14.553	-14.553
3	0.002499	0.2525	101.0	99.24	0.836	-11.818	3.200
4	0.002495	0.2539	101.8	99.37	0.704	-11.308	0.578
5	0.002484	0.2954	118.9	99.43	0.262	3.171	16.326

Table 3-5. NGK2 NO_x Sensor Calibrations and Variations

Steady State Test	Slope (volts/ppm NO_x)	Offset (volts)	Offset (ppm NO_x)	Linear Correlation Coef, R^2 Percent	Slope Variation Relative to SS1 Percent	Offset Variation Relative to SS1 Percent	Offset Variation Between Tests Percent
1	0.002492	0.2739	109.9	99.34	-	-	-
2	0.002532	0.2318	91.5	99.45	1.622	-15.631	-15.631
3	0.002512	0.2471	98.4	99.34	0.825	-9.784	6.589
4	0.002499	0.2492	99.7	99.49	0.288	-9.020	0.847
5	0.002449	0.4043	165.1	98.98	-1.687	47.626	62.262

Table 3-6. NGK3 NO_x Sensor Calibrations and Variations

Steady-State Test	Slope (volts/ppm NO_x)	Offset (volts)	Offset (ppm NO_x)	Linear Correlation Coef, R^2 (%)	Slope Variation Relative to SS1 (%)	Offset Variation Relative to SS1 (%)	Offset Variation Between Tests (%)
1	0.002404	0.2575	107.1	99.61	-	-	-
2	0.002416	0.2272	94.0	99.63	0.157	-11.787	-11.787
3	0.002401	0.2352	98.0	99.55	-0.116	-8.685	3.516
4	0.002393	0.2401	100.3	99.63	-0.444	-6.791	2.074
5	0.002307	0.4729	205.0	96.92	-4.009	83.635	97.014

Table 3-7. NGK4 NO_x Sensor Calibrations and Variations

Steady State Test	Slope (volts/ppm NO_x)	Offset (volts)	Offset (ppm NO_x)	Linear Correlation Coef, R^2 (%)	Slope Variation Relative to SS1 (%)	Offset Variation Relative to SS1 (%)	Offset Variation Between Tests (%)
1	0.002414	0.2731	113.1	99.58	-	-	-
2	0.002438	0.2407	98.7	99.57	1.020	-11.866	-11.866
3	0.002425	0.2451	101.1	99.47	0.476	-10.256	1.827
4	0.002415	0.2463	102.0	99.58	0.057	-9.817	0.489
5	0.002325	0.3168	136.3	99.63	-3.681	15.986	28.612

Figures 3-10, 3-11, 3-12, and 3-13 show the NO_x ppm value from a given sensor's output voltage based on the calibration slopes and offsets determined from a given test (i.e. SS3 output voltage processed with SS3 calibrations). Each figure represents a single NO_x sensor with all five sets of steady-state data. A +/-10 percent error envelope (manufacturer's specification) and a dashed 1-to-1 correlation line is also shown in the figures. The data in Figure 3-10 represent sensor NGK1 and show good agreement between the measured data and the NO_x values computed from the calibrations. This should be the case due to the 99 percent and greater correlation coefficients for NGK1. The five data points between 1000 ppm and 1400 ppm NO_x from the idle speed and 100 percent load condition can clearly be seen as falling outside the acceptable error envelope. This trend of exceeding the 10 percent error envelope, or being on the 10 percent error envelope, was repeated in all four NGK sensors.

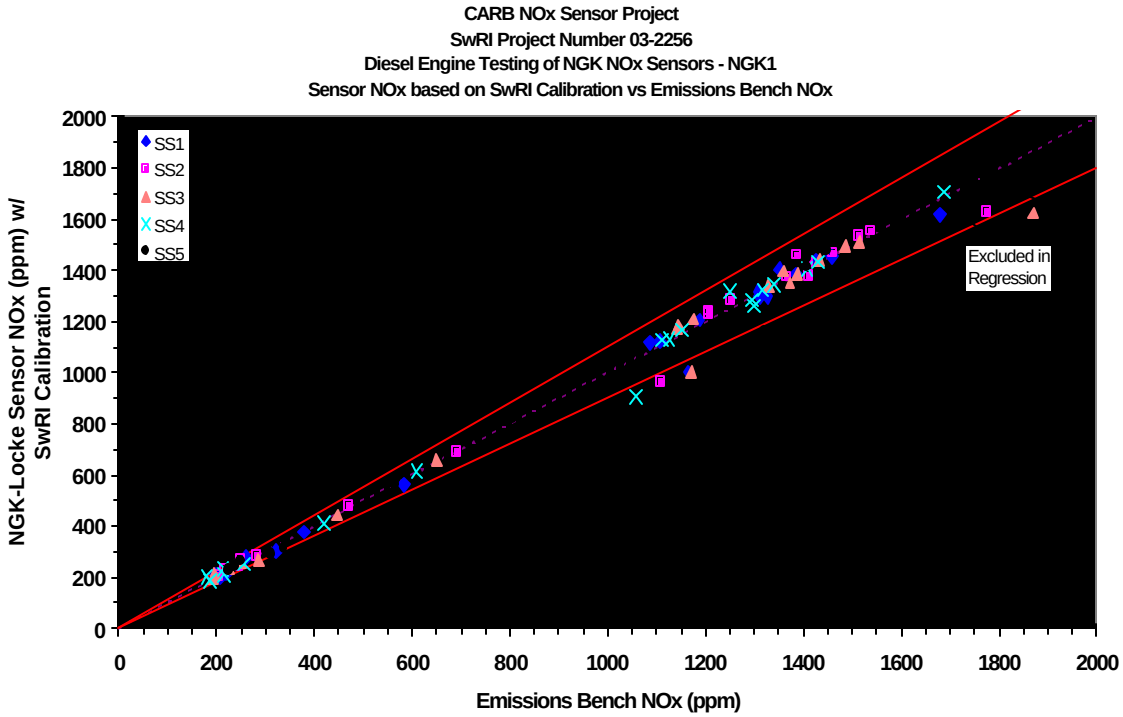

Figure 3-10. Sensor NGK1 NO_x Value as Function of Measured NO_x Emissions

Data scatter from the SS5 tests for NGK2 and NGK3 can be seen in Figures 3-11 and 3-12. However, all of the NGK2 sensor data, except the idle speed and 100 percent load condition, fell within the +/-10 percent error envelope. On the other hand, in addition to the idle speed and 100 percent load data from each steady-state test, nine other points in the SS5 data for NGK3 fell outside the +/-10 percent error envelope. These points occurred at high engine speeds and high gas velocities. Increased gas velocities are effective at cooling the sensor down, requiring precise control of the sensor heater for accurate measurements. Hence, heater control problems could be a reason for erroneous measurements in NGK3 at some conditions: recall that each sensor was paired with only one controller throughout these tests. Sensor NGK4 exhibited a tight trend similar to NGK1. One would expect the results presented in Figures 3-10, 3-11, 3-12 and 3-13 because the NO_x values for a given sensor were based upon the calibration from each set of test data.

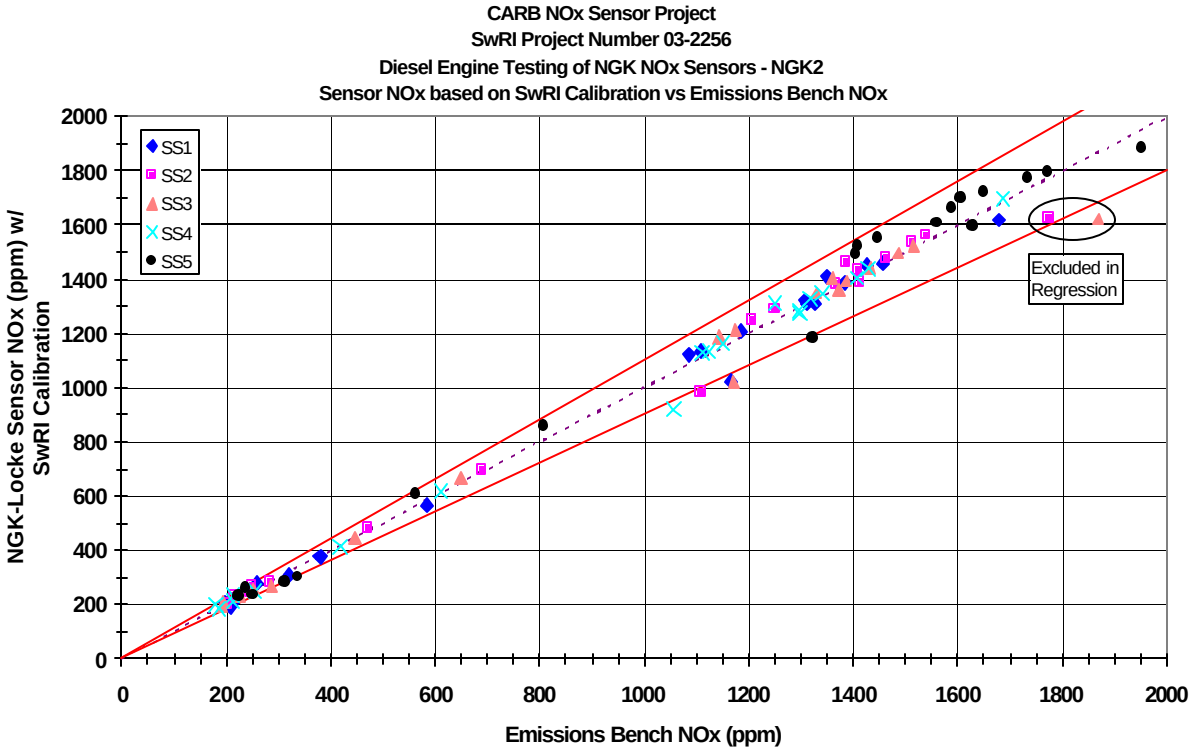

Figure 3-11. Sensor NGK2 NO_x Value as Function of Measured NO_x Emissions

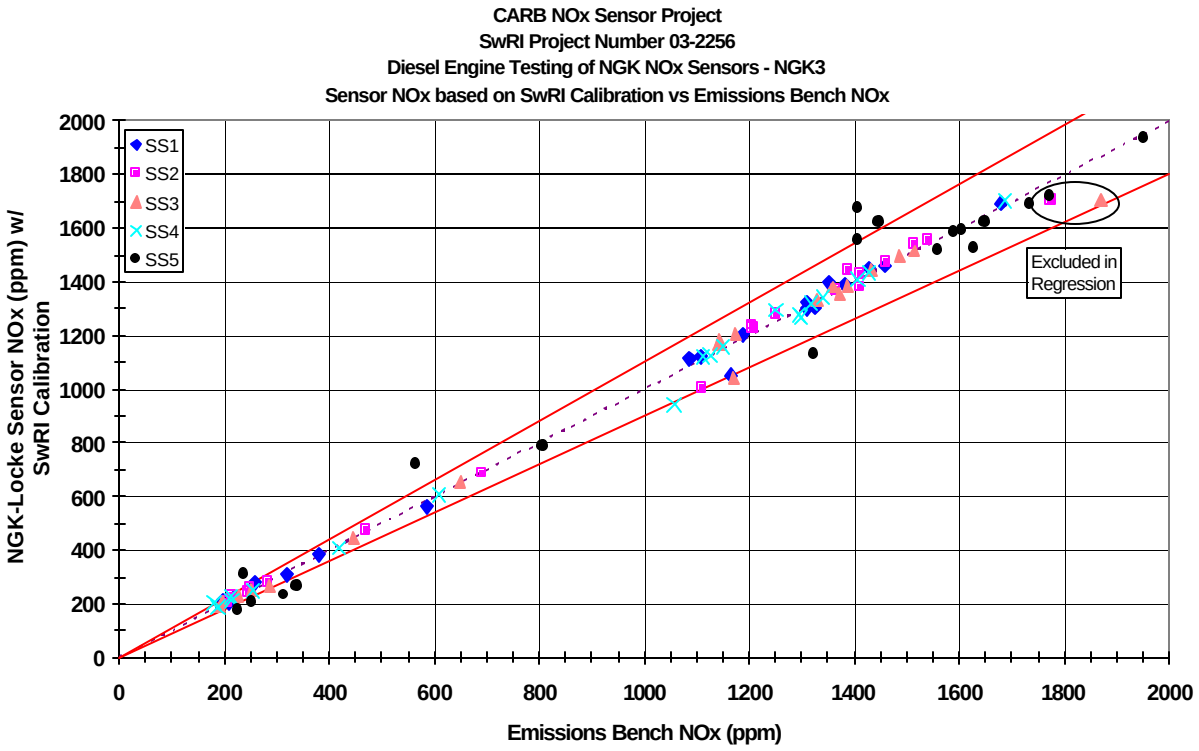

Figure 3-12. Sensor NGK3 NO_x Value as Function of Measured NO_x Emissions

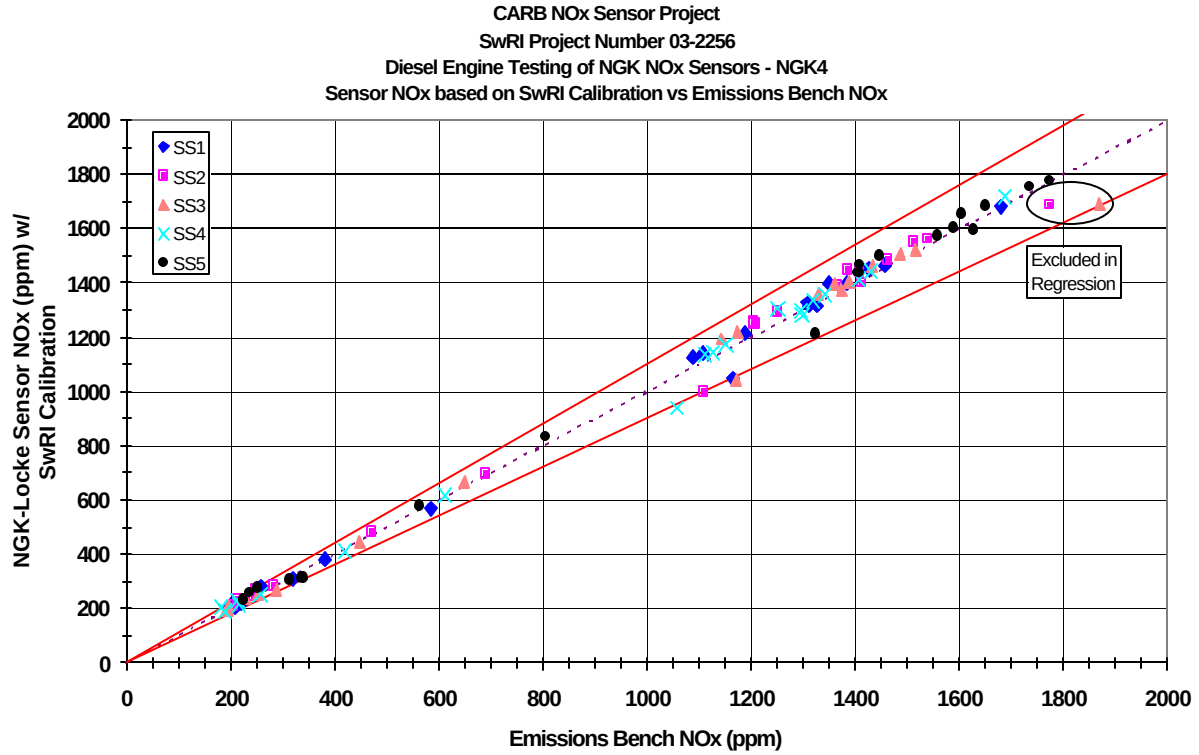

Figure 3-13. Sensor NGK4 NO_x Value as Function of Measured NO_x Emissions

A more realistic test, however, is to use the SS1 calibrations for all of the data and observe how the data falls in or out of the error envelope. In a real world application of the sensors, the end user would have only the initial calibration to compare against in subsequent calibration checks. Figures 3-14, 3-15, 3-16, and 3-17 represent sensors NGK1, NGK2, NGK3, and NGK4, respectively. Each figure shows sensor NO_x values for steady-state tests 2 through 5 for a given sensor. The NO_x values for all steady-state tests were based upon the SS1 calibrations for the respective sensor. Figure 3-14 shows that all of the NGK1 sensor data except the idle speed 100 percent load data points fall within the error envelope. Hence, the SS1 calibration was applicable for all data throughout this program. The NGK2 data in Figure 3-15 exhibited a trend similar to the NGK1 data except for a few points from the SS5 test near 250 ppm. Figure 3-16 shows the scatter in the NGK3 data from the SS5 test discussed. All other steady-state test data, however, fall within the error envelope except for the usual high CO idle speed 100 percent load condition. The NGK4, shown in Figure 3-17, is similar to the NGK1 data and indicates that the SS1 calibration could have been used for all data throughout this project.

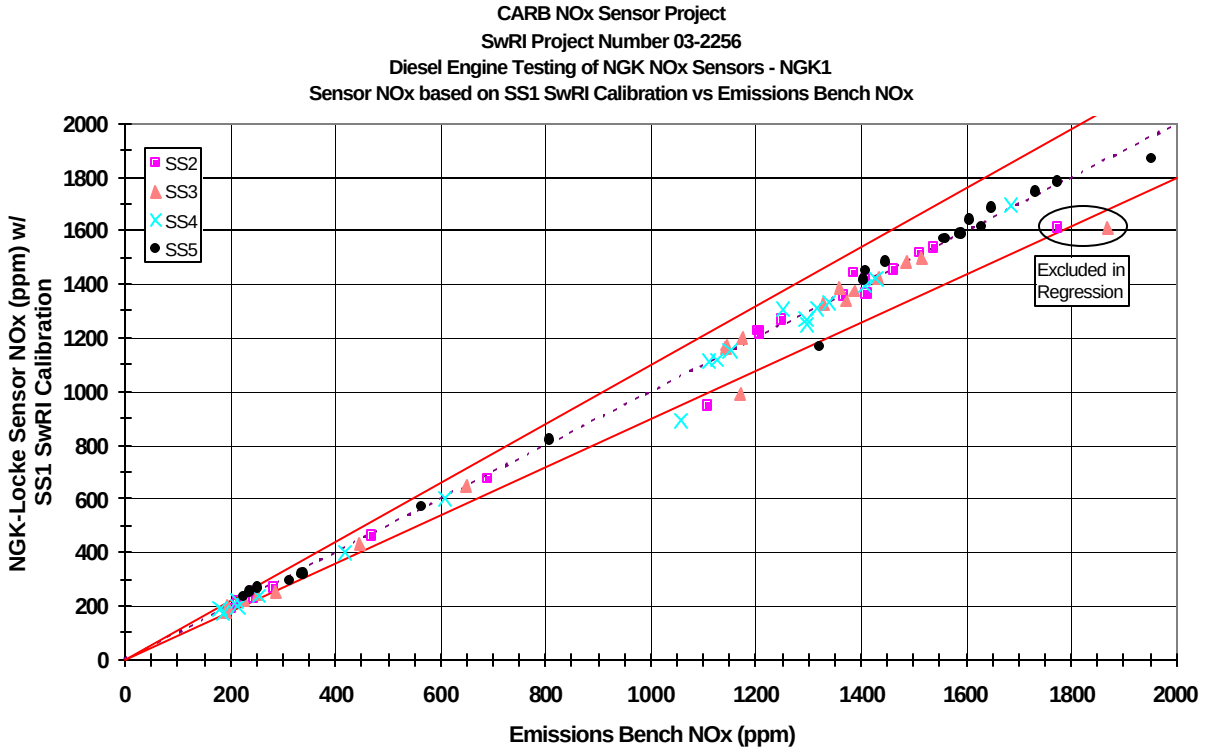

Figure 3-14. Sensor NGK1 NO_x Value Based on SS1 Calibration as a Function of Measured NO_x Emissions

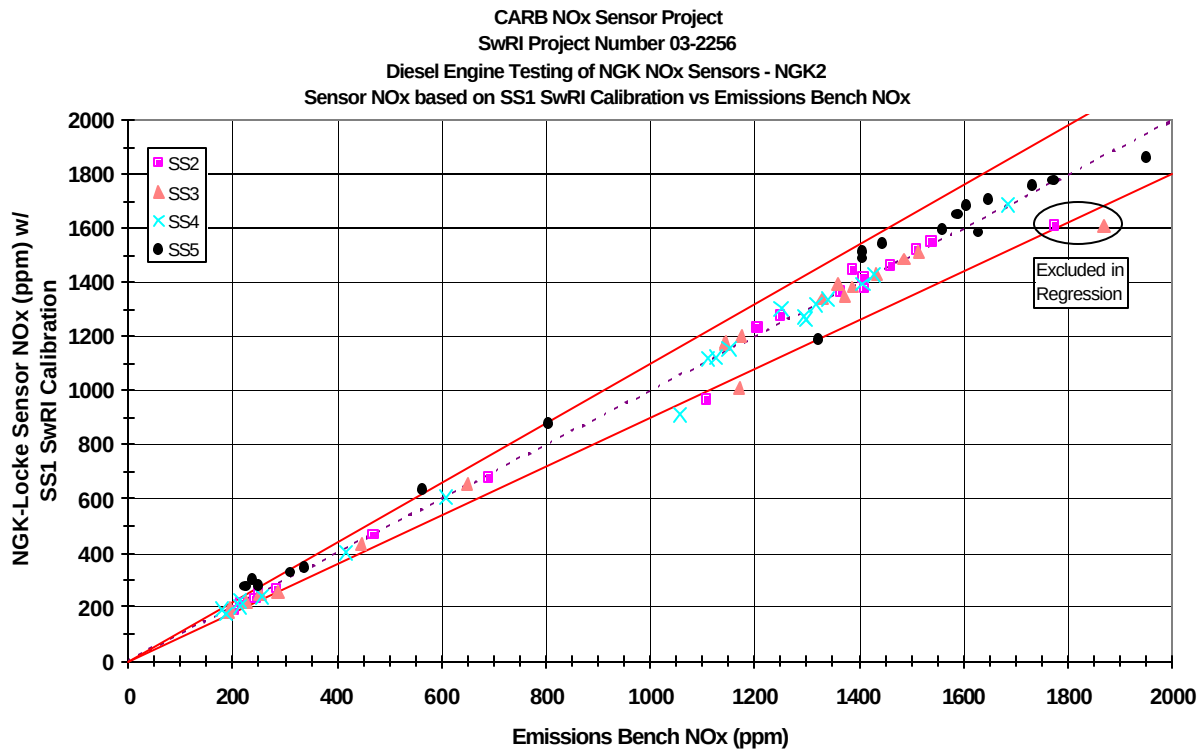

Figure 3-15. Sensor NGK2 NO_x Value Based on SS1 Calibration as a Function of Measured NO_x Emissions

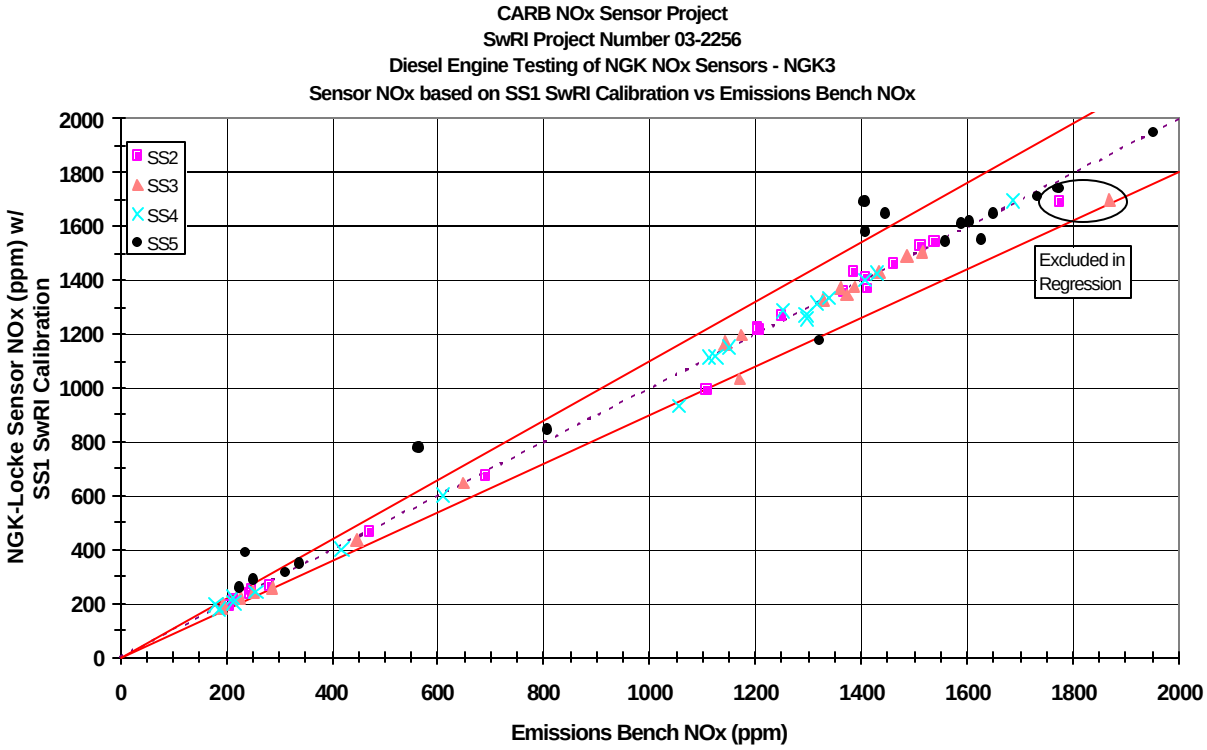

Figure 3-16. Sensor NGK3 NO_x Value Based on SS1 Calibration as a Function of Measured NO_x Emissions

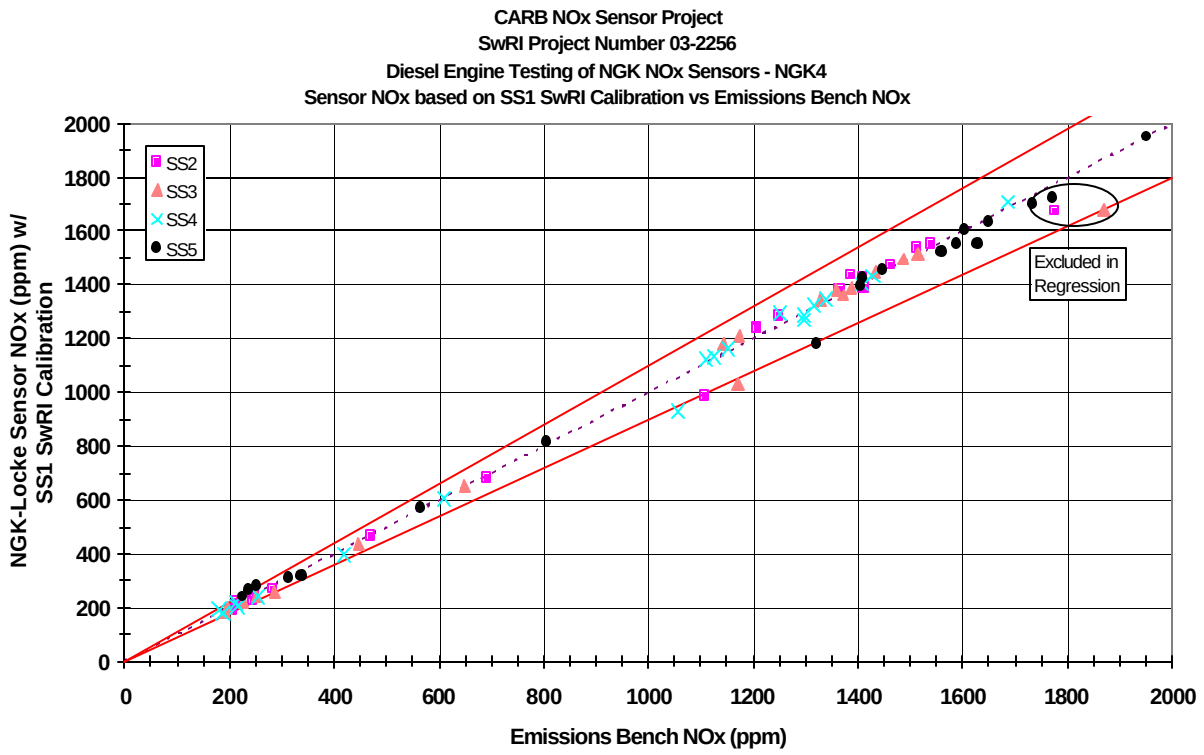

Figure 3-17. Sensor NGK4 NO_x Value Based on SS1 Calibration as a Function of Measured NO_x Emissions

3.3.2 19-Point Steady-State Test Results for NO_x Component of the NGK Insulators, Ltd. Sensors Using Factory Calibrations

The NO_x values for all sensors in a given steady-state test using the NGK supplied calibrations are shown in Figures 3-18, 3-19, 3-20, 3-21, and 3-22. All four sensors are shown in each figure with each figure representing a steady-state test. The calibrations supplied by NGK were based on a model gas apparatus and not an engine. The NGK factory supplied calibration slopes and offsets are shown in Table 3-8. The plots in the figures show that some of the NGK1 and NGK2 data fall above the error envelope's upper threshold. However, most of the data fall within the error envelope. This trend is repeated from steady-state test to stead-state test except for the SS5 data (Figure 3-22). The SS5 data shows considerable error above 1400 ppm. In addition, the scatter between sensors at the same emissions bench NO_x is noticeably larger. Hence, the NGK supplied calibrations based on the model gas apparatus would not have been adequate to represent the data for all portions of this project.

Table 3-8. NGK Insulators, Ltd. Factory Supplied Calibrations

Sensor Number	Sensor Serial Number	Controller Serial Number	Slope (volts/ppm NO_x)	Offset (volts)	Offset (ppm NO_x)
1	9E10B-1038	9EC5-017	0.002200	0.3600	163.6
2	9E10B-1044	9EC5-018	0.002203	0.3720	168.9
3	9F14A-1018	9EC5-166	0.002172	0.3520	162.1
4	9F14A-1022	9EC5-118	0.002190	0.3520	160.7

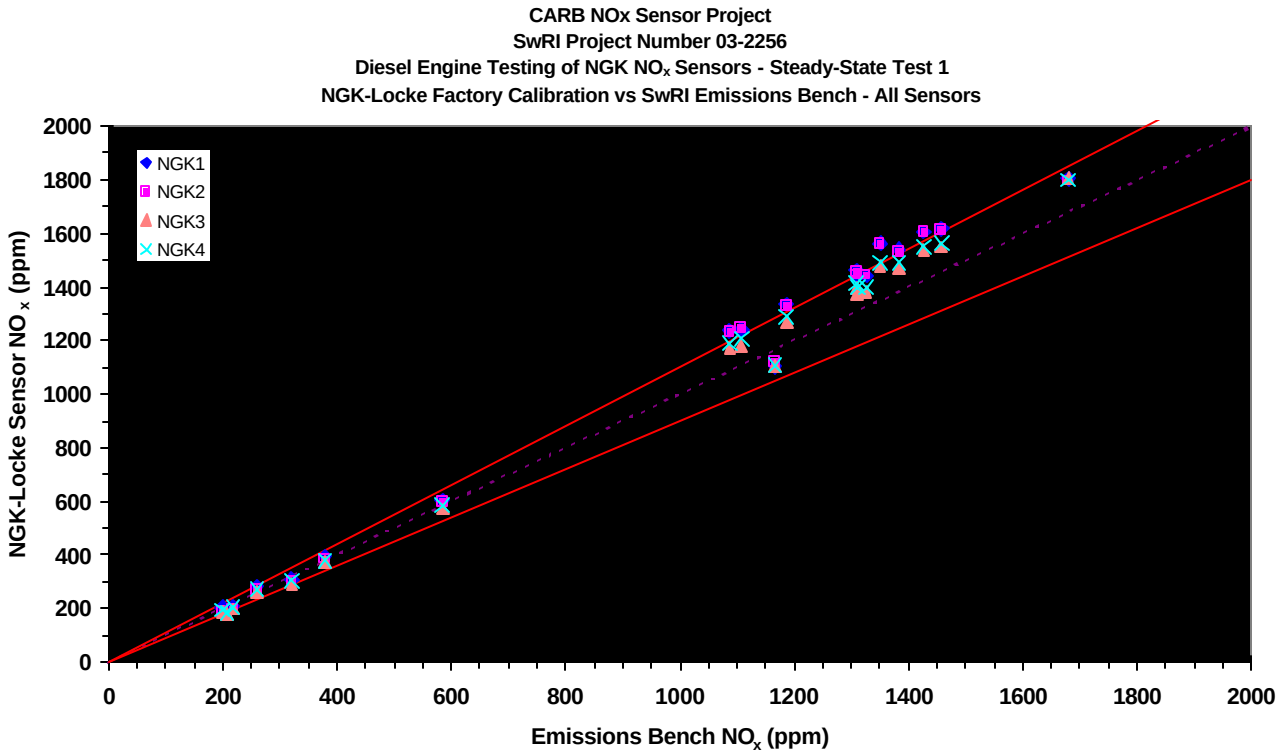

Figure 3-18. All NGK Insulators, Ltd. Sensor's NO_x SS1 Values Based on NGK Insulators, Ltd. Supplied Calibrations as a Function of Measured NO_x Emissions

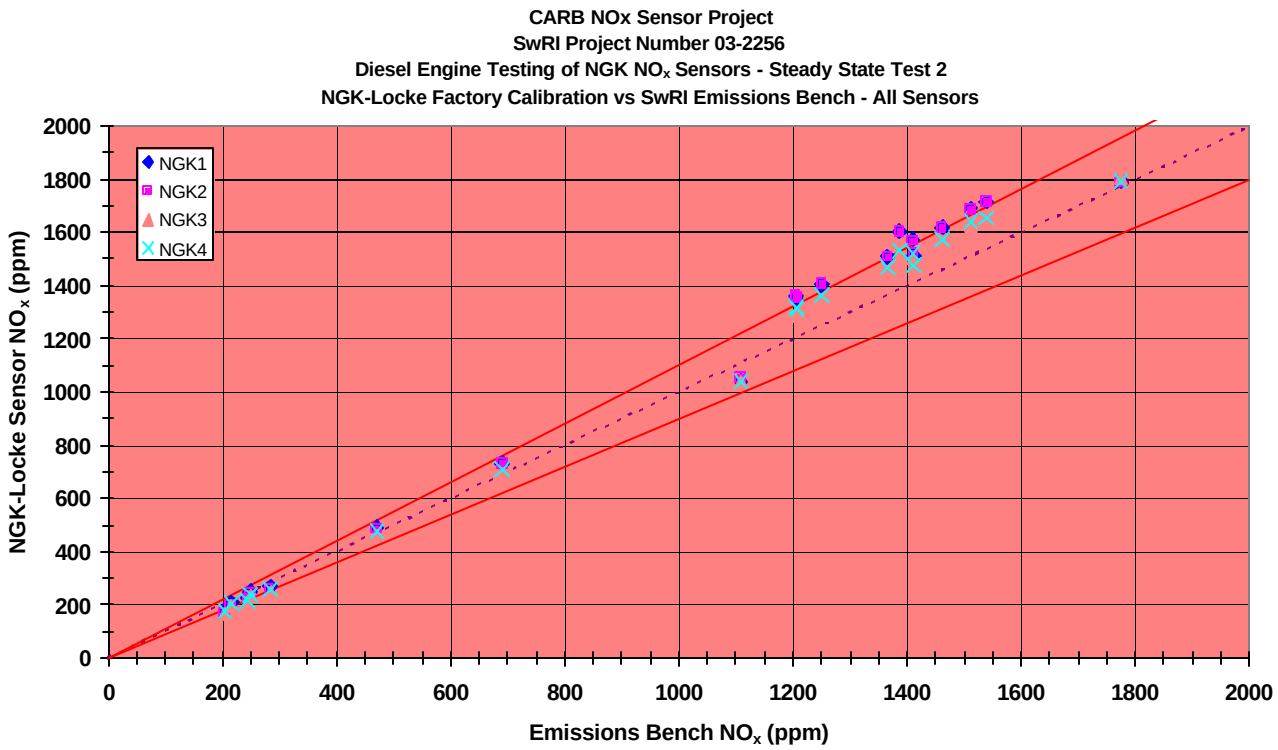

Figure 3-19. All NGK Insulators, Ltd. Sensor's NO_x SS2 Values Based on NGK Insulators, Ltd. Supplied Calibrations as a Function of Measured NO_x Emissions

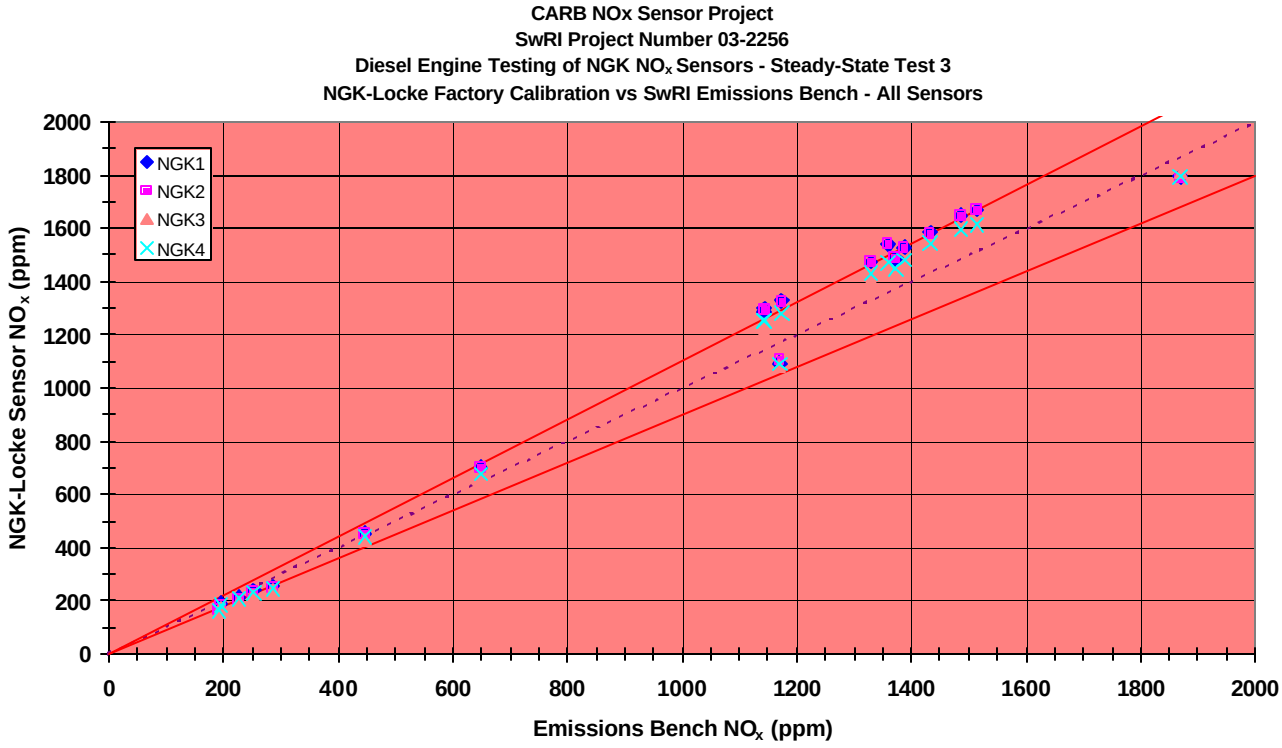

Figure 3-20. All NGK Insulators, Ltd. Sensor's NO_x SS3 Values Based on NGK Insulators, Ltd. Supplied Calibrations as a Function of Measured NO_x Emissions

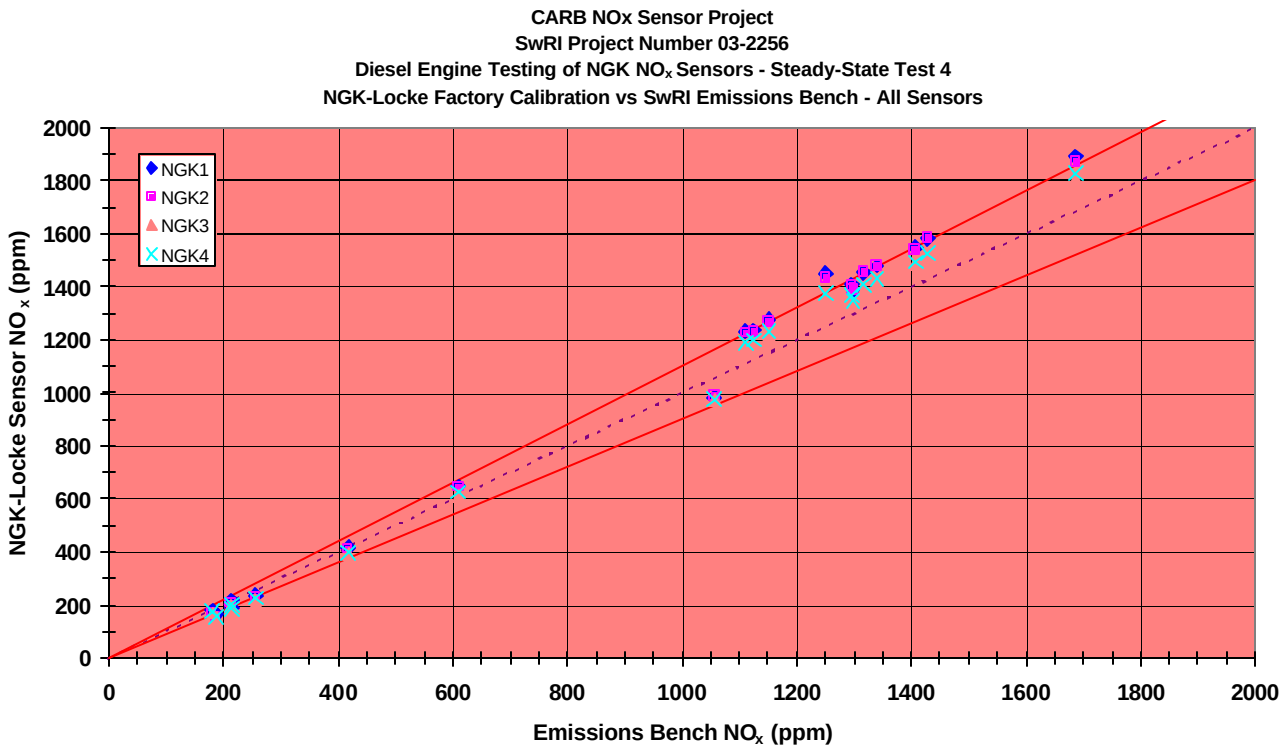

Figure 3-21. All NGK Insulators, Ltd. Sensor's NO_x SS4 Values Based on NGK Insulators, Ltd. Supplied Calibrations as a Function of Measured NO_x Emissions

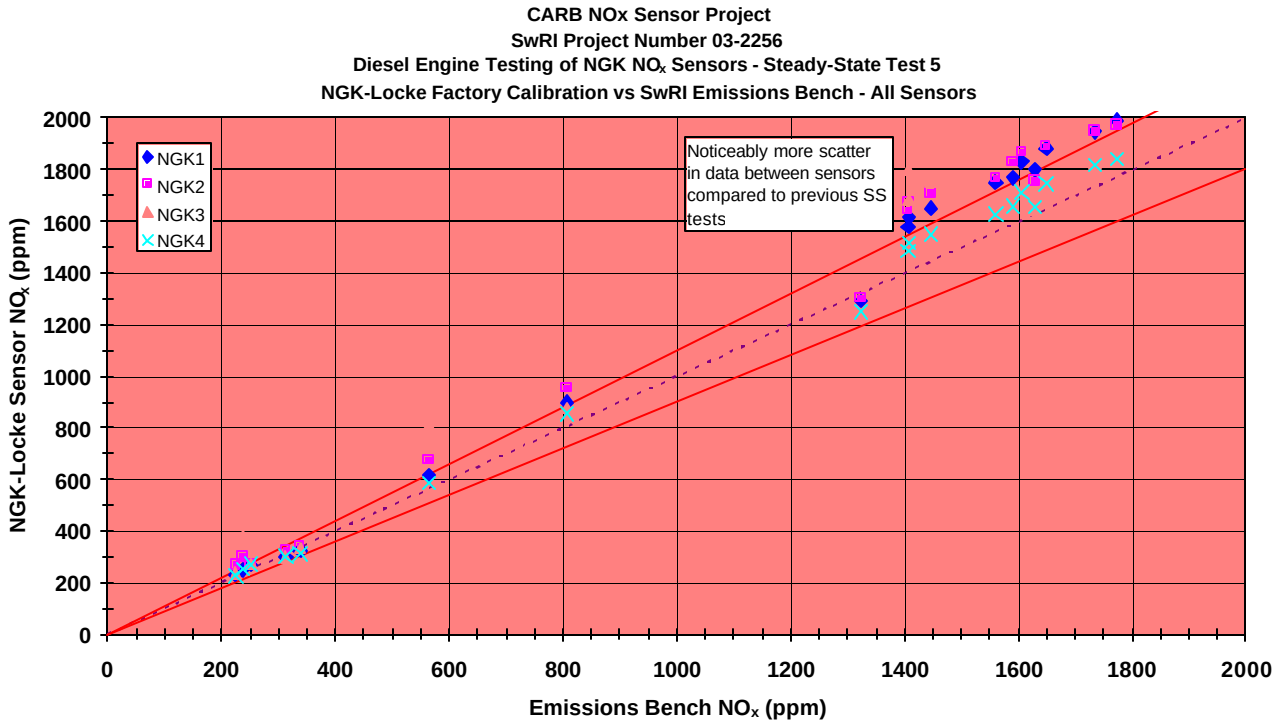

Figure 3-22. All NGK Insulators, Ltd. Sensor's NO_x SS5 Values Based on NGK Insulators, Ltd. Supplied Calibrations as a Function of Measured NO_x Emissions

3.3.3 19-Point Steady-State Test Results for O_2 Component of the NGK Insulators, Ltd. Sensors

As an added benefit to NO_x output, each sensor provides an output proportional to the O_2 concentration in the exhaust gas. Although not the focus of this project, the O_2 output voltage was analyzed since the exhaust gas must pass through the first measuring cavity where the O_2 concentration is detected. The exhaust gas then enters the second measuring cavity where NO_x is inferred.

The output from the O_2 component of each NO_x sensor is shown graphically in Figures 3-23, 3-24, 3-25, and 3-26. Each plot shows data from all five steady-state tests for a single sensor. The linear voltage to O_2 concentration function is shown for all five steady-state tests along with the linear correlation coefficient. The correlation coefficient was greater than 99 percent for each sensor across all tests, indicating a strong linear relationship between sensor output voltage and exhaust gas O_2 concentration. In each figure, the slope can be seen to be increasing from test to test while the offset decreased from test to test from the SS2 to the SS5 test. The output from NGK1 worked intermittently during the SS2 test. A temporary problem with the output electronics is suspected because the NO_x component of the sensor continued to function during the test. The output from all NO_x sensors appeared to saturate at 4.25 volts for all O_2 concentrations above 17 percent for the SS1, SS2, and SS3 tests. Data above 17 percent, were, therefore, not included in the regression analysis. An explanation is not presently available for the saturating behavior. The saturating behavior was not present during the SS4 and SS5 tests.

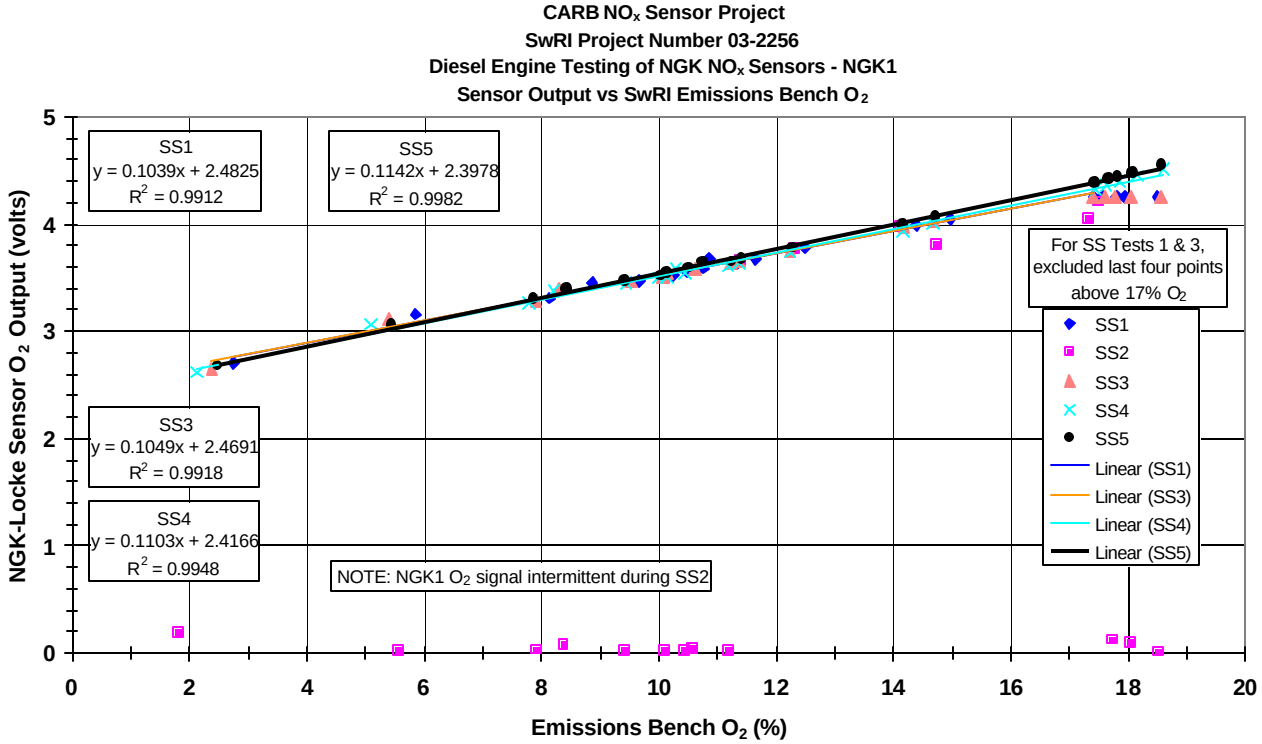

Figure 3-23. NGK1 O_2 Sensor Output Voltage as a Function of Measured O_2 Emissions

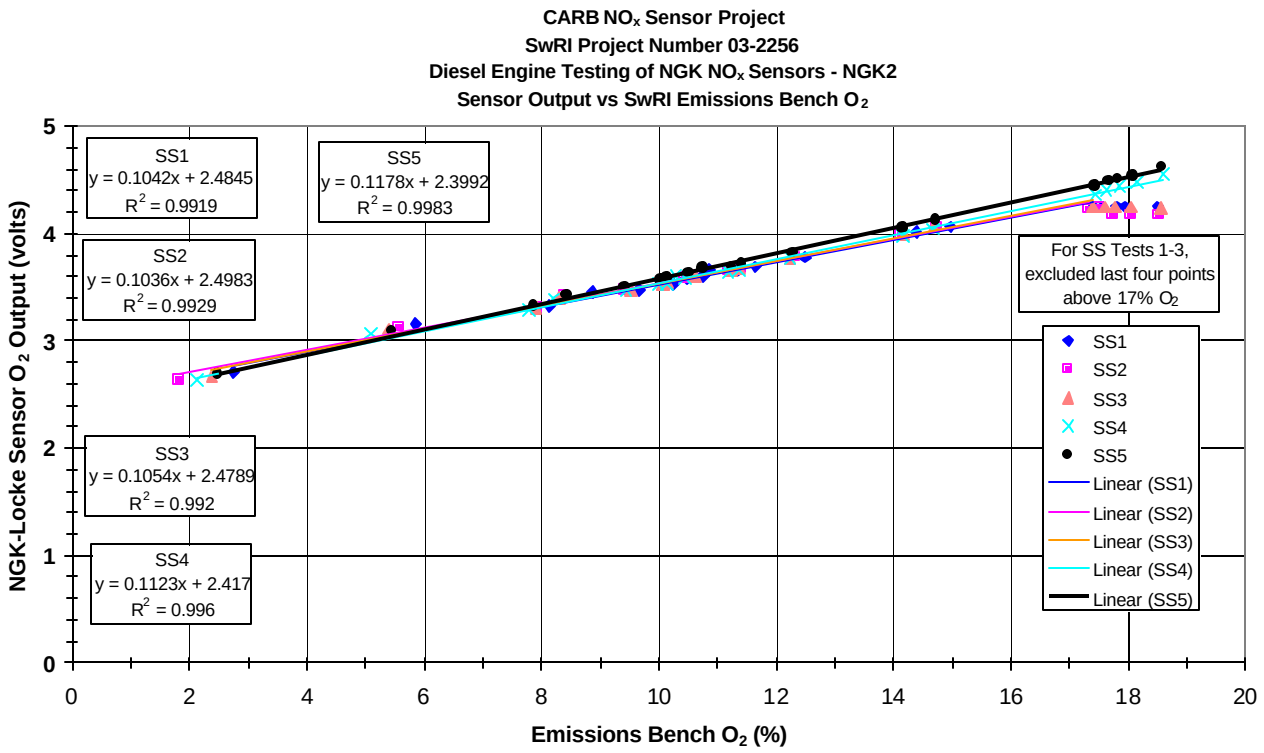

Figure 3-24. NGK2 O_2 Sensor Output Voltage as a Function of Measured O_2 Emissions

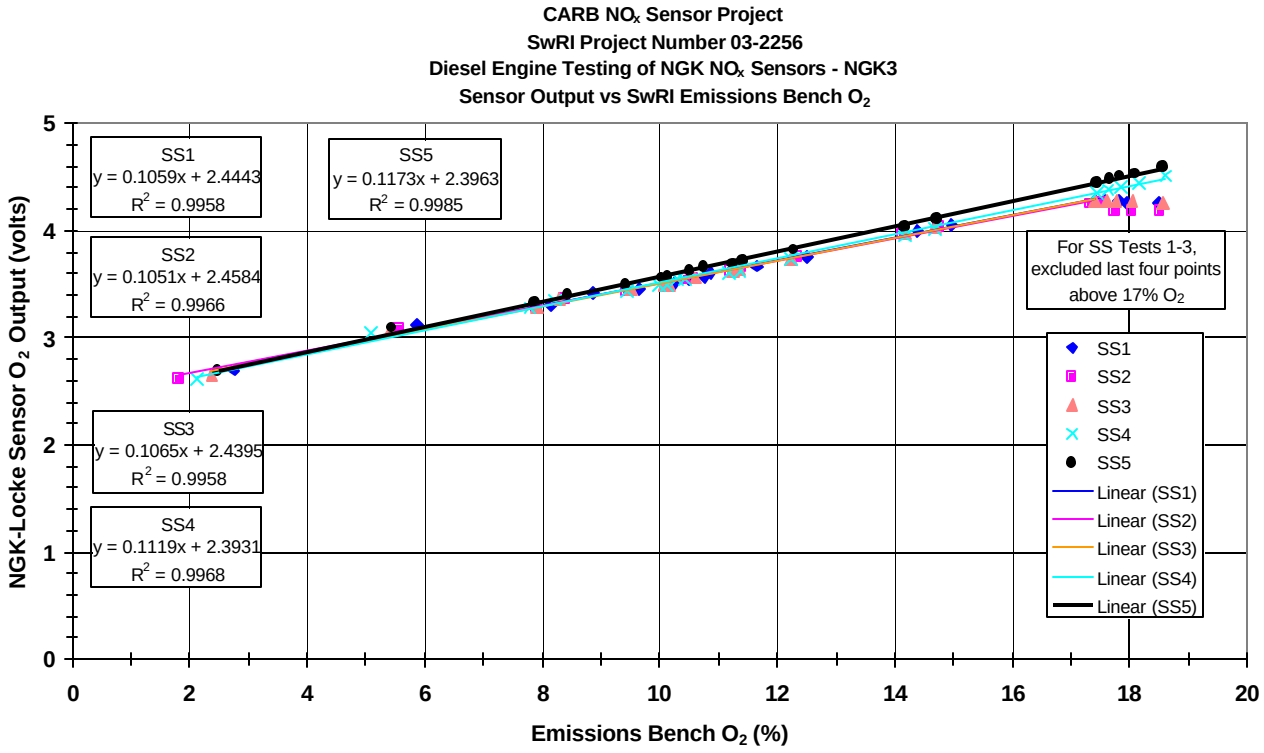

Figure 3-25. NGK3 O_2 Sensor Output Voltage as a Function of Measured O_2 Emissions

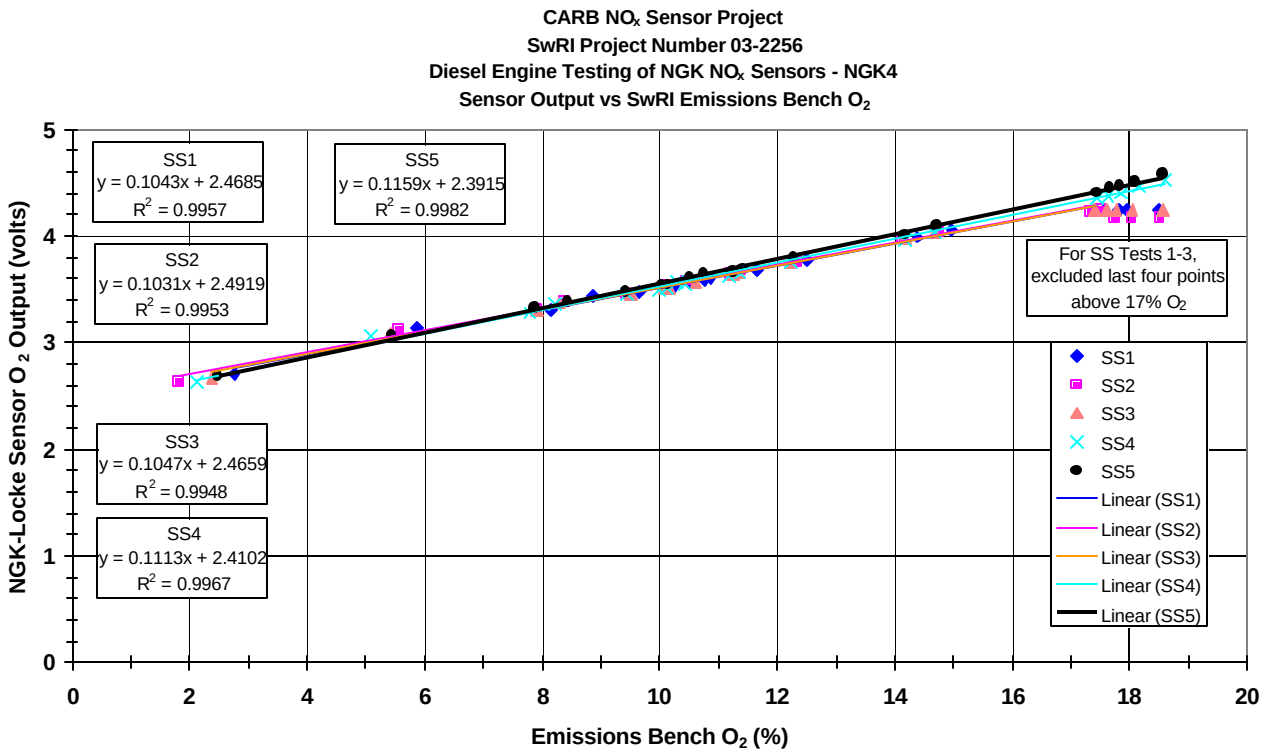

Figure 3-26. NGK4 O_2 Sensor Output Voltage as a Function of Measured O_2 Emissions

3.3.4 Interference Gas Test Results-Effect on NO_x Component Output

The effects of the interference gases on the NO_x component of the NGK combined NO_x/O_2 sensor will be discussed in individual subsections. Graphs of the data are plotted in bar chart format on a +/-10 percent scale to illustrate how the NO_x reported by the sensors falls within the +/-10 percent error envelope published by NGK; as used in the discussion of the steady-state test data above. Appropriate sensor calibrations developed from steady-state tests were used to compute sensor NO_x values. SS1 calibrations were used for interference gas test #1 (IGE1), SS4 calibrations for interference gas #2 (IGE2), and SS5 calibrations for interference gas test #3 (IGE3). SwRI Milton-Roy emissions bench measurements served as the basis for the relative comparisons. That is, the percent differences in the graphs below are relative to the NO_x measured by the emissions bench. Note that in all cases, as the interference gas mole fraction increased, the NO_x measured by the emissions bench decreased due to dilution by the interference gas. Negative relative percent differences indicate that the sensor NO_x was less than the emissions bench, and positive relative percent differences indicate that the sensor NO_x was greater than the emissions bench NO_x.

3.3.4.1 Effect of CO_2 Interference Gas

Figures 3-27, 3-28, and 3-29 show the effect of CO_2 interference gas on the NO_x component output of each sensor for each of three interference gas tests (refer to Table 2-5 for listing of the test sequence). The legend in each figure shows the interference gas mole fraction as measured by the SwRI Milton-Roy emissions bench. In Figure 3-27, it can be seen that, in

general, as the CO_2 interference gas mole fraction increased, the NO_x reported by each sensor (using the SS1 calibration for a given sensor) decreased to a maximum of -2.53 percent (NGK1) at 14.1 percent CO_2 relative to the NO_x reported by the emissions bench. All sensors exhibited a similar trend as the CO_2 mole fraction. That being that the relative percent difference between the sensor NO_x value and the emissions bench NO_x, value increased as the CO_2 interference gas mole fraction increased.

Figure 3-28 shows a trend similar to that shown in Figure 3-27. The NO_x reported by the sensors (using SS4 calibrations) increased from -0.41 percent at 10.0 percent CO_2, to –2.59 percent (NKG1) at 14.0 percent CO_2. NGK4 was least affected by increases in the interference gas.

Figure 3-29 shows the effect of CO_2 interference gas after the field demonstration was completed. NO_x sensor calibrations taken from the SS5 (post field demo) data were used to compute sensor NO_x for this test. NGK1, NGK2, and NGK4 reported NO_x values that were less than -2.0 percent variant relative to the emissions bench at the maximum CO_2 interference gas mole fraction tested of 13.8 percent. NGK2 was least affected by increases in interference gas with almost no change in NO_x relative to the emissions bench NO_x level. NGK3 exhibited differences in NO_x relative to the emissions bench from -2.0 percent to -4.0 percent.

All in all, the sensors exhibited only small changes in NO_x values relative to the NO_x values measured by the emissions bench. The change in sensor NO_x values were well within the +/-10 percent error envelope discussed during the 19 point, steady-state tests. Therefore, at constant engine out NO_x emissions, changes in the exhaust gas concentrations induced by dilution due to additional CO_2 gas have a negligible effect on sensor NO_x values.

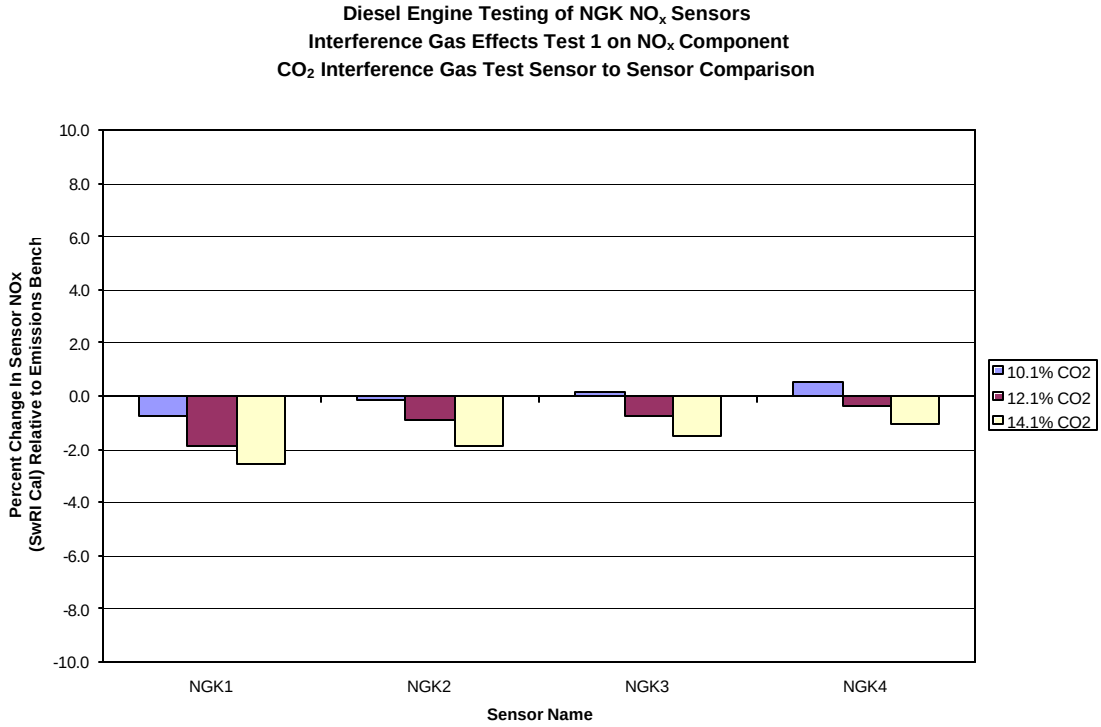

Figure 3-27. CO_2 Interference Effect on NO_x Component Interference Gas Test Number 1

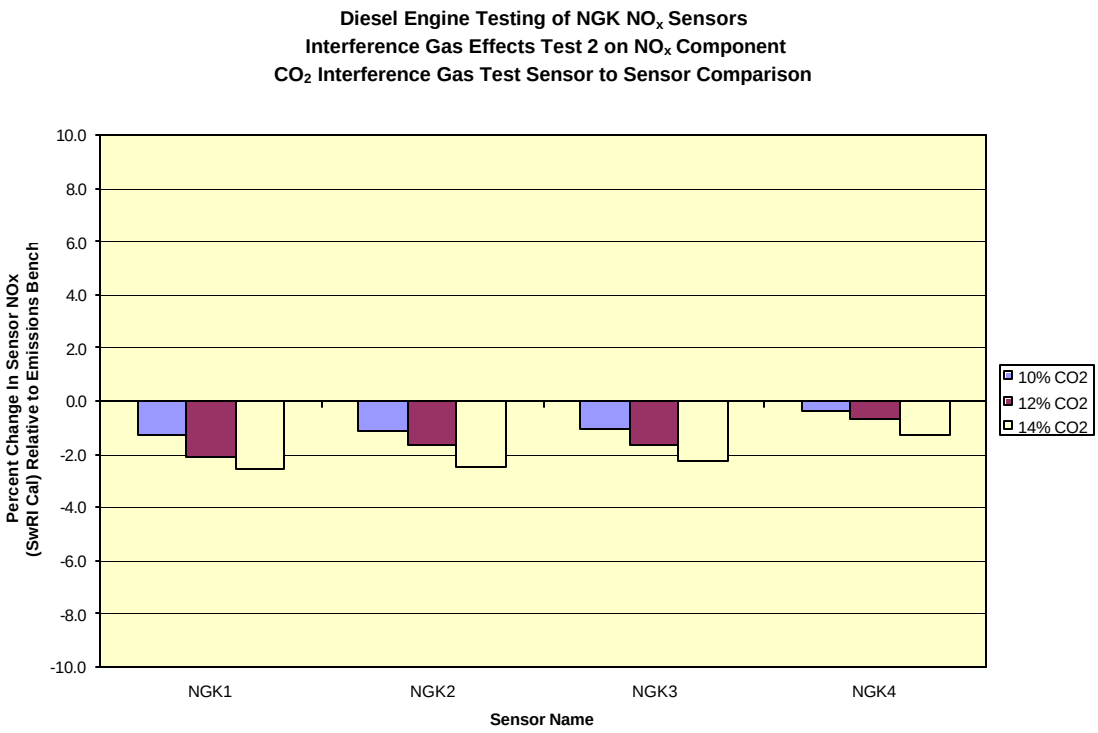

Figure 3-28. CO_2 Interference Effect on NO_x Component Interference Gas Test Number 2

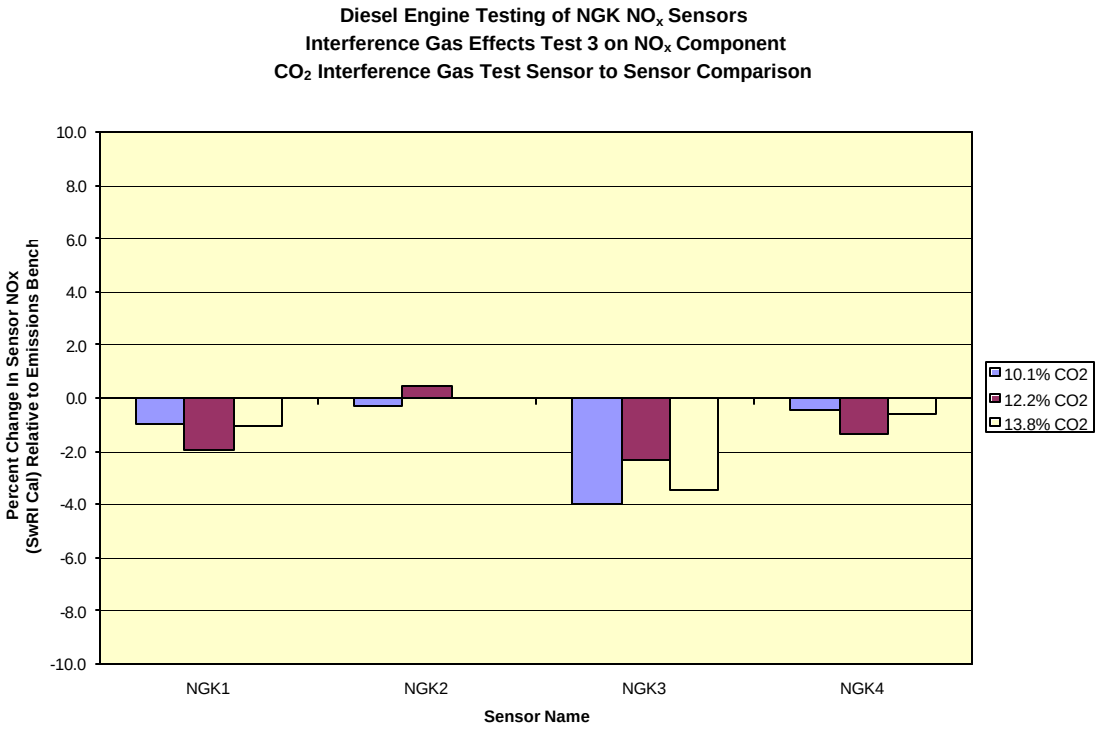

Figure 3-29. CO_2 Interference Effect on NO_x Component Interference Gas Test Number 3

3.3.4.2 Effect of O_2 Interference Gas

Figures 3-30, 3-31, and 3-32 show the effect of the O_2 interference gas on the output of the NO_x component of the NO_x sensors. The legend in each figure shows the O_2 interference gas mole fraction as measured by the SwRI Milton-Roy emissions bench. The effect of O_2 interference gas is similar to the effect of CO_2 interference gas effect, but opposite in sign. That is, the relative percent difference between the NO_x sensor value and the emissions increased in the positive direction as the O_2 interference gas increased. Figure 3-30 shows the results of the first O_2 interference gas test. All sensors exhibited nearly identical changes in sensor NO_x values (using SS1 calibrations) at a given O_2 interference gas mole fraction tested. The maximum effect occurred at 14.2 percent O_2 where the percent relative difference reached 4.89 percent for NGK2.

The second interference gas test with O_2 is shown in Figure 3-31. All four sensors exhibited nearly an identical trend and magnitude, as that shown in Figure 3-30. Using SS4 steady-state calibrations, the maximum change in sensor NO_x relative to the emissions bench was 4.54 percent and occurred in sensor NGK1.

The third interference gas test (IGE3, post field demo using SS5 calibrations) indicated significant deviations for sensors NGK2 and NGK3 relative to sensors NGK1 and NGK4, as well as from the IGE1 and IGE2 data sets for NGK2 and NGK3. Sensor NGK2 exhibited the largest percent difference relative to the emissions bench NO_x of 7.12 percent at the 12.0 percent O_2 level. Sensor NGK3 exhibited changes less than +/-2.0 percent in NO_x value relative to the emission bench across all O_2 mole fractions tested. Sensors NGK1 and NGK4 exhibited nearly identical responses to increase in O_2 interference gas. The maximum change in sensor NO_x values relative to the emissions bench NO_x was 3.81 percent and 3.60 percent respectively for NGK1 and NGK4 at an O_2 interference gas mole fraction of 12.0 percent. The decrease in the percent change in NO_x values, relative to the emissions bench NO_x between the 12.0 percent O_2 and the 13.9 percent O_2 interference gas levels, is likely the result of inadequate analyzer settling time prior to acquiring the emissions bench data, rather than a sensor anomaly or interference gas effect.

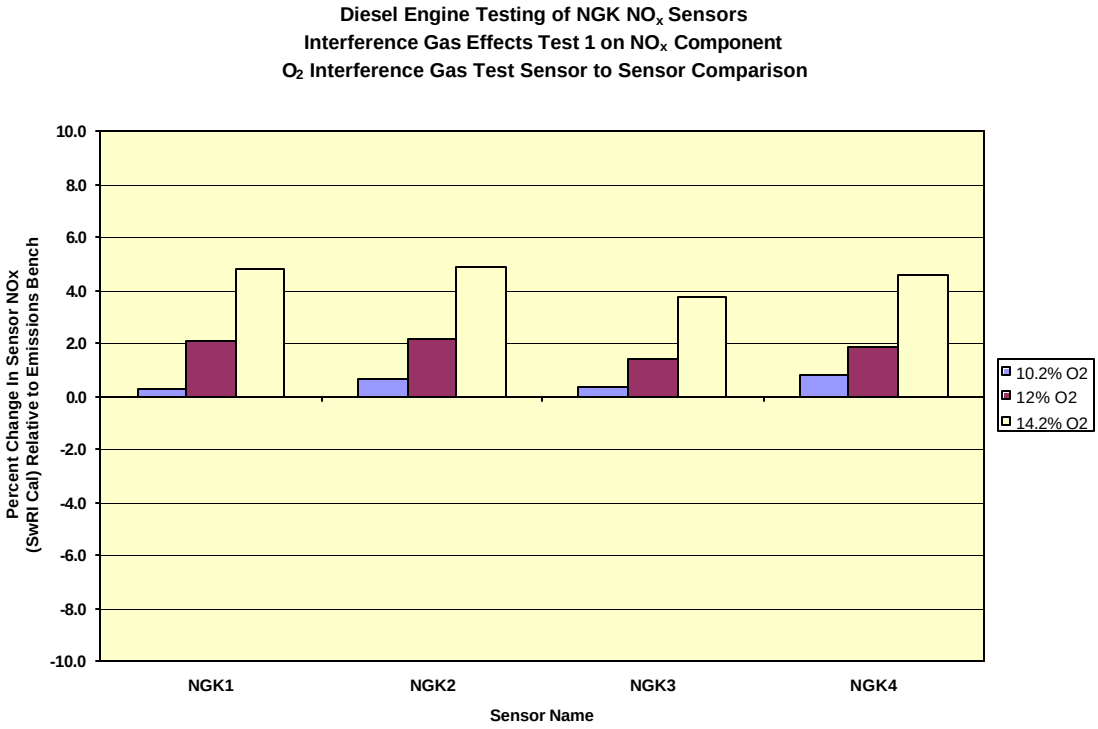

Figure 3-30. O_2 Interference Effect on NO_x Component Interference Gas Test Number

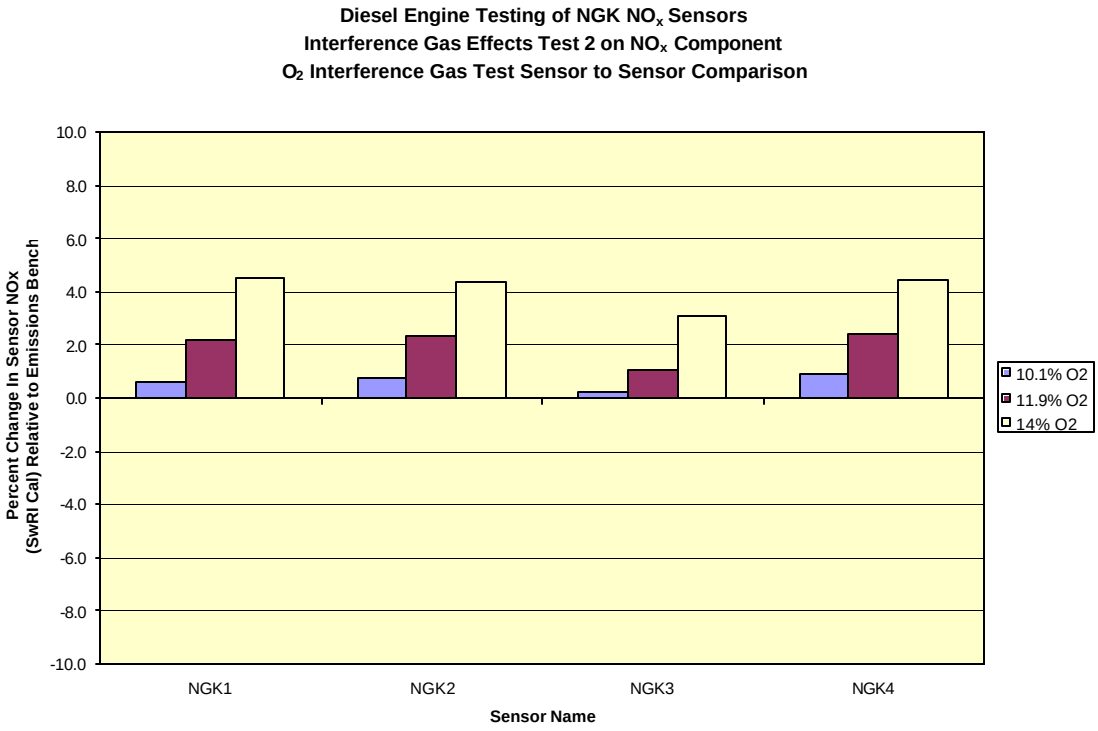

Figure 3-31. O_2 Interference Effect on NO_x Component Interference Gas Test Number 2

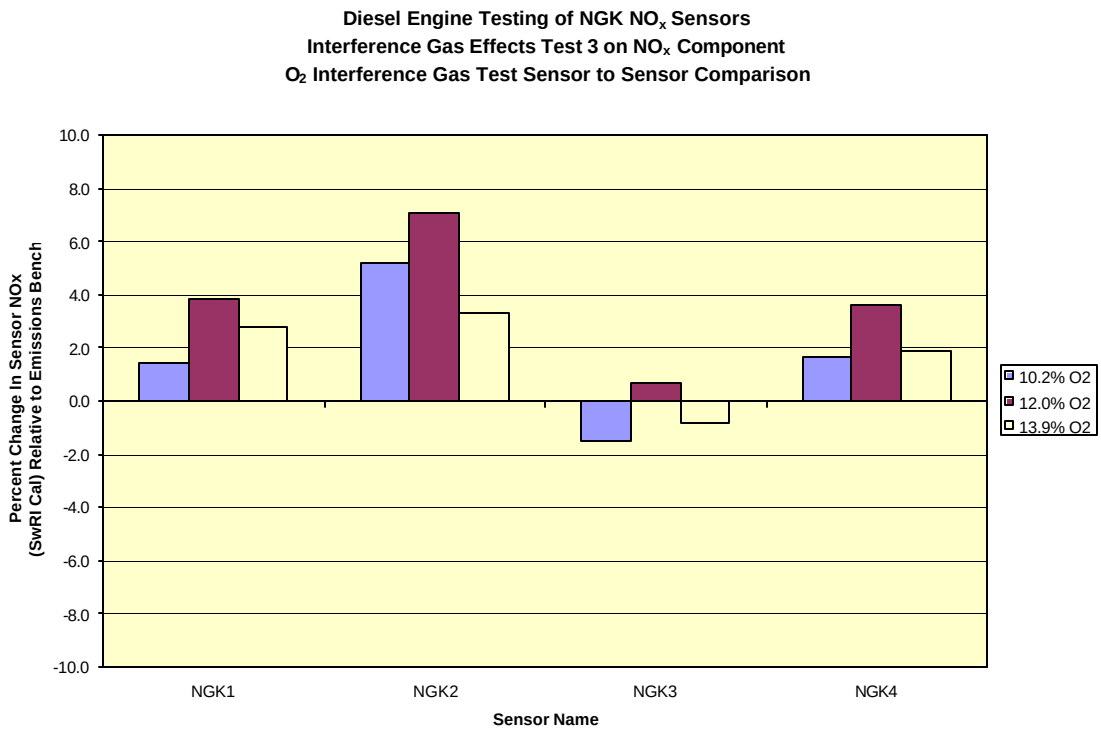

Figure 3-32. O_2 Interference Effect on NO_x Component Interference Gas Test Number 3

3.3.4.3 Effect of C_3H_6 Interference Gas

The effect of the C_3H_6 hydrocarbon interference gas is shown in Figures 3-33, 3-34, and 3-35. The effect was less than -2.34 percent for the first interference gas test and -3.26 percent for the second interference gas test, relative to NO_x concentration measured by the emissions bench. The effect of additional hydrocarbons was largest on sensor NGK3 during the third interference gas test (post field demo), reaching a maximum percent change in NO_x of –5.93 percent at 1508 ppm C_3H_6. The effect of C_3H_6 interference gas increases from nominal values of 500 ppm to 1500 ppm were small across the board, and can be consider negligible for the concentrations tested here.

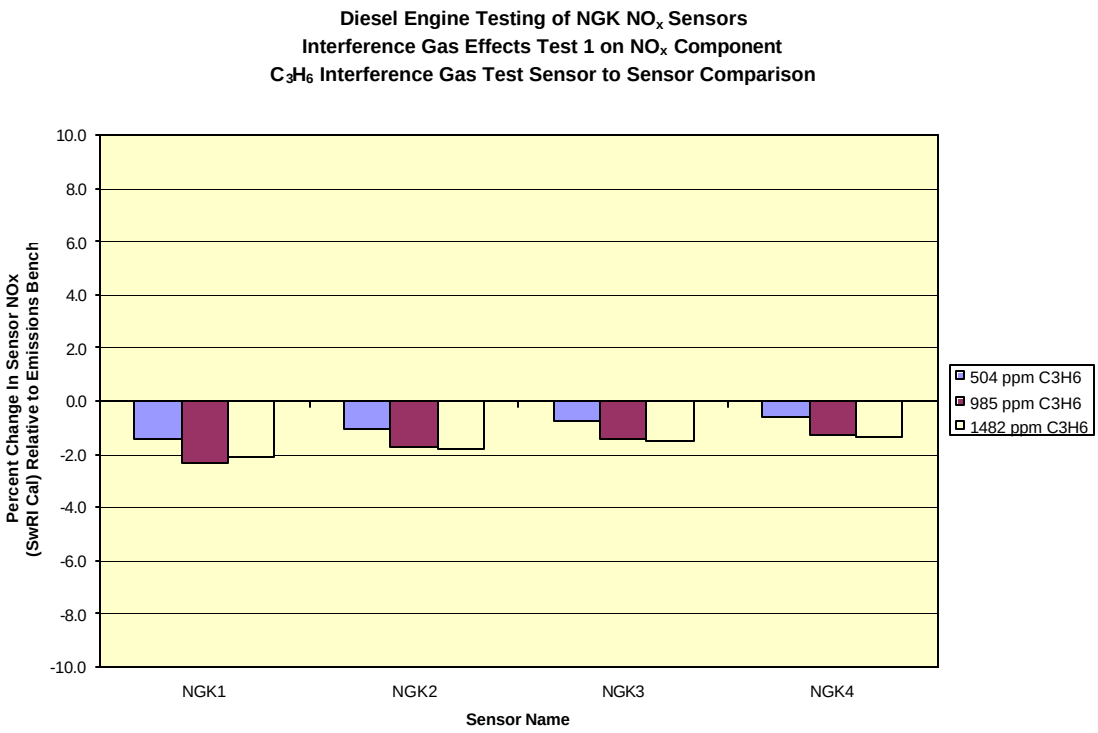

Figure 3-33. C_3H_6 Interference Effect on NO_x Component Interference Gas Test Number 1

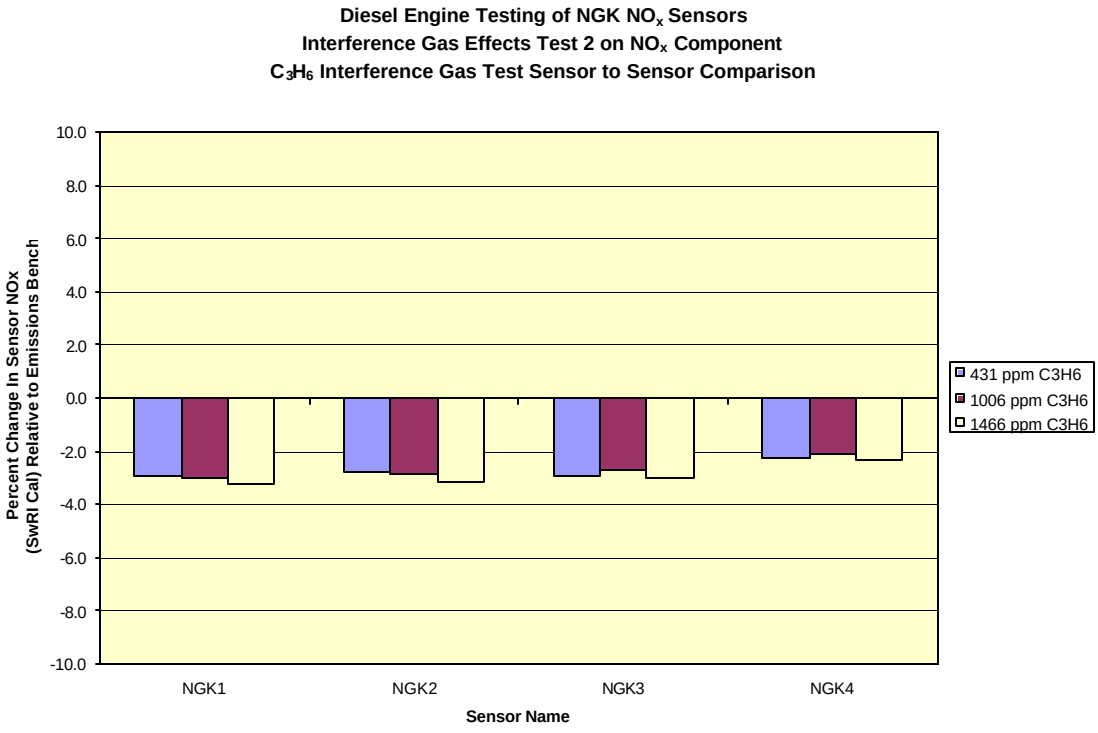

Figure 3-34 C_3H_6 Interference Effect on NO_x Component Interference Gas Test Number 2

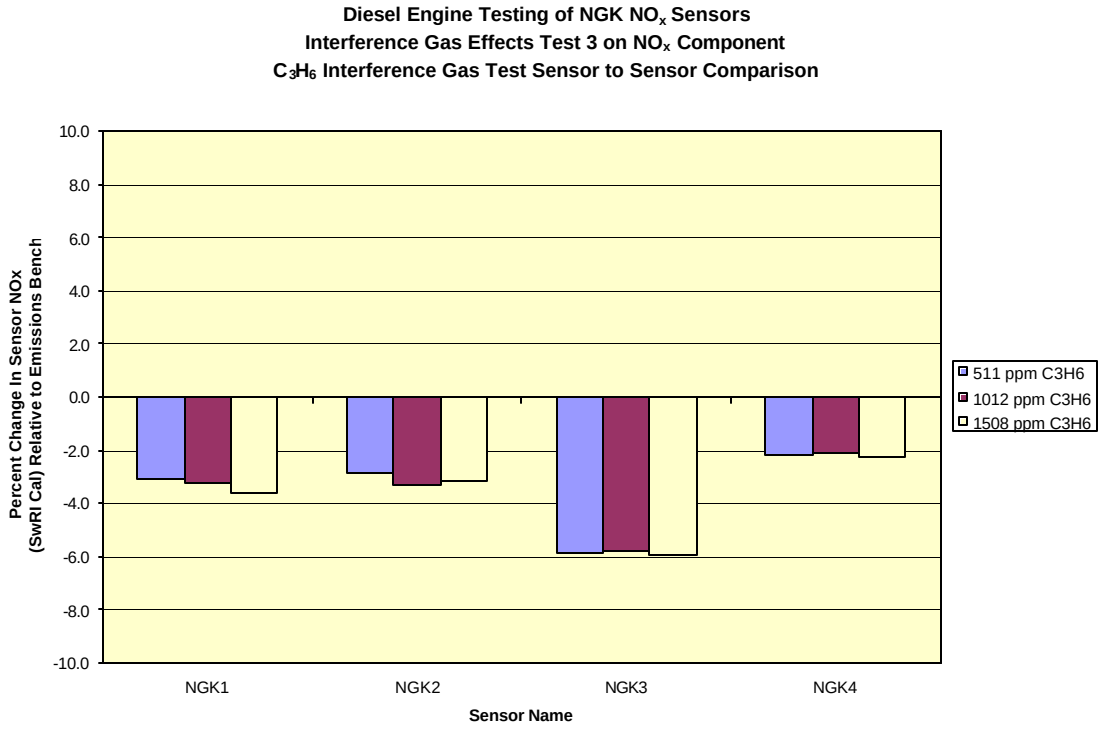

Figure 3-35. C_3H_6 Interference Effect on NO_x Component Interference Gas Test Number 3

3.3.5 Interference Gas Test Results-Effect on O_2 Component Output

The effects of the interference gases on the O_2 component of the NGK combined NO_x/O_2 sensor will be discussed in individual subsections. Graphs of the data are plotted in bar chart format on a +/-10 percent scale to illustrate how the O_x reported by the sensors falls within a +/-10 percent error envelope. Appropriate sensor calibrations developed from steady-state tests were used to compute sensor O_2 values. SS1 calibrations were used for interference gas test #1 (IGE2), SS4 calibrations for interference gas #2 (IGE2), and SS5 calibrations for interference gas test #3 (IGE3). SwRI Milton-Roy emissions bench measurements served as the basis for the relative comparisons. That is, the percent differences in the graphs below are relative to the O_2 measured by the emissions bench. Note, that in all cases, as the interference gas mole fraction increased, the O_2 measured by the emissions bench decreased due to dilution by the interference gas. Negative relative percent differences indicate that the sensor O_2 was less than the emissions bench, and positive relative percent differences indicate that the sensor NO_2 was greater than the emissions bench NO_2.

3.3.5.1 Effect of CO_2 Interference Gas

Figures 3-36, 3-37, and 3-38 show the effect of CO_2 interference gas on the O_2 component of the NGK NO_x sensor. The effect of CO_2 interference gas on the O_2 component is peculiar in that the smallest interference gas mole fraction tested resulted in the largest relative percent differences for all sensors. As the interference gas mole fraction was increased, the relative percent difference decreased slightly. This is exhibited in Figures 3-36 and 3-37. This is a real effect because the mole fraction of the CO_2 interference test gas was admitted into the

exhaust gas stream from highest to lowest concentration during first interference gas tests (IGE1), and from lowest to highest concentration during the second interference gas tests (IGE2). The maximum percent relative difference occurred in sensor NGK1 at 4.41 percent for the IGE1 tests, and again in sensor NGK1 at 6.45 percent for the IGE2 tests.

Figure 3-38 shows the results from the post-field demo tests (IGE3). Sensors NGK2, NGK3, and NGK4 exhibited increases in percent relative difference as the O_2 interference gas concentration was increased. There was almost no difference between sensor O_2 values and the emissions bench values for NGK1, NGK3, and NGK4. The large percent differences observed during the IGE1 and IGE2 test lead one to believe that a "burn-in" period may exist for the first few hours of sensor operation. The errors between the sensor O_2 values and the emissions bench values, observed during the IGE1 and IGE2 tests, are significant because the O_2 level plays a significant role in the amount of NO_x generated during the combustion event. In addition, standard O_2 or UEGO sensors implemented in natural gas and gasoline control systems typically operate with approximately 1.0 percent accuracy when relative to an emissions bench. Although these tests were conducted on diesel fuel, there is some concern that proper NO_x control via O_2 feedback could be jeopardized during the early stages of a sensor's service duty.

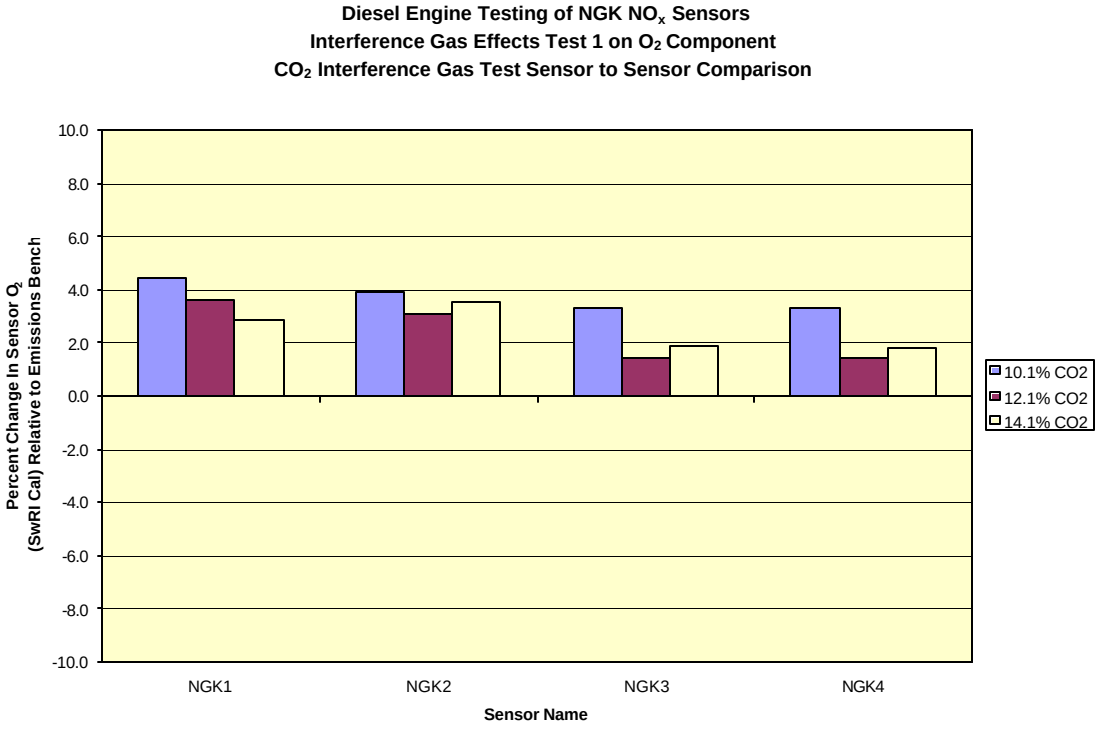

Figure 3-36. CO_2 Interference Effect on O_2 Component Interference Gas Test Number 1

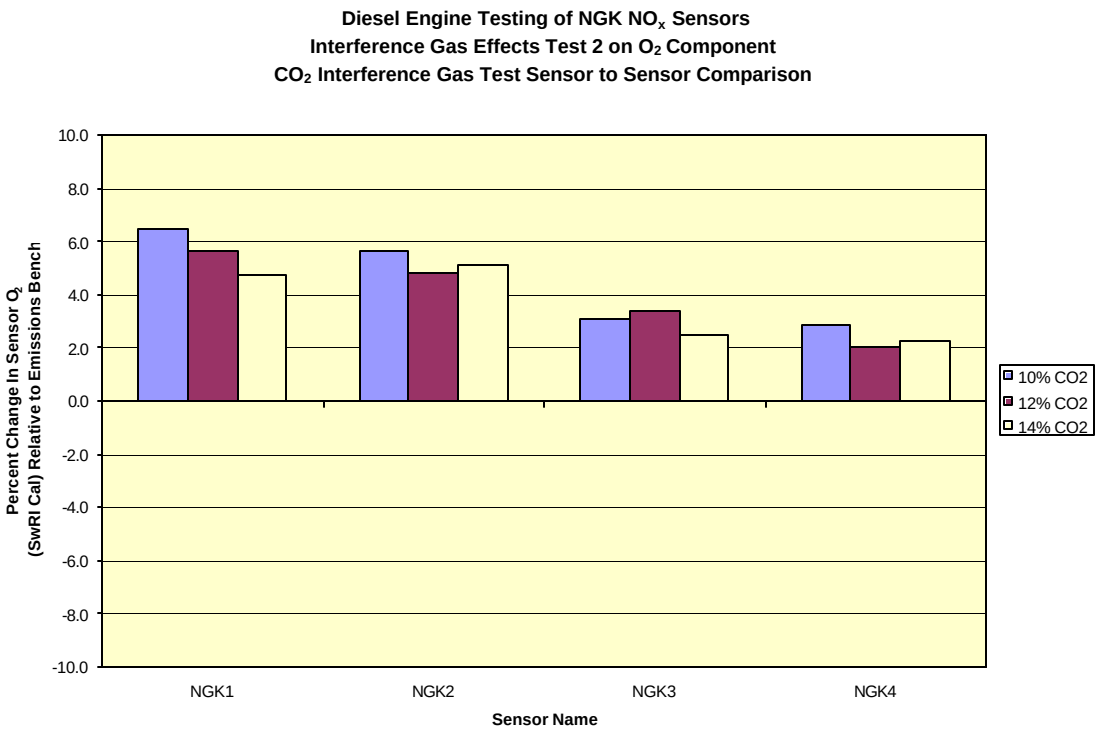

Figure 3-37. CO_2 Interference Effect on O_2 Component Interference Gas Test Number 2

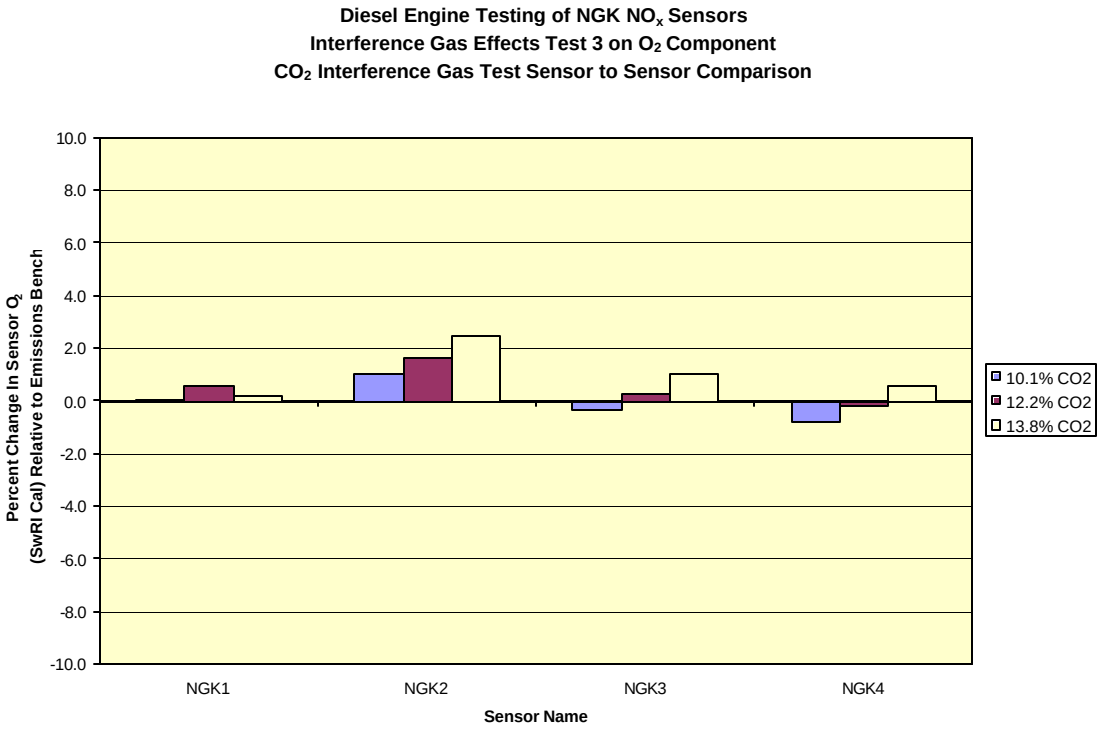

Figure 3-38. CO_2 Interference Effect on O_2 Component Output Interference Gas Test Number 3

3.3.5.2 Effect of C_3H_6 Interference Gas

Figures 3-39, 3-40, and 3-41 show how additional hydrocarbons in the exhaust gas affect the O_2 component of the sensor when compared to emissions bench measurements. A trend similar to the CO_2 interference gas tests described in §3.3.5.1 can be seen for the IGE1 and IGE2 tests. That is, larger differences between sensor values and the emissions bench exist at low interference gas concentrations, and decrease as the interference gas concentration is increased. Sensor NGK1 exhibited the largest difference relative the emissions bench values for all interference gas concentrations in the IGE1 and IGE2 tests (except NGK2 at 504 ppm C_3H_6 during IGE1).

Figure 3-41 shows that the data from the third interference gas test (IGE3) supports the "burn-in" theory presented in §3.3.5.1. The relative percent differences were smaller in magnitude, and negative, for the IGE3 tests for all sensors when compared to the same interference gas concentrations in IGE1 and IGE2. The only exception is for NGK4 wherein the magnitude in the percent relative difference was comparable, but opposite in sign. Another interesting fact is that the percent relative differences increased for NGK1 and NGK4 as the interference gas concentration increased. This is directly opposite of what was observed during the IGE1 and IGE2 tests.

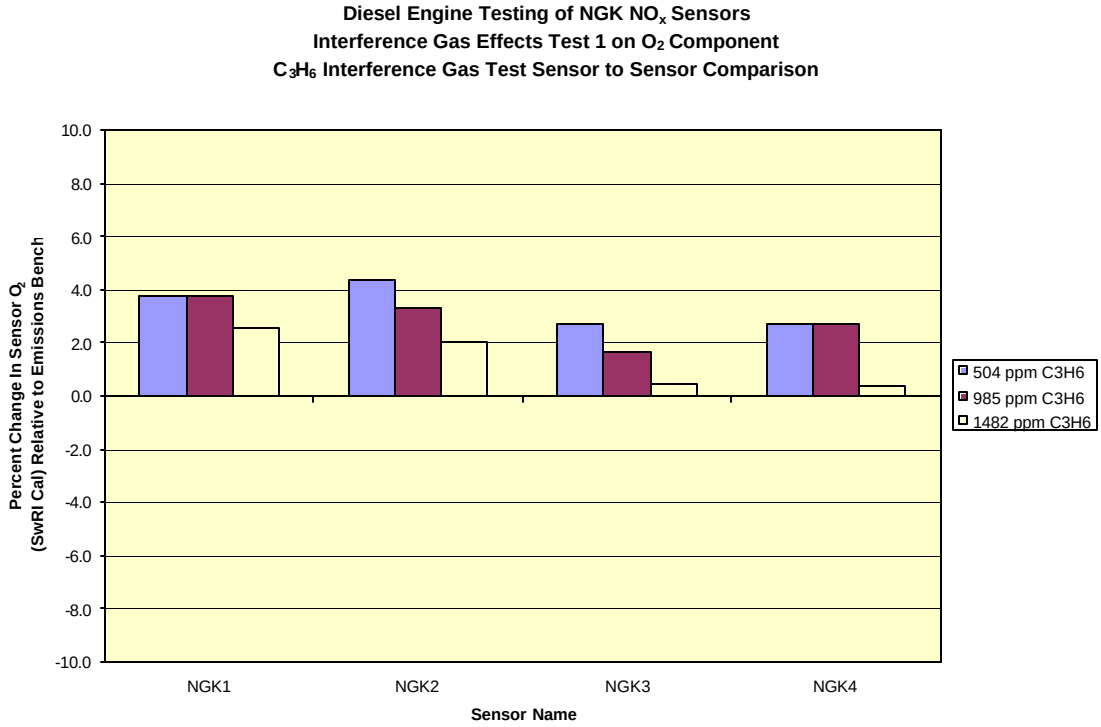

Figure 3-39. C_3H_6 Interference Effect on O_2 Component Interference Gas Test Number 1

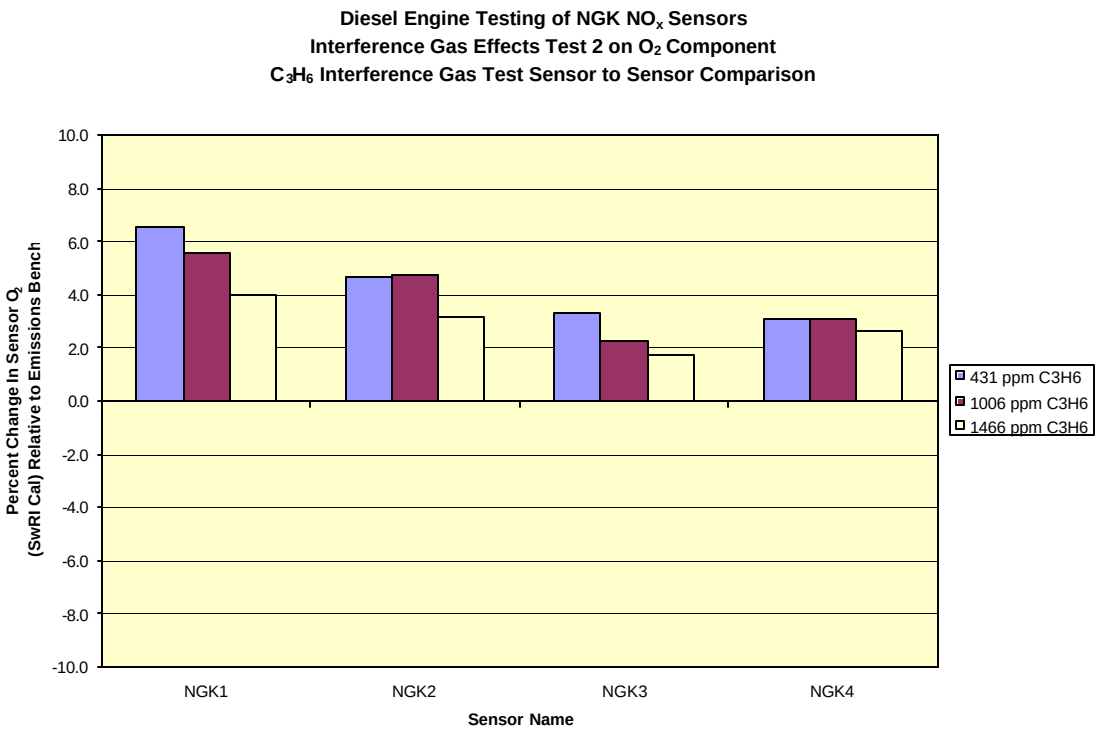

Figure 3-40. C_3H_6 Interference Effect on O_2 Component Interference Gas Test Number 2

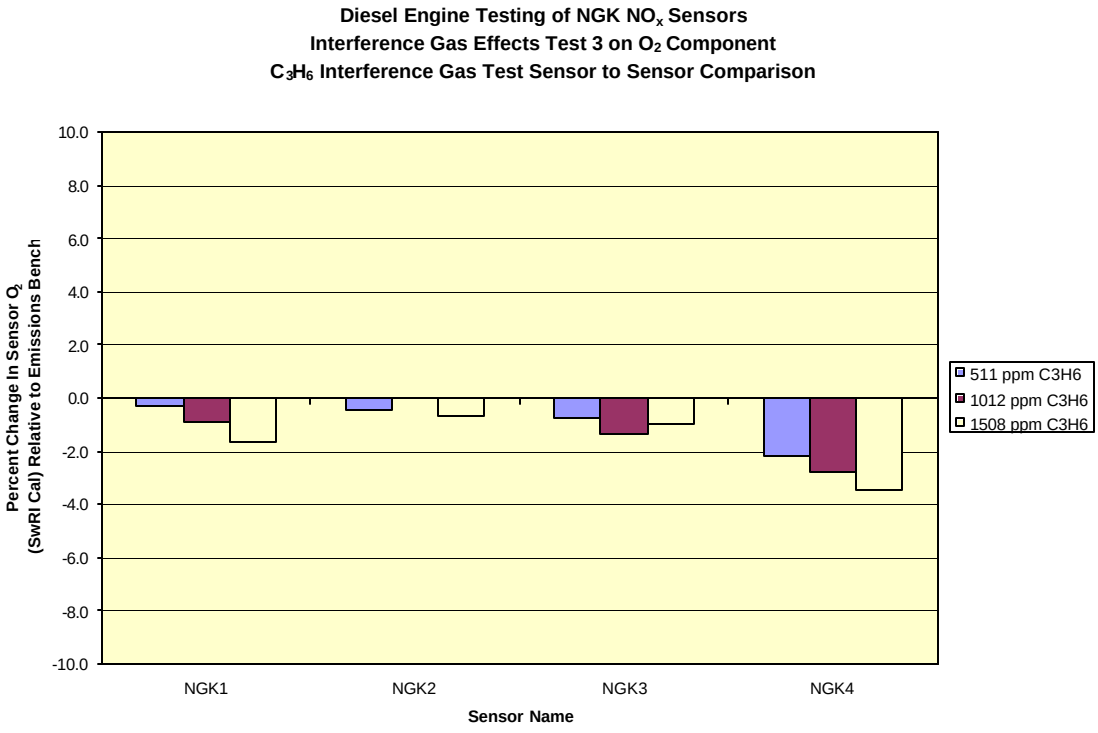

Figure 3-41. C_3H_6 Interference Effect on O_2 Component Interference Gas Test Number 3

3.3.6 Transient Test Results

Figure 3-42 shows a plot containing engine speed, torque, and pedal command for a transient test conducted at 1200 rpm. This plot is provided so the reader can gain a feel for the test technique and also to show how the engine and dynamometer responded during and after the 100 msec pedal "snap". The plot shows how engine speed and torque increase during a pedal "snap". The increase in engine speed and torque during the increase in pedal command (at approximately 32 seconds) is the result of the dynamometer controller characteristics. These tests were conducted with a wet gap eddy current dynamometer typically used for steady-state testing. However, the style and nature of these transient tests was such that it was deemed acceptable for the type of testing. All other transient tests were conducted in similar manner, but with varying starting and ending pedal command positions and engine speed (700, 1200, and 1800 rpm).

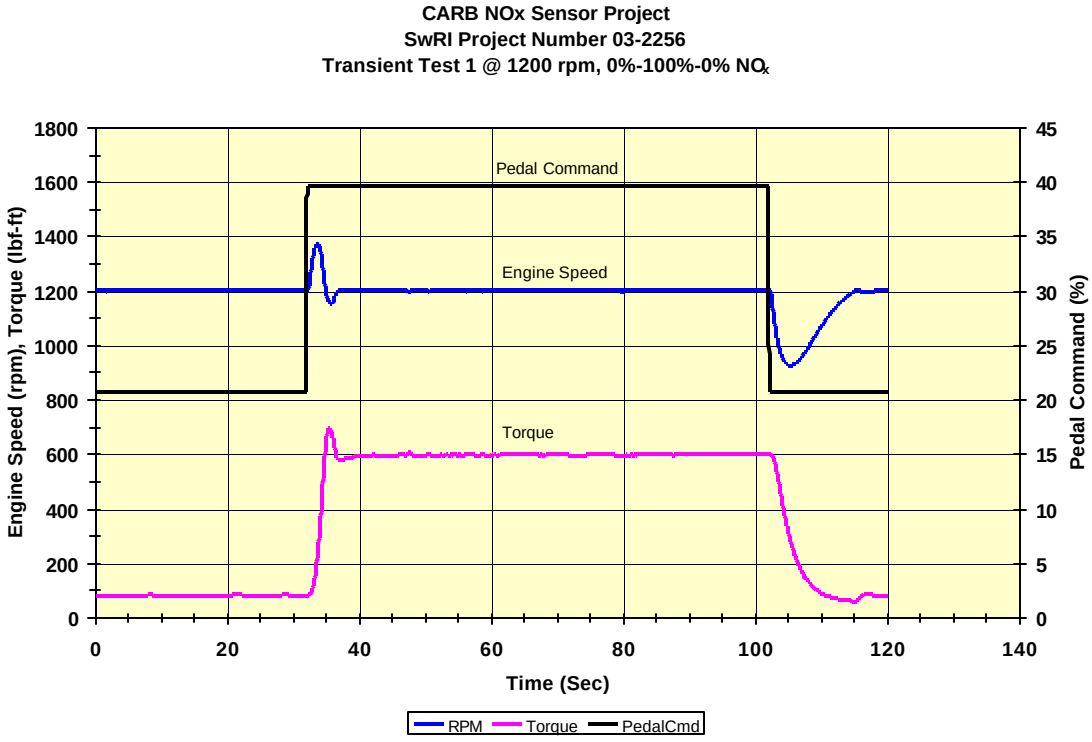

Figure 3-42. Transient Test at 1200 rpm

A total of three sets of transient tests were conducted at various points in this project. Two sets of tests were conducted before the field demonstration, and one set after the field demonstration. Data for the first two sets of transient tests were acquired at 20 Hz (50 msec) intervals. The data acquisition rate was increased to 200 Hz (5 msec) for the final tests to achieve improved accuracy and resolution of the transient response. It should be noted, that although the approach to evaluate the transient response characteristics of the sensor are adequate, the actual time constant of the sensor cannot be determined from the engine transient approach. Time constant determination requires testing the sensor in a controlled environment

where NO_x gas can be turned on and off nearly instantaneously. In addition, the Cummins CELECT production engine controller likely possesses maximum and minimum fueling ramp rates that limit fueling regardless of the magnitude of the pedal position derivative. This affects the rate at which NO_x is produced. Also, mass transport delay exists between the fuel injectors and the NGK NO_x sensors, which also affects the response characteristics when referenced to a particular time, for instance the beginning of the pedal "snap". Mass transport delay was not considered in this analysis.

In the analysis presented here, a four point, centered, finite-divided difference first derivative was utilized to determine the following:

1. Δt_1, the time differential between when the O_2 component of the sensor responded after the pedal transient was commanded for the increasing NO_x portion of the test
2. Δt_2, the time differential between when the NO_x component of the sensor responded after the pedal transient was commanded for the increasing NO_x portion of the test
3. Δt_3, the time differential between when the O_2 component responded and when the NO_x component responded for the increasing NO_x portion of the test
4. Δt_4, the time differential between when the O_2 component of the sensor responded after the pedal transient was commanded for the decreasing NO_x portion of the test
5. Δt_5, the time differential between when the NO_x component of the sensor responded after the pedal transient was commanded for the decreasing NO_x portion of the test
6. Δt_6, the time differential between when the O_2 component responded and when the NO_x component responded for the decreasing NO_x portion of the test
7. $dO_2/dt|_{Inc}$, the maximum rate of O_2 increase during the increasing NO_x portion of the test
8. $dNO_x/dt|_{Inc}$, the maximum rate of NO_x increase during the increasing NO_x portion of the test
9. $dO_2/dt|_{Dec}$, the maximum rate of O_2 decrease during the decreasing NO_x portion of the test
10. $dNO_x/dt|_{Dec}$, the maximum rate of NO_x decrease during the decreasing NO_x portion of the test

Figures 3-43 and 3-44 are plots of the first derivative of test point number 5 in Table 2-3 and provide a visual representation of the variables described in 1-10 above. A four-point central difference formula was used to accurately compute the first derivative and to minimize the effects of signal noise. Equation 8 is mathematical representation of the four point first derivative formula. The Δt in the denominator was 0.050 seconds for the first two sets of transient tests, and 0.005 seconds for the last set of transient tests (post field demo). The reference points selected for the analysis of 1-6 above were the first points after the respective derivative crossed the x-axis and continued in the same direction. The circles in Figures 3-43 and 3-44 represent these points:

$$\frac{dx_i}{dt} = \frac{(-f(x_{i+2}) + 8 \cdot f(x_{i+1}) - 8 \cdot f(x_{i-1}) + f(x_{i-2}))}{12 \cdot \Delta t} \tag{8}$$

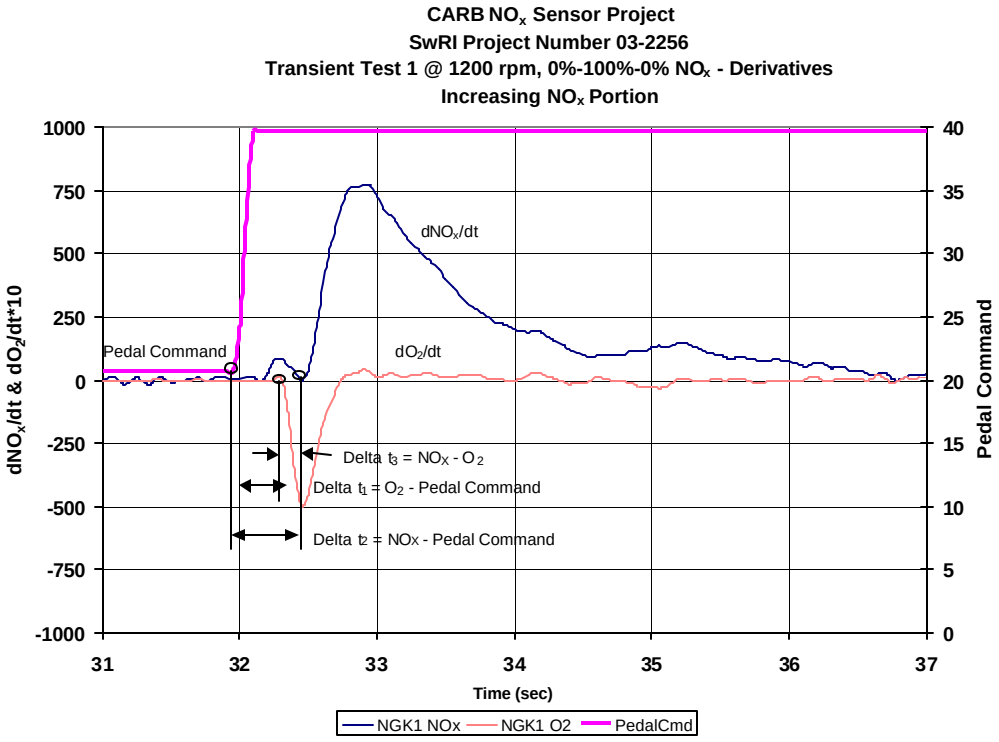

Figure 3-43. Increasing Portion of Transient Test Definitions

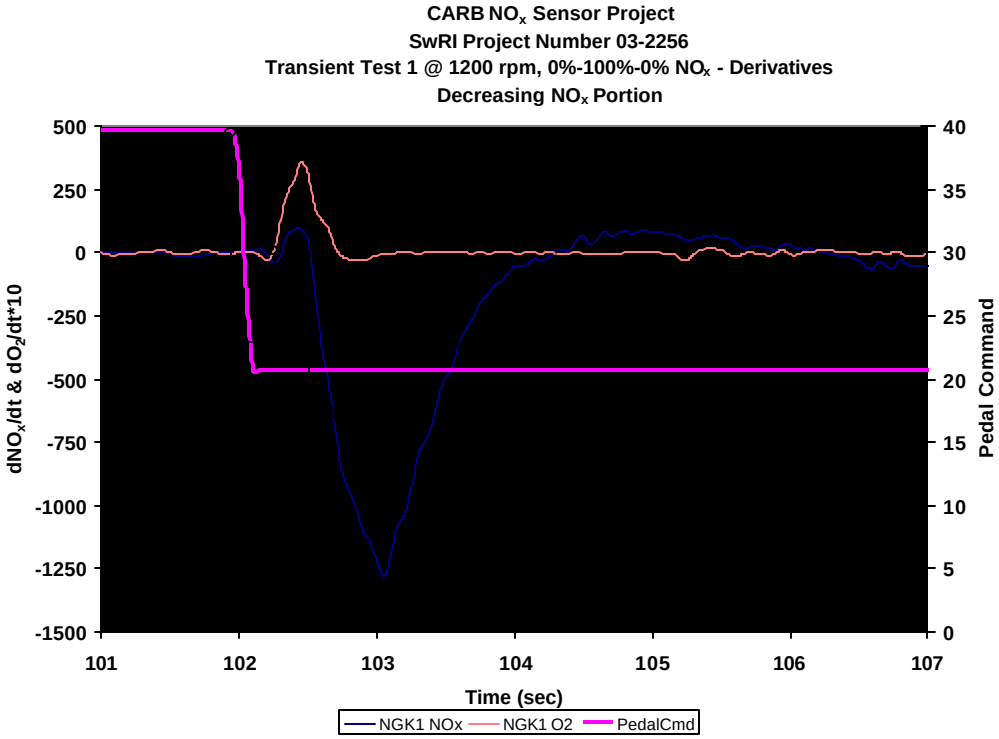

Figure 3-44. Decreasing Portion of Transient Test Definitions

The plots show the time rate of change in NO_x and O_2 increase or decrease during the transient. The O_2 derivative was scaled by 10 so both curves could be viewed on the same axis. In Figure 3-43, the O_2 can be seen decreasing while the NO_x increases. The opposite is true in Figure 3-44.

Data similar to that shown in Figure 3-43 and 3-44, were reduced for the first and third set of transient test data for a given engine test speed. These data are shown in Figures 3-45 to 3-56. Each figure shows data for all four sensors at a given engine speed and transient test number (Transient Test #1 = pre-field demo, Transient Test #3 = post field demo). The figures show the elapsed time from when the O_2 sensor responded to when the NO_x component of the sensor responded (Δt_3 or Δt_6). The legend entries in each figure correspond to a particular transient test. For instance, 25-100-25 represents the 25 percent of maximum NO_x, to maximum NO_x, back to 25 percent of maximum NO_x transient. Figure 3-45 shows that approximately 100 to 150 msec elapsed before the NO_x component of the sensor responded when the engine was run at 700 rpm. The data taken for the 50-100-50 NO_x transient indicate that the NO_x component responded before the O_2 component. This is physically impossible in an increasing NO_x case since exhaust gas must pass through the O_2 measuring cells first. Therefore, these data are considered suspect and should not be used to characterize the sensor.

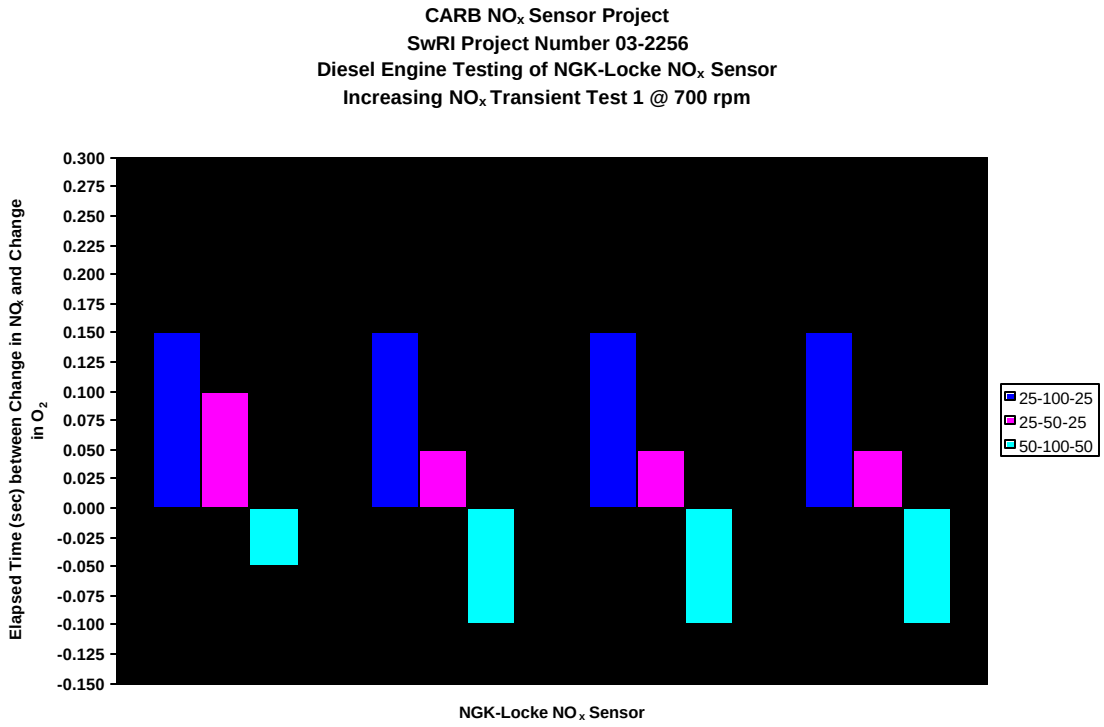

Figure 3-45. Reduced Data for Increasing NO_x Portion of Transient Test Number 1 at 700 rpm

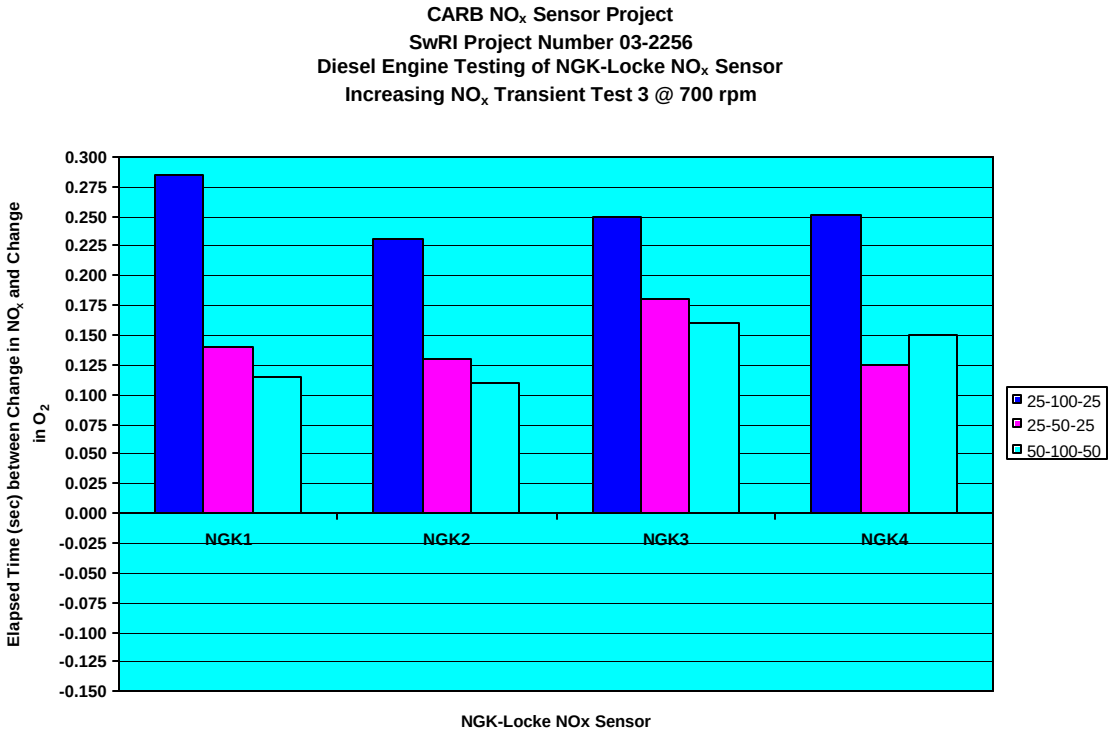

Figure 3-46. Reduced Data for Increasing NO_x Portion of Transient Test Number 3 at 700 rpm

Figure 3-46 shows the same data as in Figure 3-45, but for the post field demo transient tests. These data were taken at a higher resolution than the pre-field demo data and therefore, should be more accurate. The data in Figure 3-46 indicate that the response time of the sensors has increased for the largest NO_x transient (25-100-25). The range in elapsed times was between 230 msec and 285 msec for the 25-100-25 transient. The 25-50-25 and the 50-100-50 transient data had elapsed times ranging from 125 msec to 180 msec and from 110 msec to 160 msec, respectively.

Figures 3-47 and 3-48 show reduced data for the decreasing portion of the NO_x transients at 700 rpm. The elapsed times (Δt_6) ranged between 200 and 300 msec for the pre-field demo data. Figure 3-48 shows that all sensors, after the field demo, exhibited nearly the same elapsed times for the 25-100-25 decreasing portion of the test at approximately 117 msec. However, NGK3 and NGK4 showed marked increases in elapsed times for the 25-50-25 tests over NGK1 and NGK2. The elapsed time for the 50-100-50 test shows that the elapsed time was approximately –100 msec. This would indicate that the NO_x component of the sensor responded first, which is plausible during a decreasing NO_x transient. The decrease was associated with a reduction in engine load, and hence exhaust gas flow rate and pressure. Therefore, the NO_x measuring cavity could evacuate the "old" gas faster than it fills with "new" gas.

Figures 3-49 and 3-50 show the elapsed times for the increasing NO_x portions of the tests at 1200 rpm. Figure 3-49 shows that the elapsed time ranged between 100 and 200 msec.

However, this data is only accurate to +/-50 msec. The reduced data in Figure 3-50 represents the post-field demo tests and shows that the elapsed times ranged between 220 msec and 440 msec, depending on the magnitude of the NO_x transient. All sensors had similar elapsed times for all tests except the 0-25-0 transient. Sensors NGK1 and NGK2 showed elapsed times of 440 msec and 389 msec compared to 285 msec and 284 msec for NGK3 and NGK4, respectively.

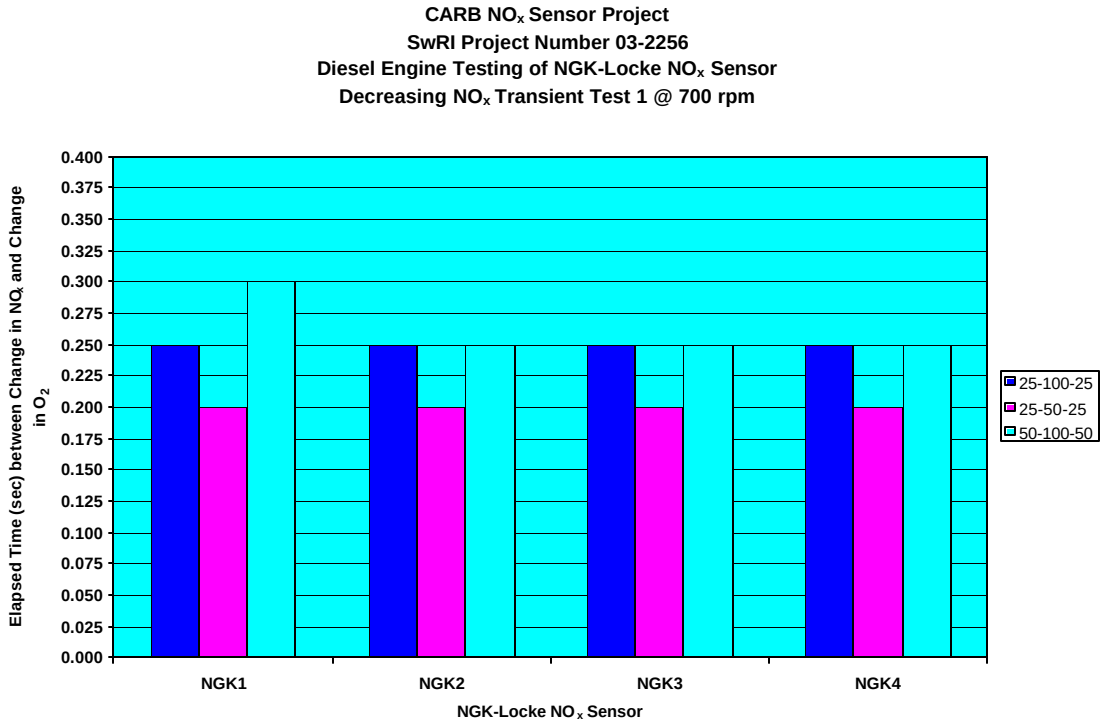

Figure 3-47. Reduced Data for Decreasing NO_x Portion of Transient Tests Number 1 at 700 rpm

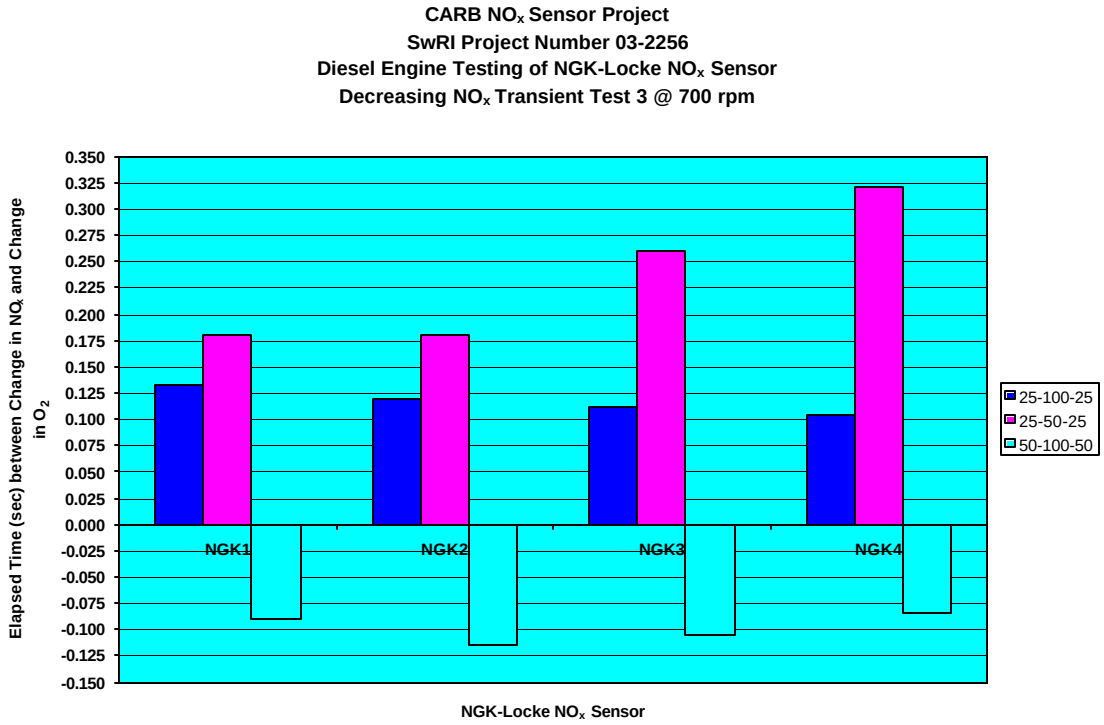

Figure 3-48. Reduced Data for Decreasing NO_x Portion of Transient Tests Number 3 at 700 rpm

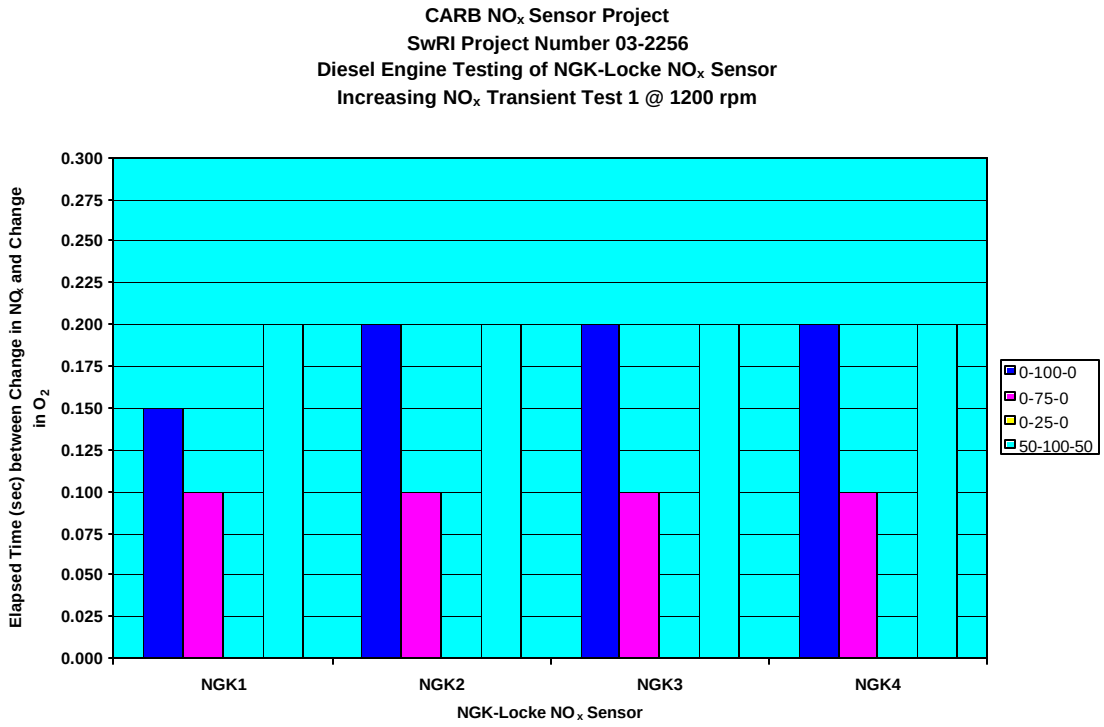

Figure 3-49. Reduced Data for Increasing NO_x Portion of Transient Tests Number 1 at 1200 rpm

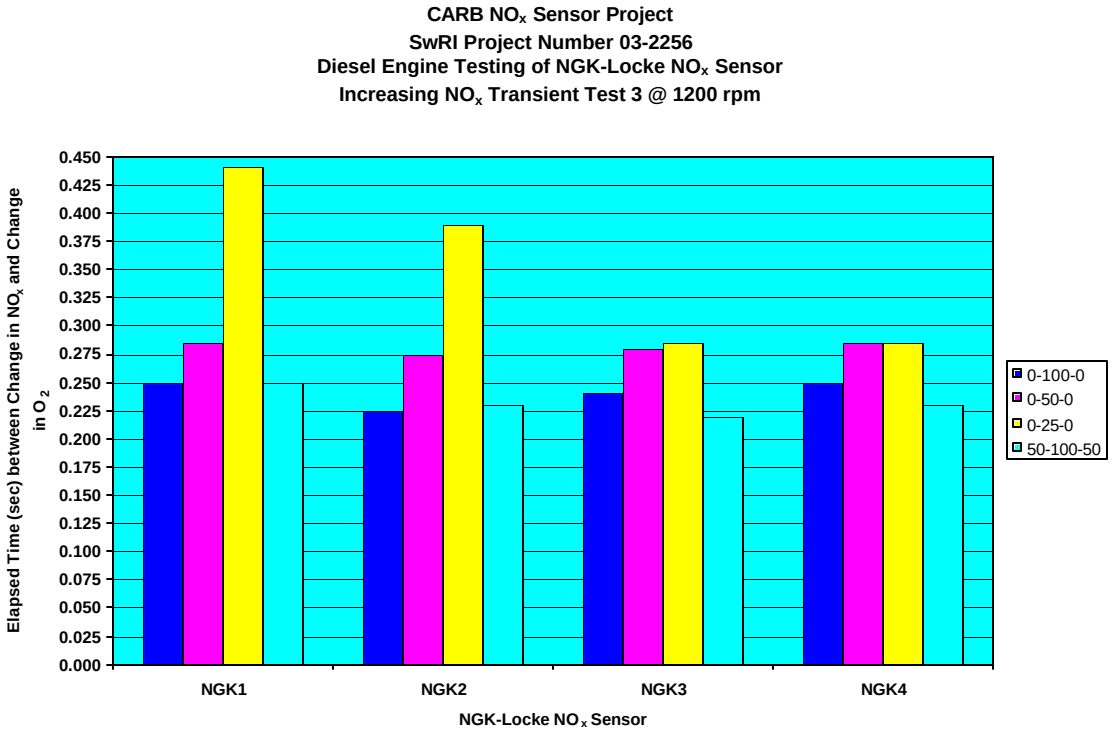

Figure 3-50. Reduced Data for Increasing NO_x Portion of Transient Tests Number 3 at 1200 rpm

Figures 3-51 and 3-52 show the reduced data for the decreasing NO_x portion of the 1200 rpm tests for pre- and post-field demo data (Test #1 and #3), respectively. Figure 3-51 shows that the elapsed time during the decreasing transients ranged between 100 and 300 msec for all tests. NGK1 had the longest elapsed during the 0-100-0 transient test. Figure 3-52 shows the reduced data for the post-field demos transient tests (Test #3). These data show that the NGK1 had the longest elapsed times of all the sensors for every test but the 0-25-0 transient. The NGK1 elapsed times were greater than 200 msec for all tests. Whereas, the elapsed times were a combined average of 118 msec in the 0-100-0 and 0-50-0 transients for the NGK2, NGK3, and NGK4 sensors. All sensors exhibited nearly the same elapsed times during the 0-25-0 transient of approximately 360 msec.

Figures 3-53 and 3-54 show reduced data for the 1800 rpm increasing portion of the NO_x transients. Figure 3-53 shows that the elapsed time for all sensors ranged between 150 msec and 300 msec across all tests for the pre-field demo tests. Sensor NGK1 generally exhibited the longest elapsed times. However, these data were compiled from data that is only accurate to 50 msec, and NGK1 is within 50 msec of the other sensors. Figure 3-54 shows the reduced data for the post-field demo transient tests. Again, the post-field demo data is accurate to +/-5 msec due to the increased acquisition rate. The post field demo data show that NGK1 is more on par with the other three sensors, but still had the longest elapsed times between the O_2 and NO_x components of the sensor. In general, the elapsed time of the responses ranged between 100 and 200 msec for all tests but the 0-25-0 transient tests. The elapsed time ranged from 280 and 290 msec for the small 0-25-0 transient.

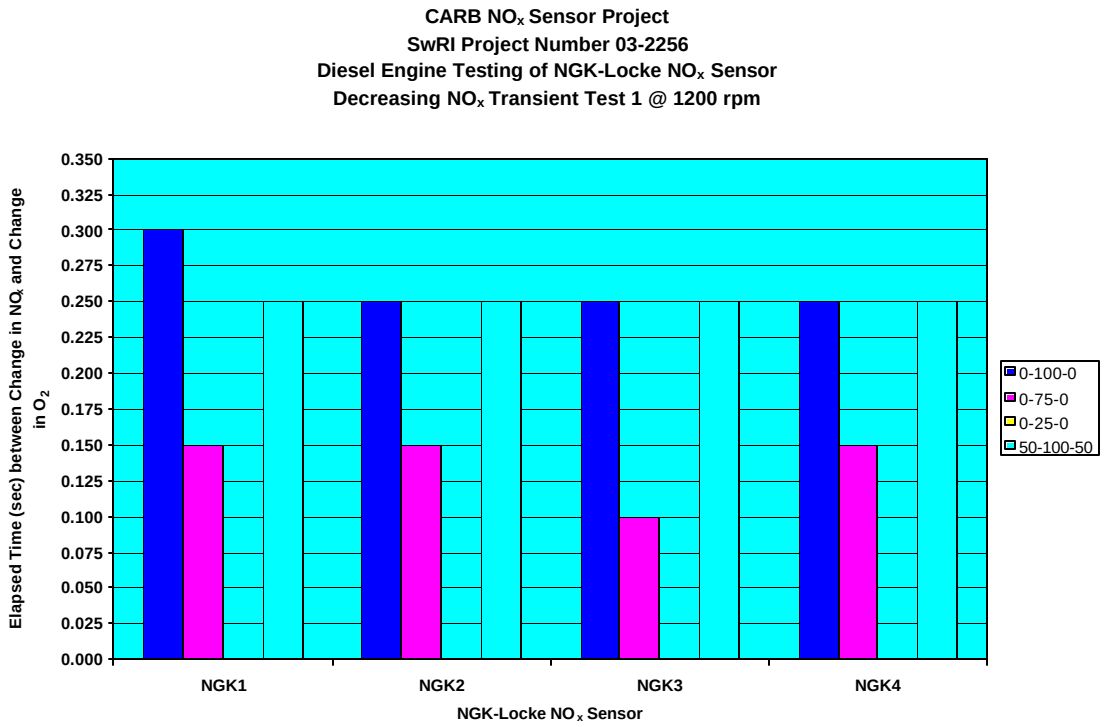

Figure 3-51. Reduced Data for Decreasing NO_x Portion of Transient Tests Number 1 at 1200 rpm

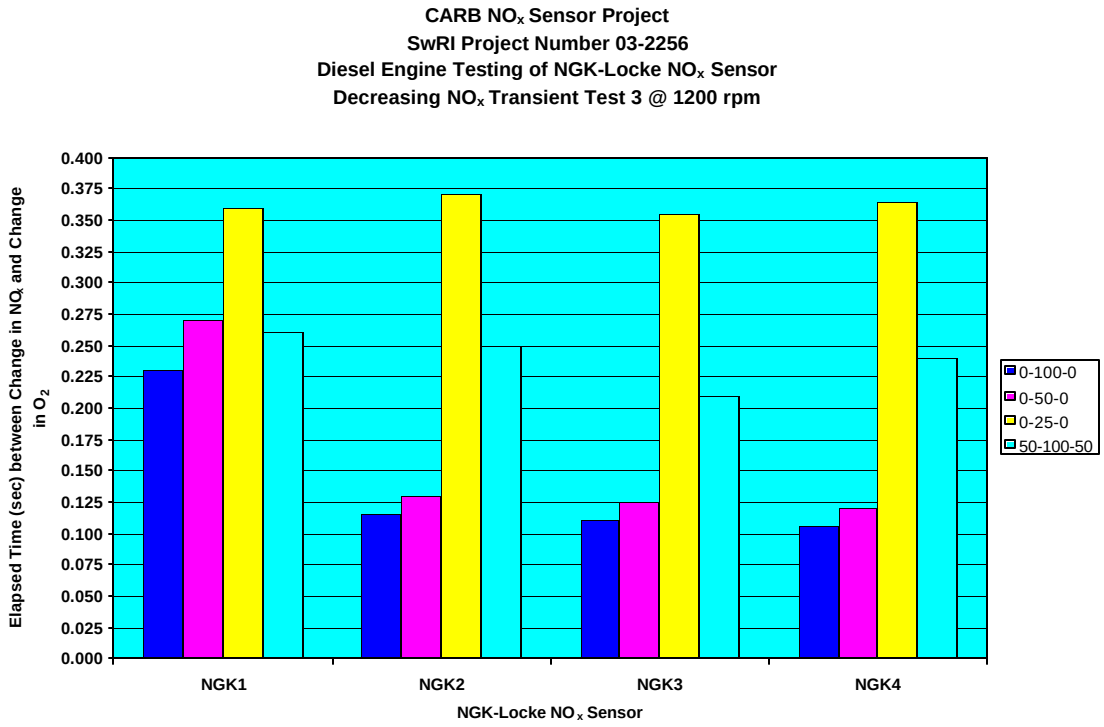

Figure 3-52. Reduced Data for Decreasing NO_x Portion of Transient Tests Number 3 at 1200 rpm

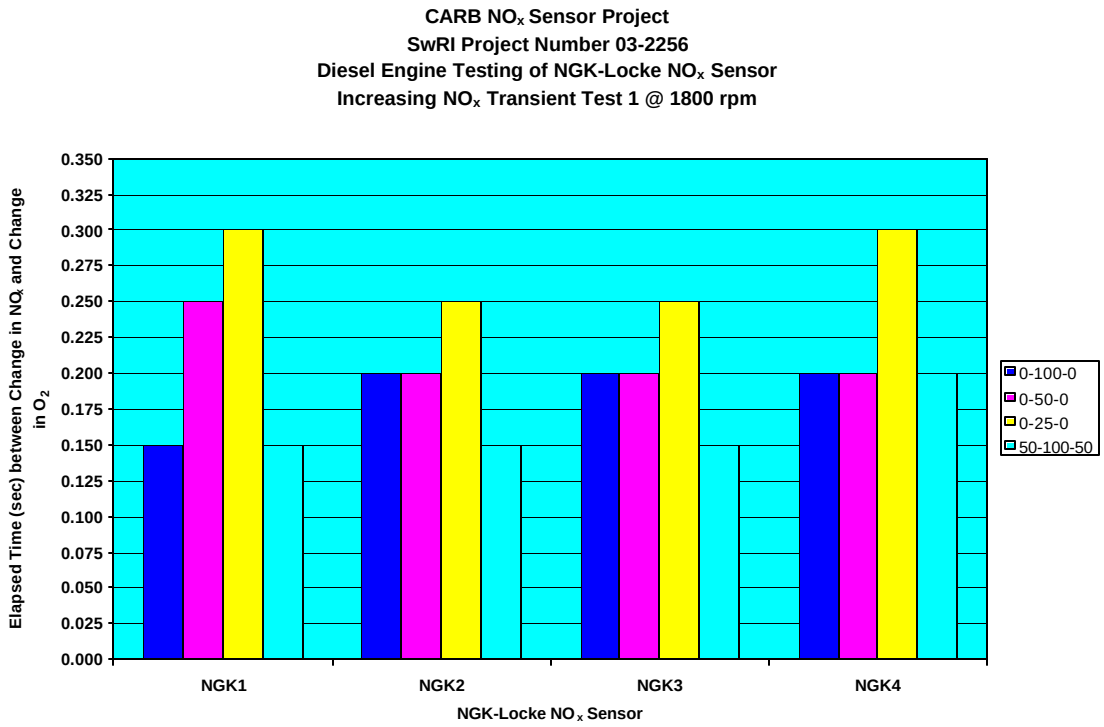

Figure 3-53. Reduced Data for Increasing NO_x Portion of Transient Tests Number 1 at 1800 rpm

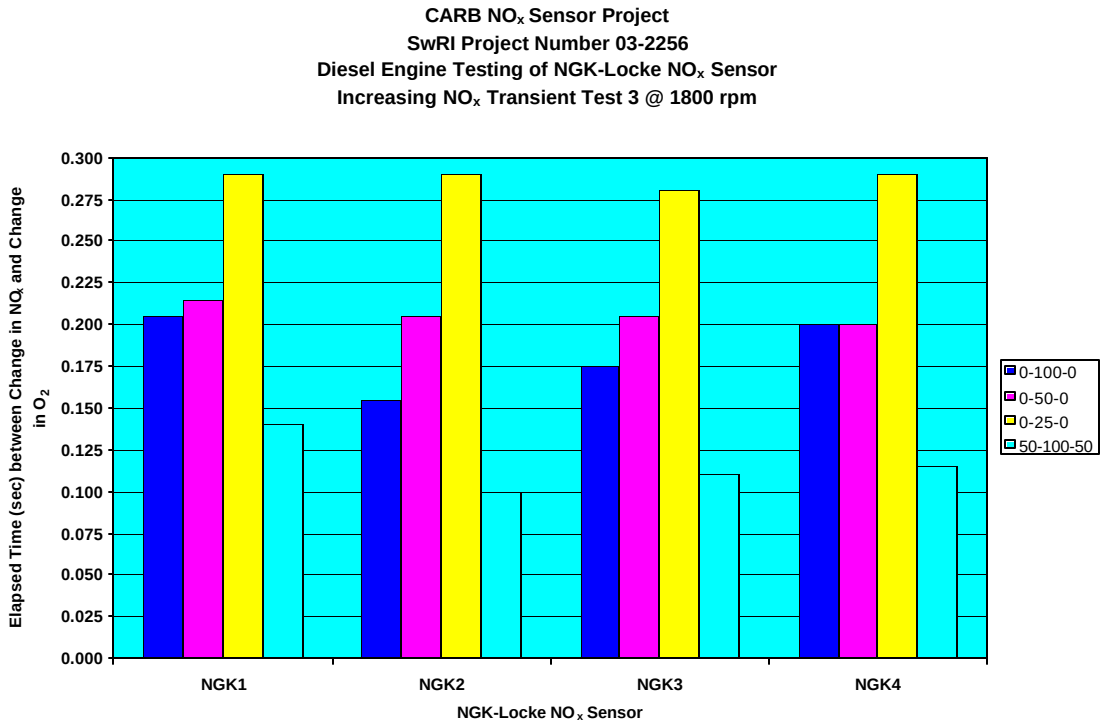

Figure 3-54. Reduced Data for Increasing NO_x Portion of Transient Tests Number 3 at 1800 rpm

Figures 3-55 and 3-56 show the elapsed times for the decreasing portion of the transients at 1800 rpm. Figure 3-55 shows that the elapsed time ranged between 100 and 200 msec for all tests except the 0-25-0 transient during transient tests #1. The elapsed time was 250 msec for all sensors for the 0-25-0 transient. Figure 3-56 shows the elapsed time for the post-field demo transient tests. The elapsed times were similar to the pre-field demo data in that the range was generally between 100 msec and 200 msec. Sensor NGK1 again showed the longest elapsed times for every test compared to the other three sensors. Sensor NGK1 was installed closest to the turbo outlet in the laboratory test engine. Another peculiarity of sensor NGK1 is that the elapsed times increased as the transient magnitude decreased, whereas, in the other sensors, the trend was exactly the opposite (excluding the 50-100-50 test).

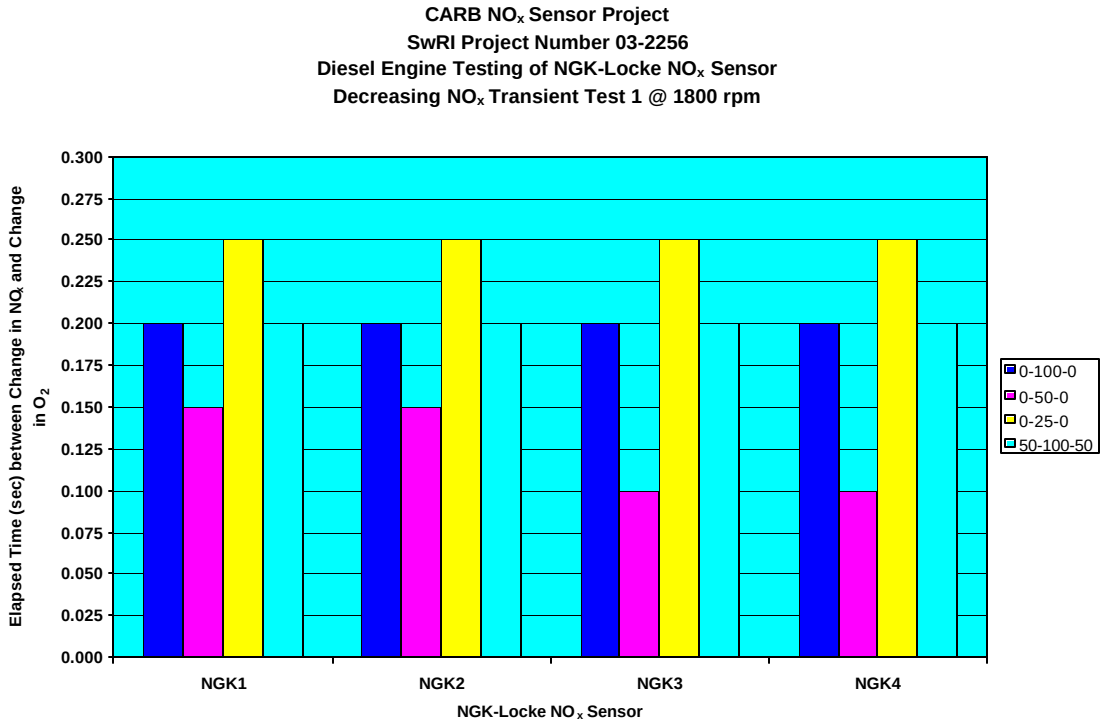

Figure 3-55. Reduced Data for Decreasing NO_x Portion of Transient Tests Number 1 at 1800 rpm

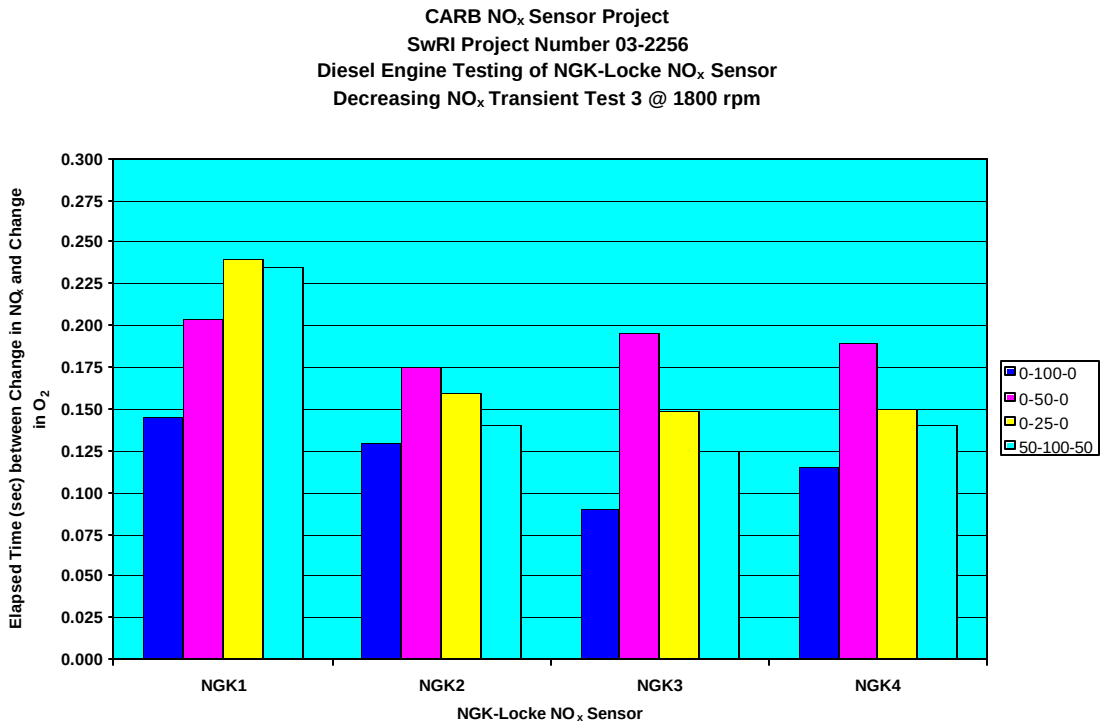

Figure 3-56. Reduced Data for Decreasing NO_x Portion of Transient Tests Number 3 at 1800 rpm

3.3.7 Histogram Analysis of Field Demonstration NO_x Sensor Data

Histogram data was taken by the dataloggers on the field demonstration vehicles at 40 Hz. Twenty-five "bins" were allocated for each logged variable. Histogram data files were downloaded, via cellular phone, once per week or when a reliable communication link could be established and maintained. The dataloggers provided a mechanism for SwRI to determine the functionality of the NO_x sensors. That is, were they still working or could a shift be observed during run time? The dataloggers were removed after six months instead of 50,000 miles. The long haul truck accumulated 48,188 miles while the short haul truck accumulated 35,277.

A mathematical method was developed to reduce an entire NO_x histogram plot to a single *average* histogram NO_x value. This allowed histograms downloaded on different dates (mileage) to be compared on a single graph for the duration of the field demonstration. Shifts in one NO_x sensor's output could then be easily compared to the output of the other NO_x sensor installed on the same vehicle. Another method would have been to integrate the NO_x from each sensor over time and compare the results. The mathematical expression used to determine the average histogram NO_x value is shown in Equation 9.

$$\overline{NO}_{x,histogramj} = \frac{\sum_{i=1}^{i=25} NO_{x,i} \cdot \#readings_i}{\sum_{i=1}^{i=25} \#readings_i} \qquad (9)$$

The $NO_{x,i}$ is the NO_x value for a given bin (e.g. 100, 200, 300, etc.). The "#readings" is the number of readings at the i^{th} bin value. The summation in the denominator is simply the total number of readings for the entire histogram.

Figure 3-57 shows a bar chart of the average histogram NO_x for the long haul truck as a function of approximate truck mileage. Each bar represents a complete histogram for a given sensor. The bar chart shows that the average NO_x difference between NGK1 and NGK3 was similar up to the 35,757 mile mark. At this point, NGK3 began to diverge from NGK1. Figure 3-58 shows the difference between the average NO_x values (average NO_x for NGK1 minus average NO_x for NGK3). The difference was approximately 25 ppm up until the 35,757 mile mark. From there it increased to a maximum of 274 ppm at 44,892 miles. The average histogram NO_x for NGK3 was higher than that of NGK1 for every average histogram entry.

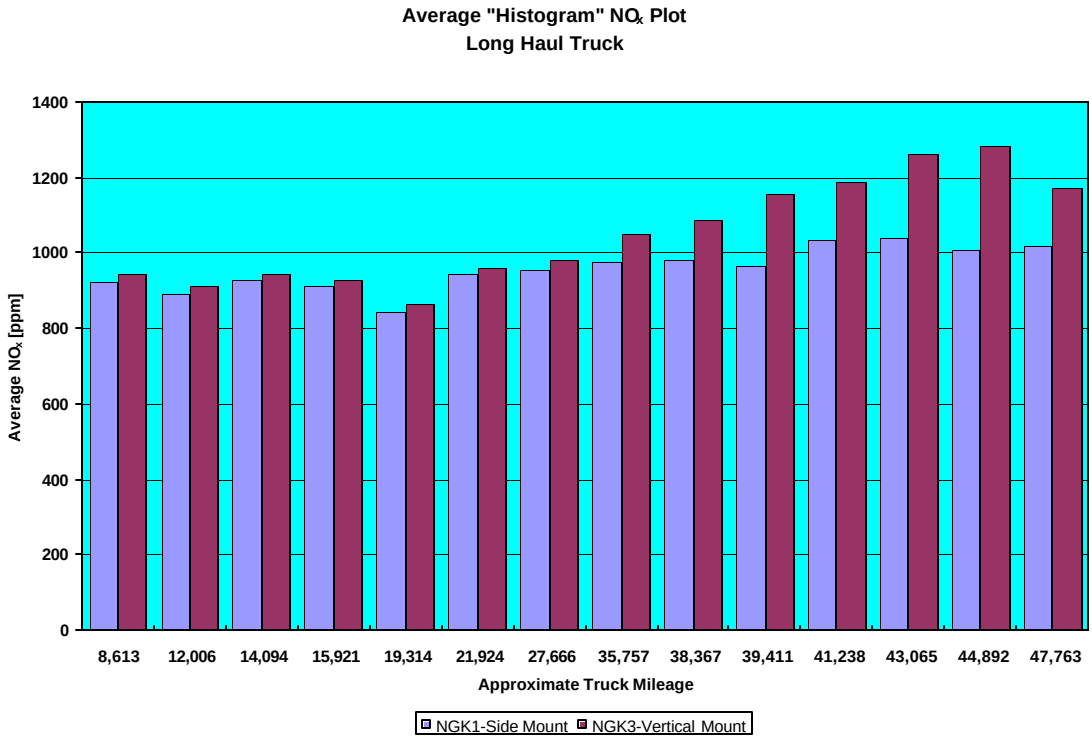

Figure 3-57. Average Histogram NO_x Comparison for Long Haul Truck

Figures 3-59 and 3-60 show the same style of data for the short haul truck as Figures 3-57 and 3-58. Figure 3-59 shows the average histogram NO_x for sensors NGK2 and NGK4 installed on the short haul demonstration vehicle. The two sensors appear to be very similar, although NGK2 had a higher average histogram NO_x than NGK4. No large deviations between the two were evident. Figure 3-60 shows the difference between NGK2 and NGK4. The difference in average histogram NO_x was less than 20 ppm for the first 7,500 miles. The difference between the sensors increased to 30 ppm up to the 25,659 mile mark. At 35,078 miles, the difference between the two sensors increases to 82 ppm.

It is interesting to note that the vertically mounted sensors NGK2 (short haul) and NGK3 (long haul) reported more NO_x than the two side mount sensors (NGK1 and NGK4). Vertically mounted sensors imply that the sensor was installed vertically in the exhaust system, or pointing toward the ground; that is, exhaust gas must flow vertically up into the measuring cavity, thus reducing the chance that particulate matter or some other debris could obstruct internal passage ways in the sensor. Horizontally mounted sensors were installed such that the center line of the sensor was nearly parallel to the ground. See Figure 2-6 for clarification.

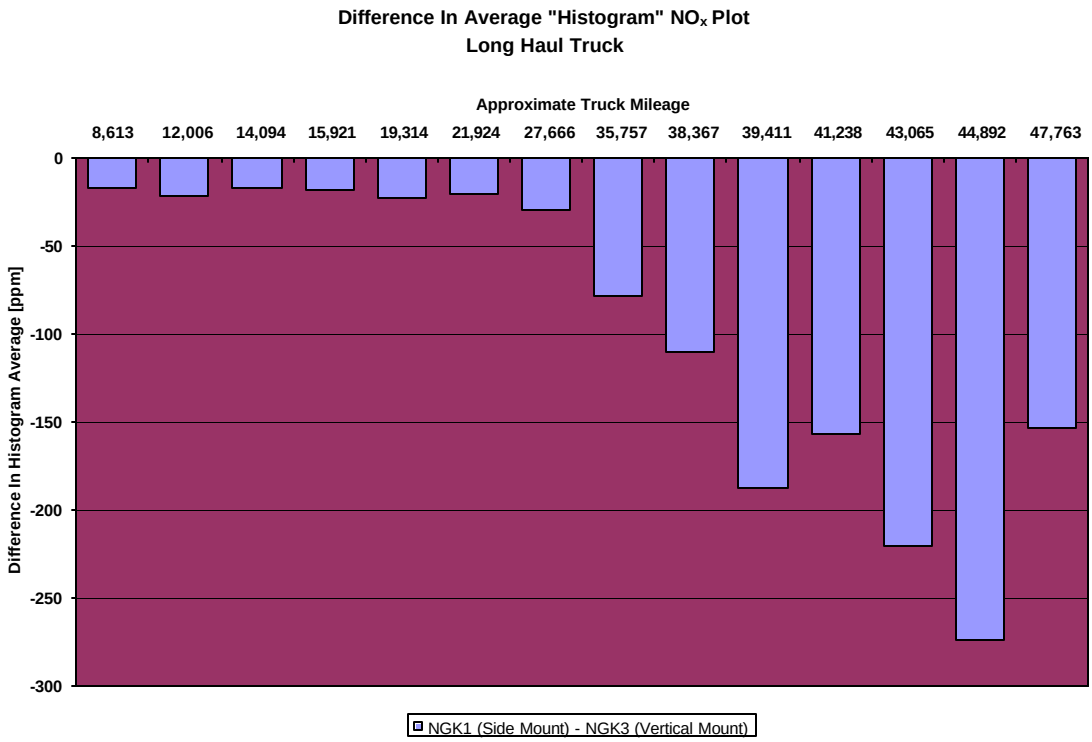

Figure 3-58. Difference in Average Histogram NO_x for Long Haul Truck

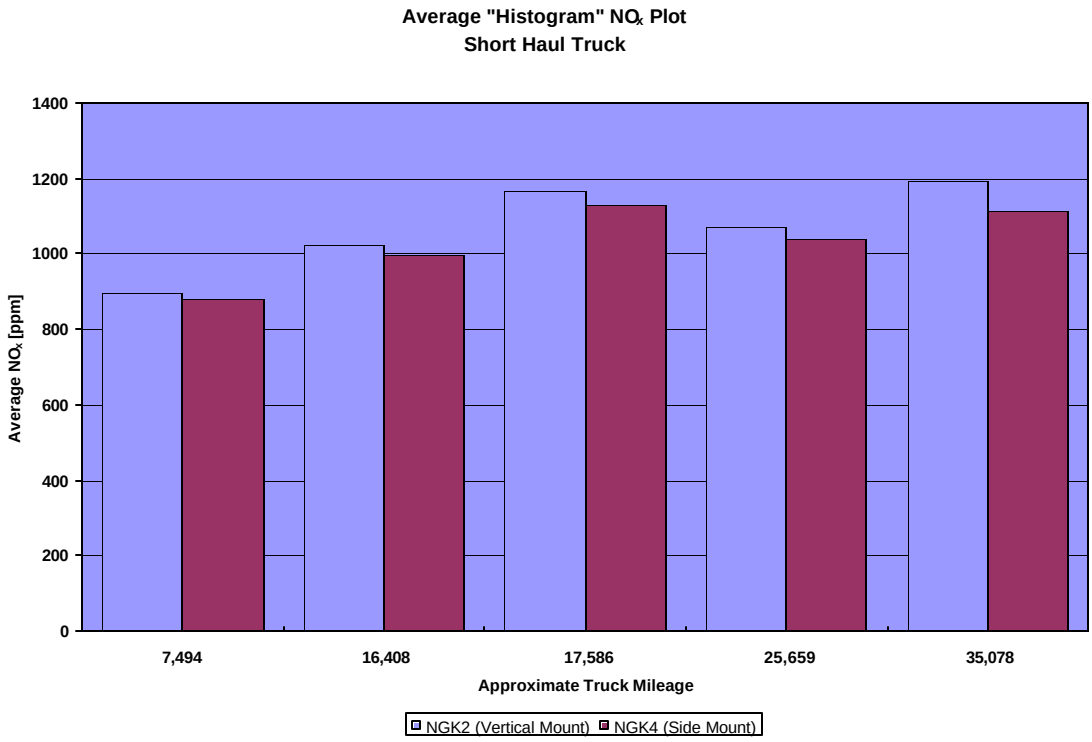

Figure 3-59. Average Histogram NO_x Comparison for Short Haul Truck

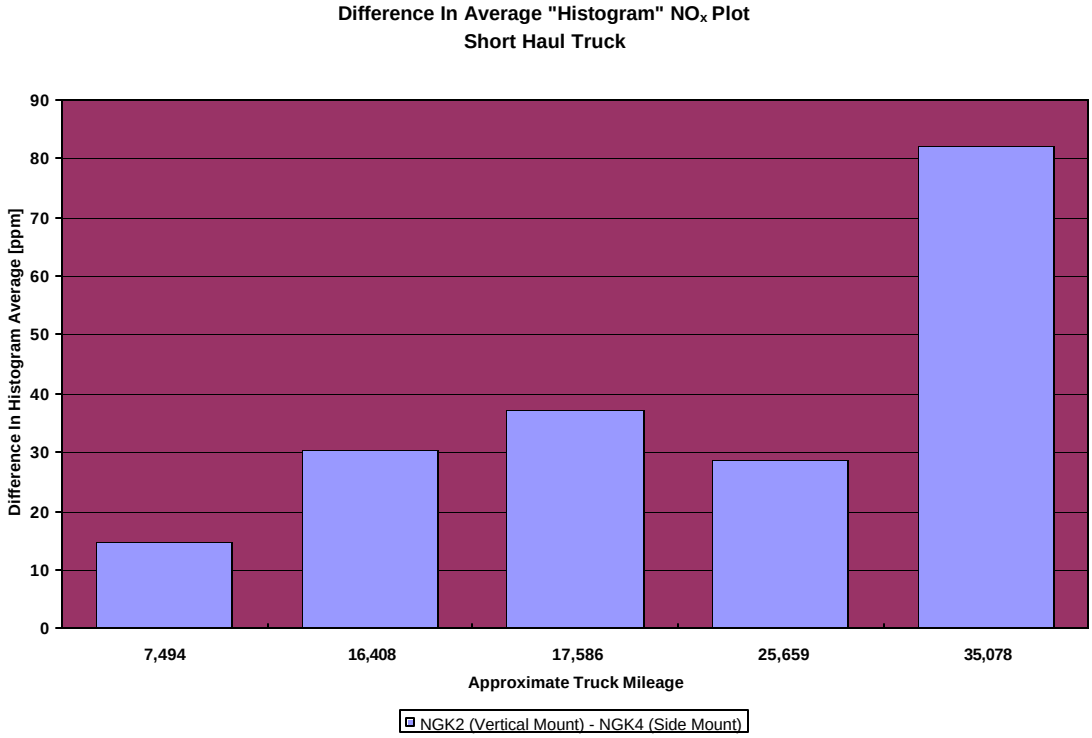

Figure 3-60. Difference in Average Histogram NO_x for Short Haul Truck

3.3.8 Presentation of Some Long Haul Time Data Acquired During the Field Demonstration

Five hard drives, consisting of raw datalogger files with a combined total of 4.157 Gbytes of raw data, were acquired and post processed and concatenated to 30-minute intervals of data for each day of operation. Only 739.9 Mbytes of data were acquired on the short haul due to hard drive and mother board failures encountered throughout the six month field demonstration. Examples of post-processed long haul data are presented here to provide the reader with a view of the type of data collected by the SwRI dataloggers, and the operating characteristics of the NGK sensors. Due to the large volume of data acquired, only a brief glimpse is presented. Excel spreadsheet files of the concatenated files for both the long haul and short haul trucks, as well as a plot macro, have been delivered to CARB on compact discs should one desire to view additional data.

Figures 3-61 to 3-66 represent the first day of operation after the datalogger was installed. Figures 3-67 to 3-72 represent the last day of operation prior to hard drive removal on February 14, 2000. There are six plots for each block of 30 minute data. The date of data acquisition is listed in the title block of each plot. The six plots contain real time data of some of the variables listed in Table 3-9. The plots have been annotated, where appropriate, since the plots are presented in gray scale.

Table 3-9. Time Domain Data Plot Descriptions

Plot Number	Variables Plotted
1	Predicted NO_x and computed NO_x in ppm from the output voltage of each sensors NGK1 and NGK3 using the SS4 calibration.
2	Computed O_2 concentration from the output voltage of NGK1 and NGK3 using the SS4 calibration.
3	Raw NO_x, and O_2, and pedal position sensor voltages.
4	Percent difference in raw NO_x and O_2 voltages relative NO_x sensor NGK1.
5	Manifold air temperature (MAT), manifold air pressure (MAP), exhaust pressure near NO_x sensors (PSens), and exhaust gas temperature (Exh T) near NO_x sensors.
6	Vehicle speed and engine speed

The 30 to 60 minute interval of time domain data, acquired on September 18, 1999, are presented in Figures 3-61 to 3-66. Figure 3-61 shows that NO_x sensor NGK1 and NGK3 yield nearly identical results, while the NO_x model under-predicted NO_x, but followed most transient trends. The error between the NO_x model and the sensor values is most likely due to injection timing effects. Injection timing was not available, and therefore, not used in the NO_x model. The O_2 sensor component traces in Figure 3-62 are in good agreement, but slight variation can be seen from one sensor to the other.

Figure 3-63 shows raw voltages from the NGK1 and NGK3 sensor NO_x components, along with the pedal position sensor voltage. Again, good agreement can be seen between the NO_x sensors output voltages. The pedal position voltage can be seen dropping to 0.5 volt on occasion. This indicates that the engine is either idling or cruise control has been activated. Analysis of the vehicle and engine speeds in Figure 3-66 can be used to determine the idle or cruise control condition. Figure 3-64 shows the percent difference in NO_x sensor voltage and O_2 sensor voltage relative to sensor NGK1 (i.e. sensor to sensor variation). The relative difference in NO_x sensor voltage is approximately +/-10 percent, and less than +/-5 percent for the O_2 sensor voltage. The large spikes in the plot are typically the result of a fuel cut condition where the NO_x sensor output voltage approaches 0.0 volts, and the internal sensor heater attempts to maintain a 1562°F (850°C) measuring tip temperature under cool exhaust gas conditions. Figure 3-65 shows the MAT, MAP, PSens, and Exh T. The MAP can be used as an indication of load. The Exh T follows the MAP with a slight delay. As MAP increases, combustion temperatures increase as indicated by increased exhaust temperatures. Higher MAPs indicate higher engine loads. The pressure at the NO_x sensors (PSens) can be seen to be nearly constant at 14.5 psia throughout the entire 30 minutes. Figure 3-66 shows that the engine spent approximately 20 minutes at idle in this 30 minute data set.

The next 30 minute interval presented is from the 570^{th} minute to the 600^{th} minute of operation on February 14, 2000. Figure 3-67 shows that the engine was operating at high NO_x levels, between 1200 and 1600 ppm, for most of the 30 minute interval. A clear shift between NGK1 and NGK3 can be seen in this plot near the 595^{th} minute. In addition, NO_x ppm computed from the output of NGK1 is consistently less than that representing NGK3. The predicted NO_x is under predicting NO_x by nearly a constant ratio, although transients are represented well. The offset between the predicted NO_x and the sensor NO_x could have been removed via additional calibration, and potentially through the addition of new independent parameters such as injection timing.

The O_2 traces in Figure 3-68 are in as good agreement as the O_2 traces presented from the September 18, 1999 data. This is confirmed in the relative difference of the O_2 sensor output voltage shown in Figure 3-69. Figure 3-69 also shows that there was a relative percent difference that was consistently negative between the NGK1 and NGK3 NO_x component output. Figure 3-69 and Figure 3-72 indicate that the cruise control was active nearly the entire 30 minutes and may indicate why the variation in the NO_x relative difference is less “noisy” than the September 18, 1999 data. In other words, the injection timing and duration were probably very stable since the engine was loaded instead of idling. The engine controller varies injection timing and probably injection duration during idle, which can have a significant effect on NO_x production. The MAP trace in Figure 3-71 shows that the transients were small and that the load on the engine quasi steady-state. The Exh T trace can again be seen following the MAP trace. As shown in Figure 3-72, engine speed was approximately 58 mph for most of this 30 minute data set.

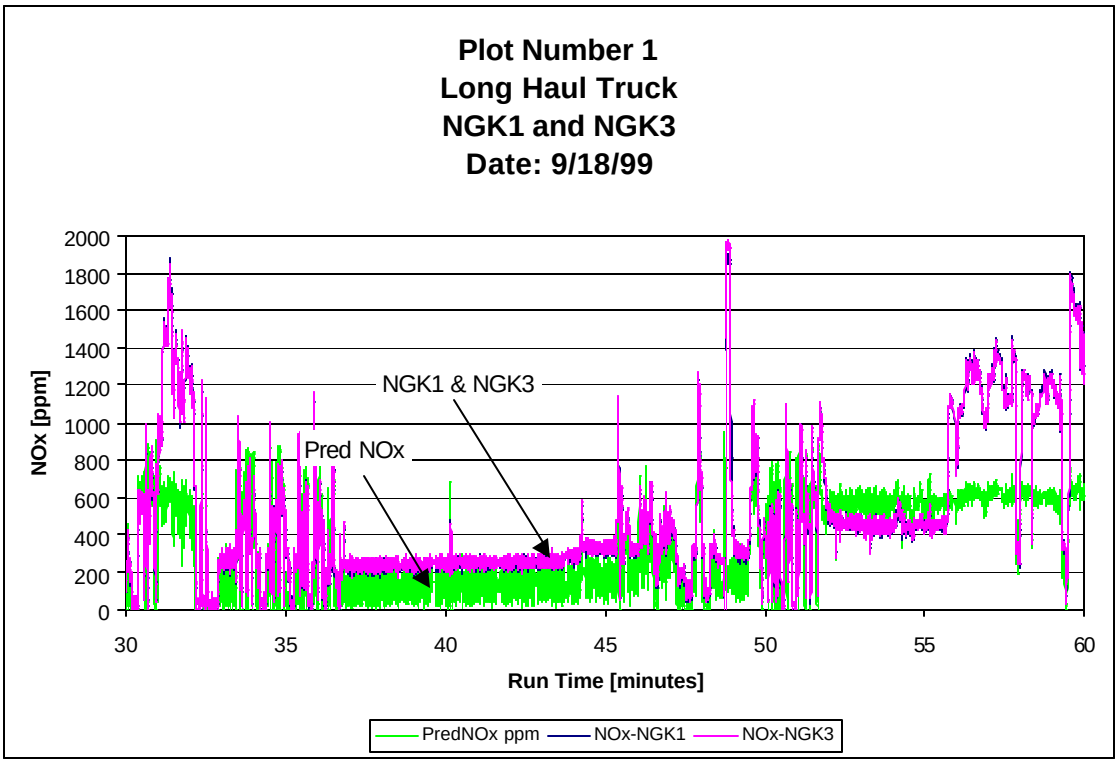

Figure 3-61. NGK NO_x Sensor NO_x and Predicted NO_x on Long Haul Truck Acquired September 18, 1999

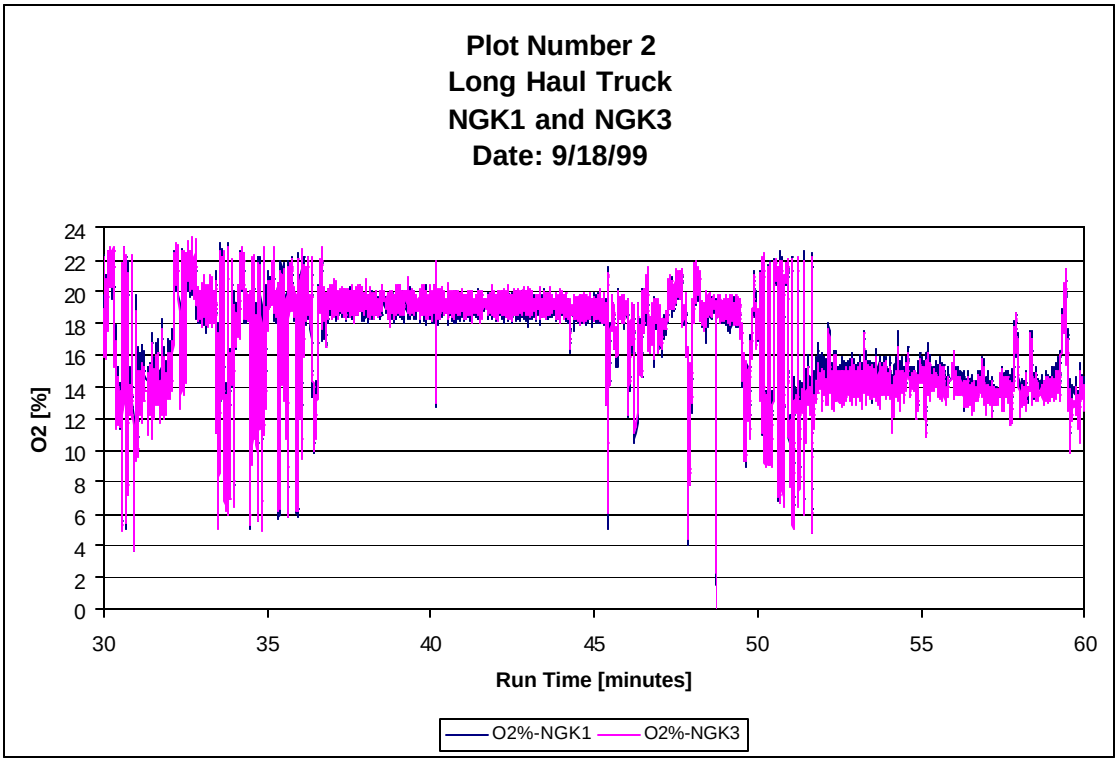

Figure 3-62. NGK Sensor O_2 on Long Haul Truck - Acquired September 18, 1999

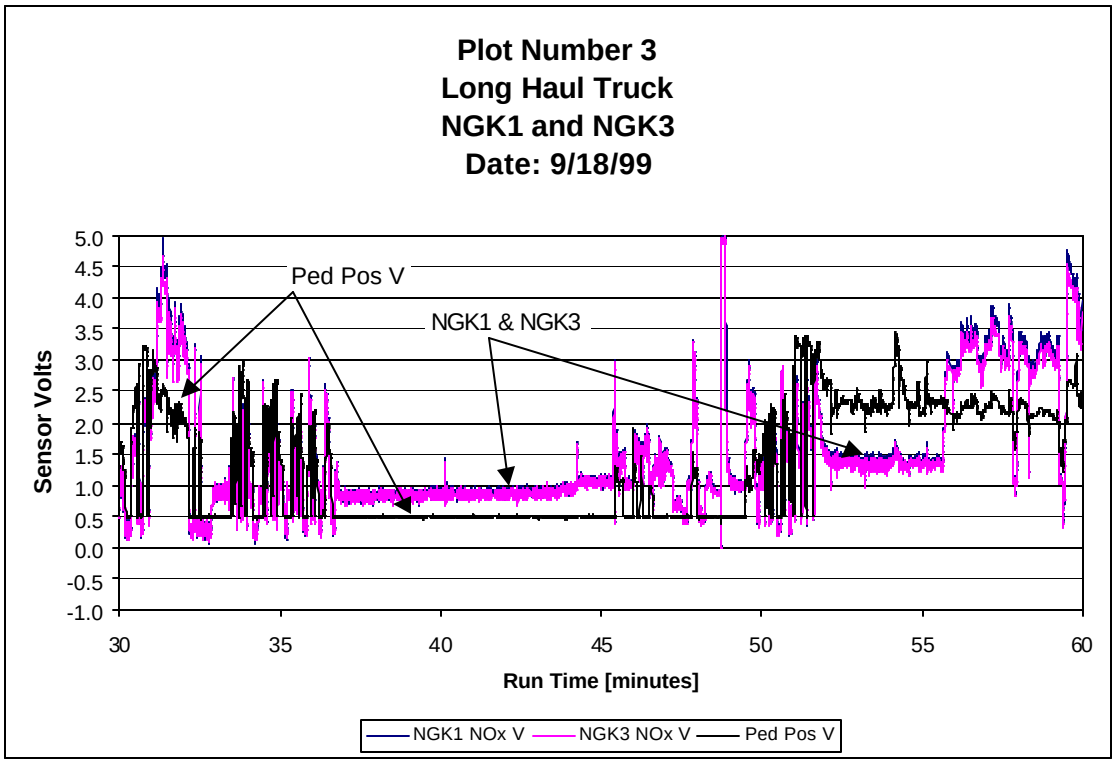

Figure 3-63. NGK NO_x Sensor and Pedal Position Sensor Output on Long Haul Truck - Acquired September 18, 1999

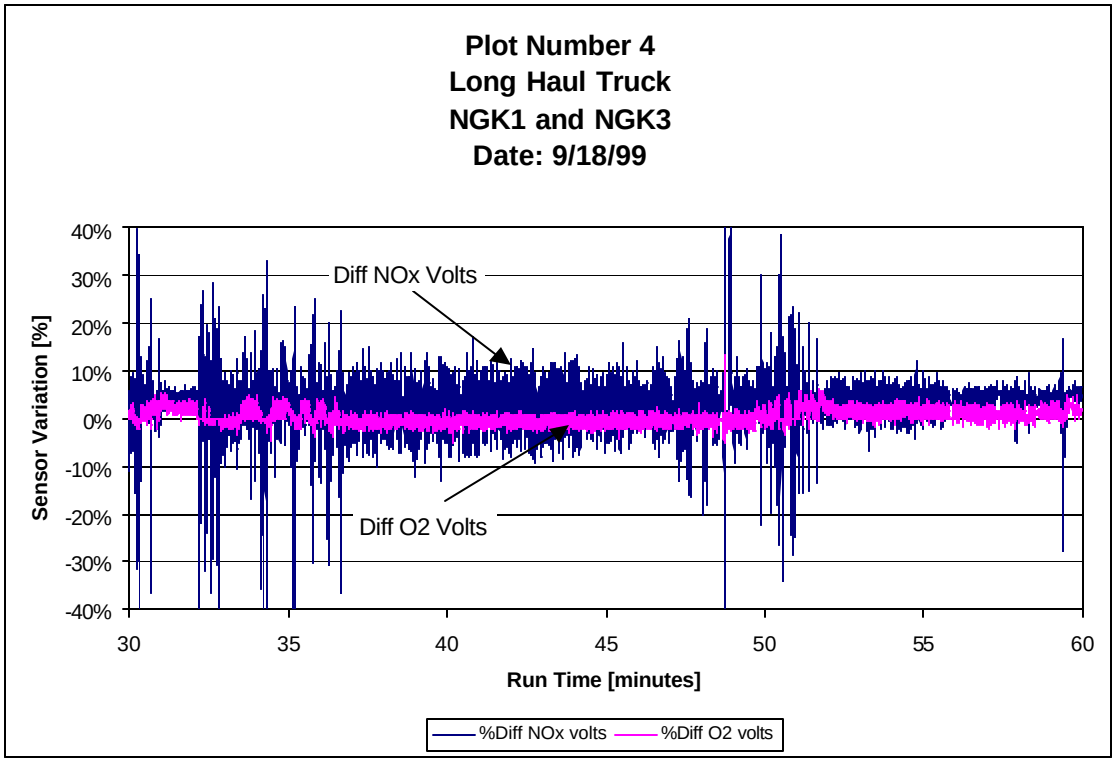

Figure 3-64. Sensor-to-Sensor Variation for NO_x and O_2 Components of NGK Sensor on Long Haul Truck - Acquired September 18, 1999

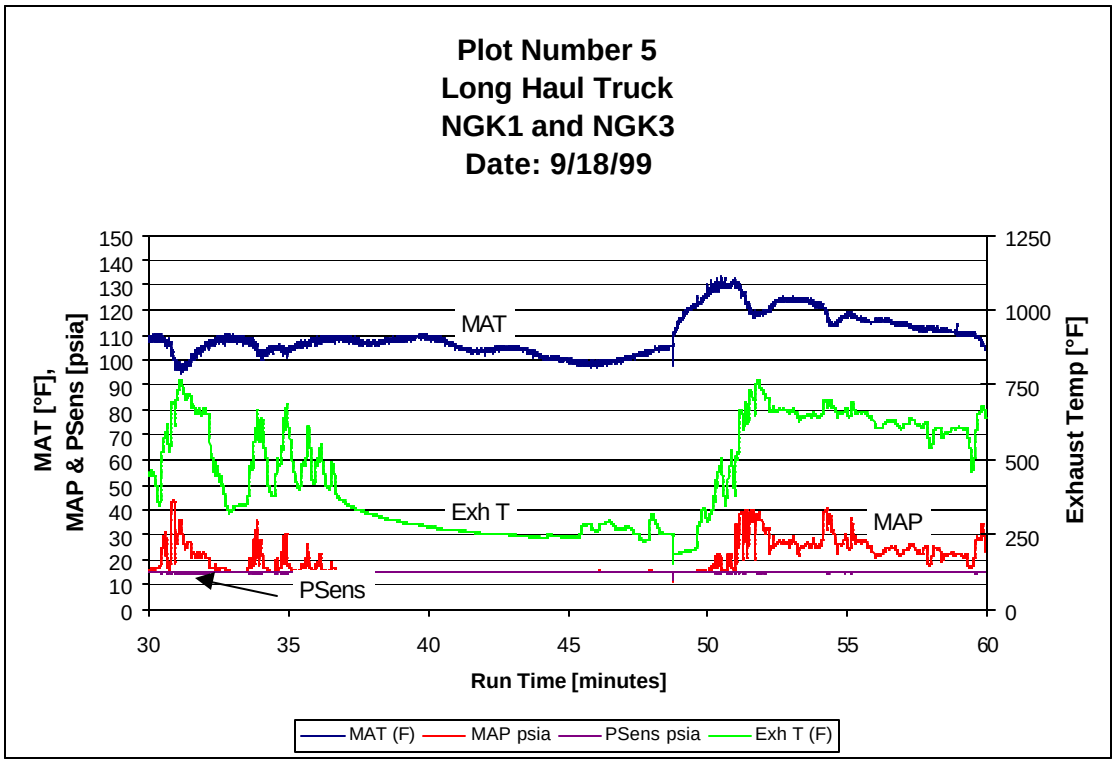

Figure 3-65. Manifold Air Temperature (MAT), Manifold Air Pressure (MAP), Exhaust Gas Temperature at NGK Sensors, and Exhaust Pressure at NGK Sensors on Long Haul Truck - Acquired September 18, 1999

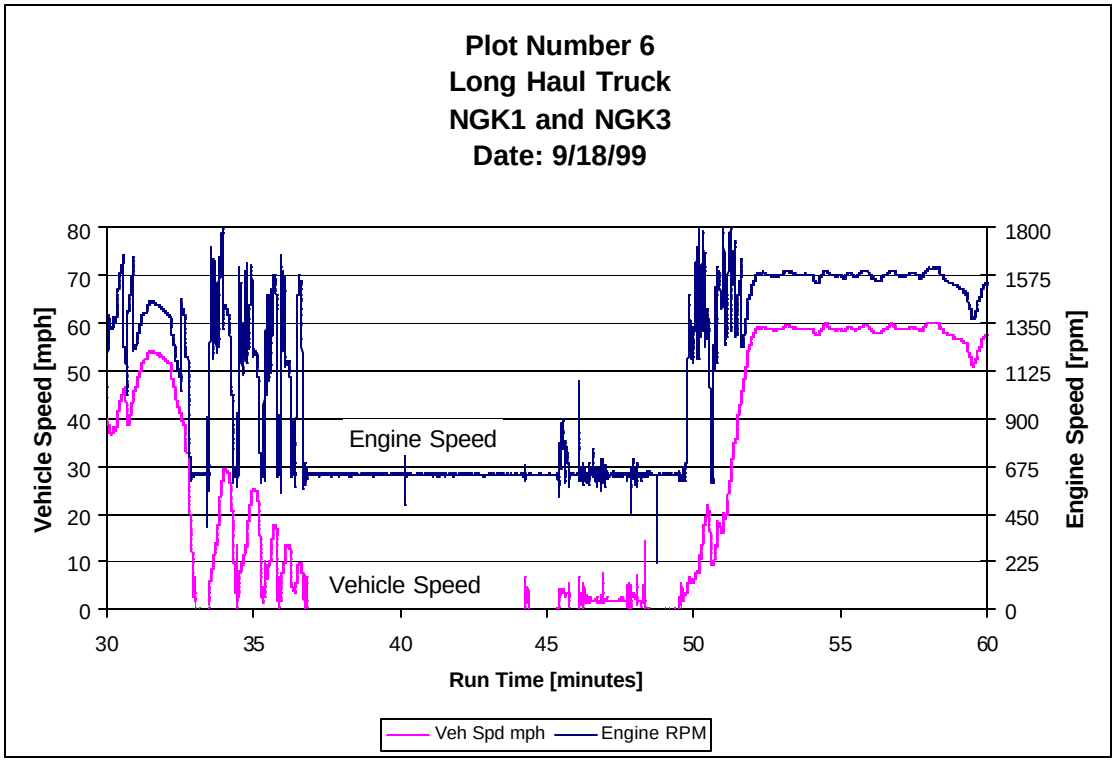

Figure 3-66. Engine Speed and Vehicle Speed on Long Haul Truck - Acquired September 18, 1999

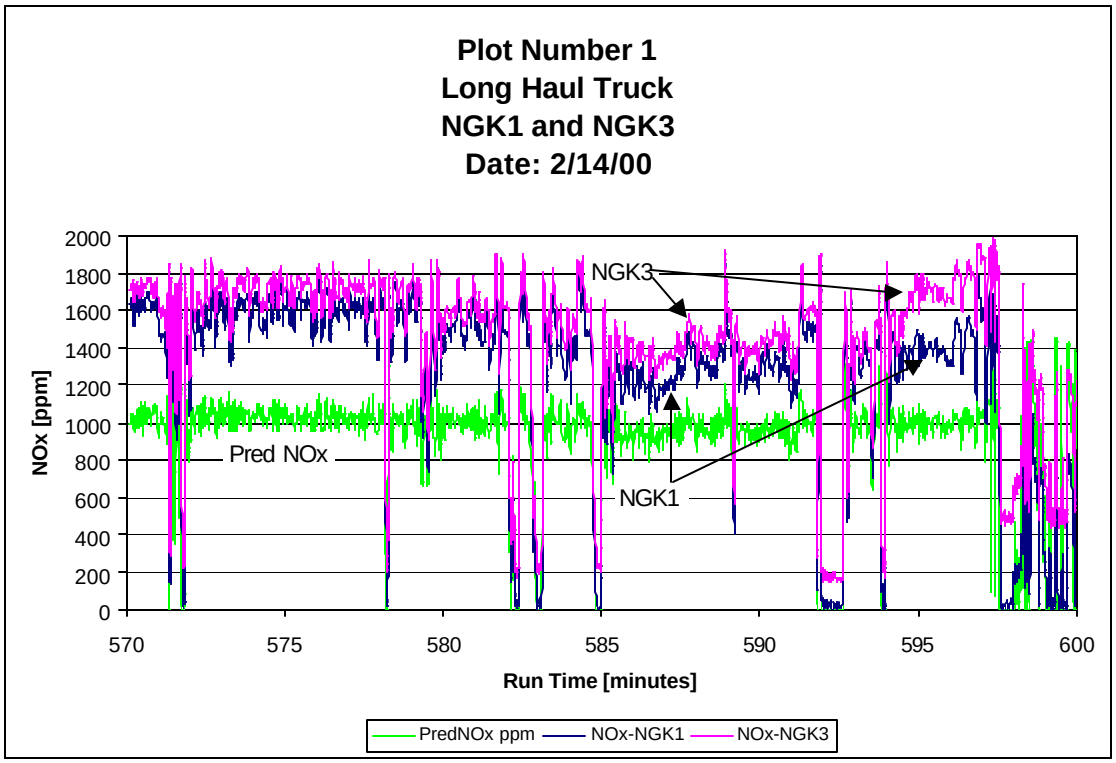

Figure 3-67. NGK NO_x Sensor NO_x and Predicted NO_x on Long Haul Truck - Acquired February 14, 2000

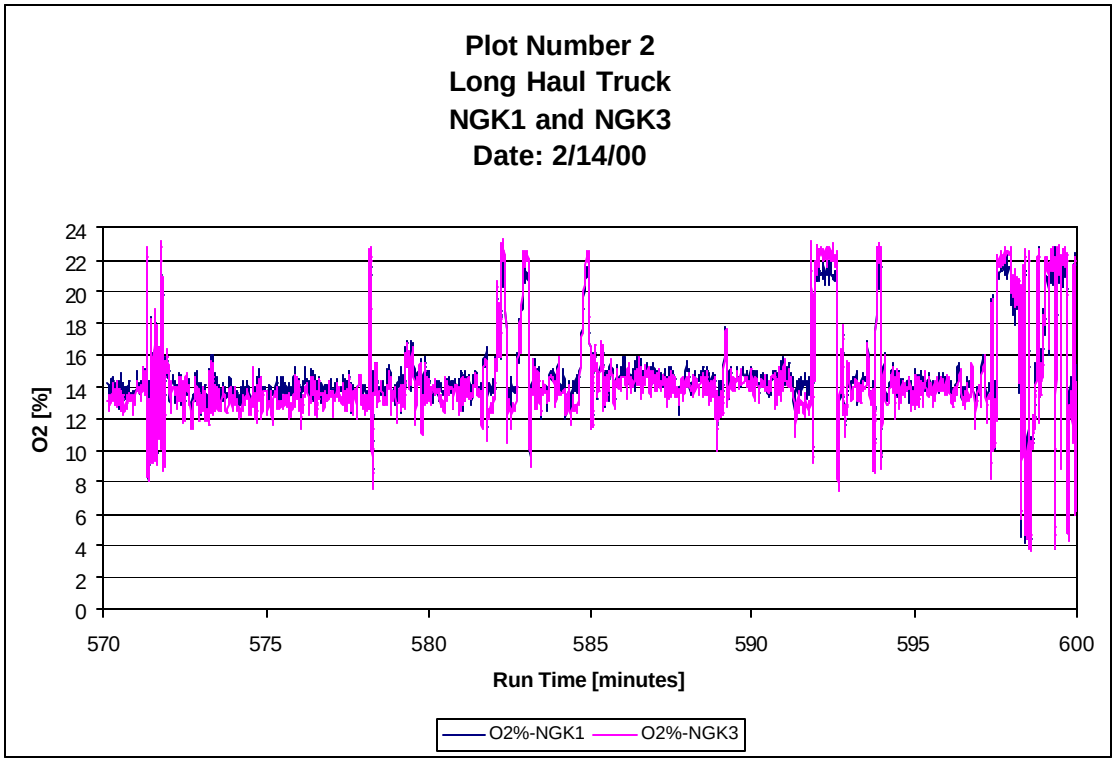

Figure 3-68. NGK Sensor O_2 on Long Haul Truck - Acquired February 14, 2000

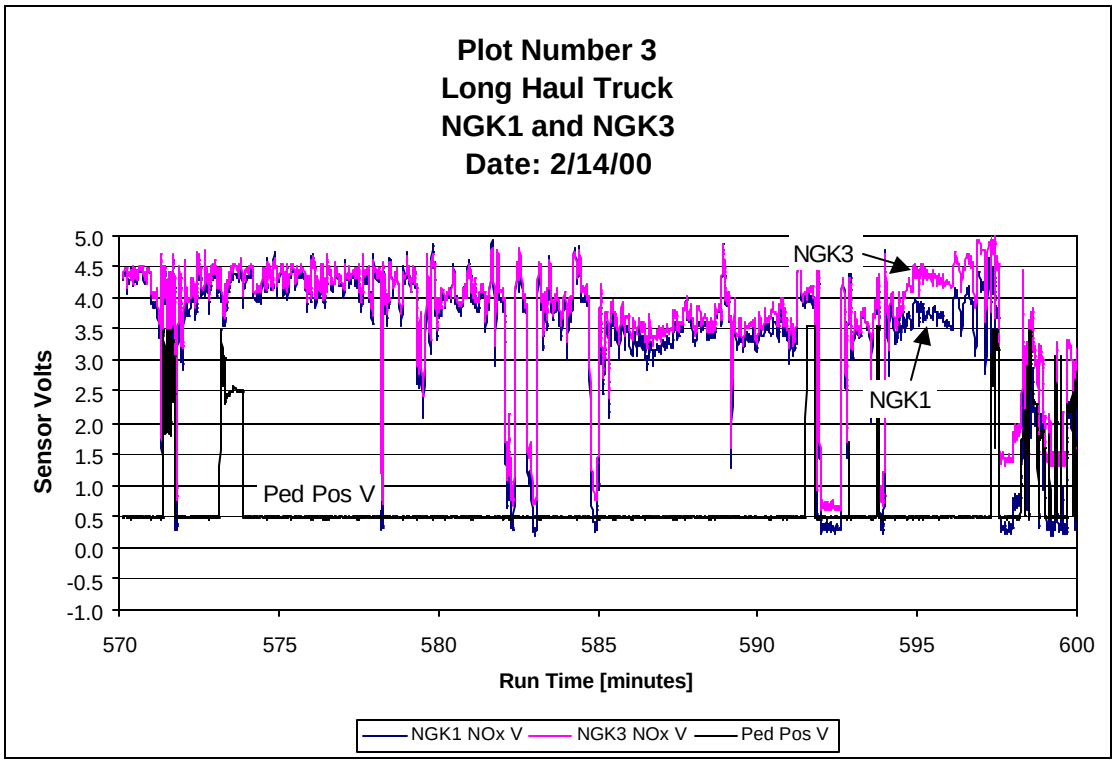

Figure 3-69. NGK NO_x Sensor and Pedal Position Sensor Output on Long Haul Truck - Acquired February 14, 2000

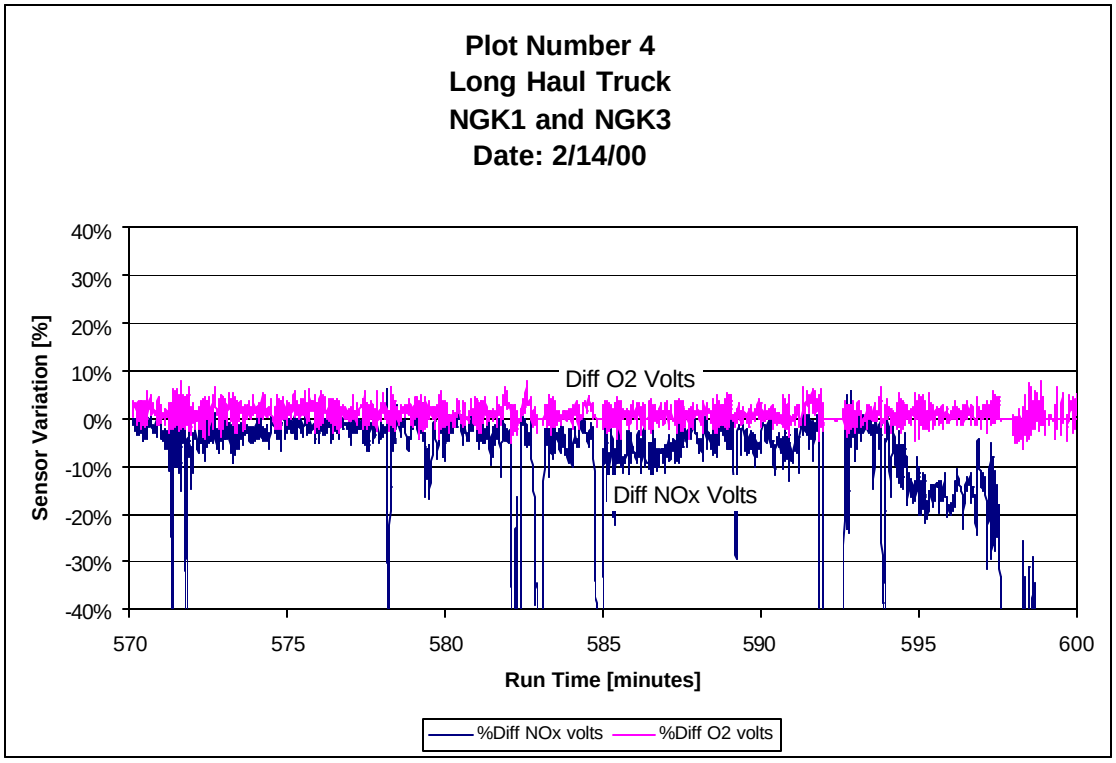

Figure 3-70. Sensor-to-Sensor Variation for NO_x and O_2 Components of NGK Sensor on Long Haul Truck - Acquired February 14, 2000

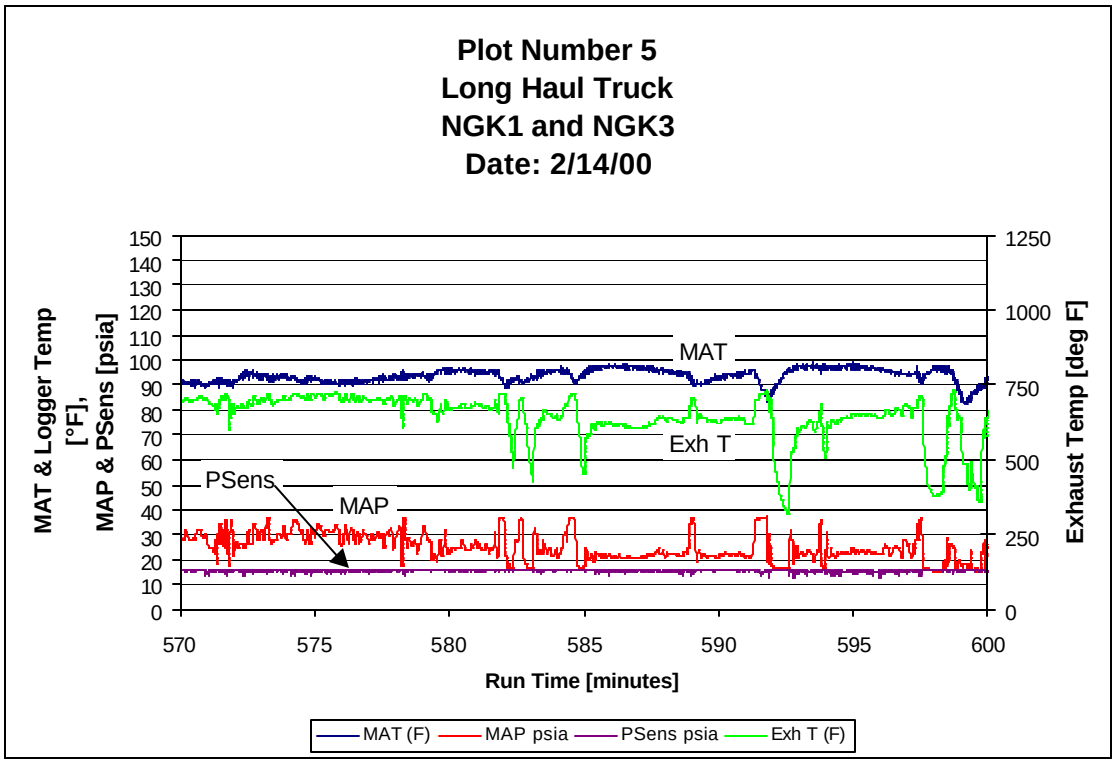

Figure 3-71. Manifold Air Temperature (MAT), Manifold Air Pressure (MAP), Exhaust Gas Temperature at NGK Sensors, and Exhaust Pressure at NGK Sensors on Long Haul Truck - Acquired February 14, 2000

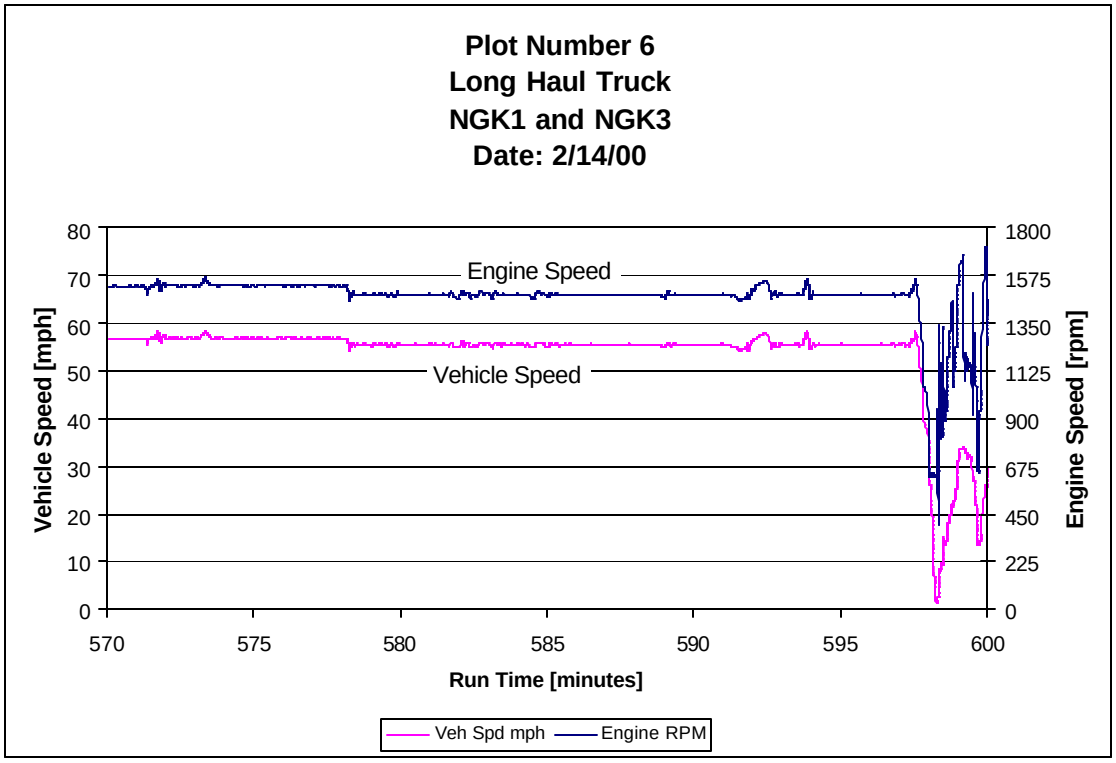

Figure 3-72. Engine Speed and Vehicle Speed on Long Haul Truck - Acquired February 14, 2000.

4.0 SUMMARY AND CONCLUSIONS

4.1 Summary

Four, 5th generation, prototype NGK Insulators, Ltd. combined NO_x/O_2 sensors with a maximum NO_x range of 2000 ppm, were procured for this project. Two of the sensors were tested under steady-state conditions in an inline 6-cylinder, John-Deere 8.2 Litre, turbocharged and aftercooled, natural gas fueled engine. All four sensors were also evaluated on a new, inline 6-cylinder, 1995 Cummins M11, turbocharged and aftercooled, diesel fueled engine over a variety of steady-state, interference gas, and transient tests. Low aromatic (10 percent max), low sulfur, CARB DF2 specification diesel fuel was used for all laboratory diesel engine tests at SwRI. Laboratory tests were conducted at SwRI before and after a six-month field demonstration in Sacramento, California.

4.2 Testing in Natural Gas Engine Exhaust Conclusions

The two sensors tested on the natural gas engine performed well in the natural gas engine exhaust environment. The linear curve fits developed by SwRI had correlation coefficients greater than 99.5 percent for both sensors. However, the calibrations differed by an average of 15.9 percent in the slope and –25.2 percent in the offset relative to the NGK factory supplied calibration. The NGK calibrations were based on a model gas arrangement with synthetic gas and not actual exhaust gas. The synthetic gas did not represent diesel or gasoline exhaust gas composition. The model gas apparatus test gas concentrations were 0-2000 ppm NO_x, 3 percent H_2O, and N_2 making up the remainder.

The O_2 component of the sensors ehxibited strong linearity with correlation coefficients greater than 98.8 percent, but with a significant shift in offset compared to the NGK factory supplied calibrations based on model gas. The NGK factory supplied calibrations were derived from data taken from a model gas having concentrations of 0-18 percent O_2, 3 percent H_2O, and N_2 making up the remainder. The difference in offset shifts the calibration curve by approximately 1.5 O_2 percent. This was expected and is not unusual since the hydrogen-to-carbon ratio of the fuel plays a significant role in the output of wide range universal exhaust gas oxygen sensors with regards to fuel type. The hydrogen-to-carbon ratio of natural gas at SwRI is typically greater than 3.85 whereas, it is on the order of 1.85 for common gasolines. All in all, the sensors performed well on the natural gas engine and exhibited strong linearity. NGK would need to provide natural gas calibrations for both the NO_x and O_2 components for the sensors.

4.3 Steady-State Testing in Diesel Engine Exhaust Conclusions

The four NGK sensors performed well throughout this test program. There was a minor glitch with the O_2 output of NGK1 early in the program, in that there was no output during the first steady-state test. In addition, the O_2 component of all four sensors appeared to saturate at 4.25 volts at O_2 mole fractions greater than 17.0 percent during the first three sets of steady-state

tests. This was not observed during the fourth and fifth sets of steady-state tests. There is currently no explanation for the saturating behavior, although one could theorize that a burn-in, or de-greening period was being observed. However, NGK does not believe that a burn-in period was occuring. All sensors exhibited strong linearity. Although the slopes and offsets changed from steady-state test to steady-state test, the very first calibration (SS1) for the NO_x component of the sensors could have been utilized throughout this project before and after the field demonstration. All of the data, with the exception of some post field demonstration data from NGK2 and NGK3, fell within the accuracy/error envelope published by NGK. This fact is borne out in Figures 3-14, 3-15, 3-16, and 3-17. The post field demonstration steady-state test (SS5) data had measurement errors that were on average –0.029% for NGK1, 5.490% for NGK2, 8.788% for NGK3, and 0.029% for NGK4 when using the SS1 calibrations. Low speed high load conditions, where CO can approach 1.0 percent by volume, decrease all NO_x sensor's output for a given NO_x level. This effect can lead to a 10 percent error in NO_x. However, it is rare that an engine would encounter such a condition (e.g. 100 percent load at idle speed).

The data scatter in NGK3 is likely due to faulty heater control and/or deterioration in the main pump cell as addressed by NGK. All of the data scatter in NGK3 was representative of high gas flow conditions. A NGK suggested design improvement to reducing the NGK3 data scatter is to reduce the cool-down rate of the measuring tip, and possibly reduce the main pump cell load be decreasing orifice area of the first diffusion path.

4.4 Diesel Engine Interference Gas Effect Testing Conclusions

Interference gases appear to have only a slight effect on the NO_x and O_2 components of the NGK sensors. In fact, the results of all interference gas tests on the NO_x component of the NGK sensor were within the +/-10 percent error envelope (relative to emissions bench measurements) published by NGK. Therefore, one could state that none of the interference gases had an effect on the NO_x component of the sensor since the error envelope of the sensor was not exceeded. Both the O_2 and NO_x components of the NGK sensor exhibited a "burn-in" period. During the "burn-in" period interference gases seem to have a larger effect than after. However, the length of the burn-in period is not known and specific tests should be conducted; although NGK does not believe a "burn-in" period exists.

4.5 Diesel Engine Transient Testing Conclusions

The transient tests conducted at 700 rpm, 1200 rpm, and 1800 rpm confirmed that the NO_x component of the sensor responds on average between 100 msec and 200 msec after the O_2 component of the sensor. NGK has stated the same. There does not appear to be an aging effect on the transient response of the sensor based on the limited field testing conducted during this work. A response time between 100 msec and 200 msec means that this is an additional time that will elapse after the O_2 component responds. The O_2 component will respond first, usually in 50 msec, since exhaust gas must pass through the O_2 measuring cavity before it diffuses into the NO_x measuring cavity. As additional information, consider that the mass transport delay of exhaust gas from the cylinder to the NO_x sensor, is approximately 85 msecs for a sensor located

approximately 1 foot from the turbo outlet with the engine running at 1800 rpm, and an atmospheric intake manifold air pressure or boosted, to say 34 psia (235 kPa). Hence, it is clear that the O_2 component is faster than the mass transport delay, and can adequately and rapidly sense changes in the air to fuel ratio. However, some mass transport delay filtering may be required to accurately *phase* the measured NO_x emissions with the engine conditions that generated the NO_x.

A true test for the time constant was not performed during this evaluation. Therefore, the elapsed times or response times of the sensors should not be considered as the sensor's time constant, but only as the time lag of the NO_x component to respond after the O_2 component has responded. This the only time that could be measured with confidence during this project. Determining the true response of the sensor would require a measuring "block" or cavity where NO_x gas could be admitted in a nearly digital fashion. With this approach, a trigger could be used to initiate data collection to determine the 33 to 66 percent or 10 to 90 percent response time.

4.6 Overall Conclusions of the NGK NO_x Sensor

This project has proven that the NGK sensor can measure NO_x, and the output of the sensor is linear for the NO_x, and O_2 components. In addition, the measurement accuracy is acceptable with regard to the manufacturer's published accuracy limits, and the response of the sensor is fast enough to be implemented into a closed loop control strategy, in one form or another. Moreover, the post field demonstration steady-state test (SS5) data had measurement errors that were on average –0.029% for NGK1, 5.490% for NGK2, 8.788% for NGK3, and 0.029% for NGK4, when using a calibration derived from the very first set of test data (SS1 data). The average measurement errors listed above are relative to the NO_x measured by the SwRI Milton-Roy emissions bench. Hence, the very first steady-state sensor calibrations could have been used for all portions of this project and produced data that were within NGK's published accuracy limits, on average.

However, based on the limited field testing conducted during this program, the present sensor design needs improvement to maintain measurement accuracy for extended periods of time. The data scatter in the NGK3 sensor post field demonstration steady-state data (SS5), shown in Figure 3-16, supports the previous statement. Further investigation is required to fully quantify reliability issues and their impact on a production engine control system in long term, heavy-duty, diesel engine emissions control applications. In the present prototype form, the sensors are not suitable for implementation into heavy-duty, diesel engine emissions control systems.

In the present form, the sensors and power electronics (controllers) can not be powered by a conventional vehicle battery due to a strict 14.0 ±0.5 dc volt requirement. However, NGK is currently developing the power electronics for use with conventional battery systems in the 9 to 16 volt range. Therefore, power electronics will not likely be a problem in future sensor controllers.

The interference gas effects are presently of little concern, if the sensor is placed in the exhaust system, since the exhaust gas species distribution changes proportionately. The sensors would likely never encounter a gas composition similar to the ones resulting from the addition of the interference gases. However, advanced control algorithms might suffer from interference gas effects if a sensor is used in the intake system or a selective catalytic reduction system (SCR). For example, the use of a NO_x sensor for EGR rate control could be difficult since O_2 in the fresh air could skew the NO_x result. In addition, NH_3, one of the main reagents in SCR systems, is presently interpreted as NO_x. In the present design, NH_3 is decomposed to NO by catalytic activity in the first internal cavity. Recall that the function of the first internal cavity is to decompose NO_2 into NO and O_2. The catalytically created NO is decomposed to N_2 and O_2 and accounted for in the second internal cavity. Thus, the measurement is erroneous. Therefore, it may prove difficult to implement a sensor using the same or similar technology as the NGK NO_x sensor downstream of a SCR system.

Assuming a durable sensor, and based on SwRI's experience in the development of advanced engine control strategies and algorithms, the NGK NO_x sensor is suitable for inclusion in a closed loop air to fuel ratio algorithm. In fact, the NGK NO_x sensor is equally suitable for other conceptual control algorithms that affect the production of NO_x during the combustion event. In this context, one can envision closed loop control of an emissions regulated parameter directly; that being NO_x. With this in mind, closed loop NO_x control algorithms can be developed and tested to determine the NO_x sensor's optimum usage and influence on existing general air to fuel ratio control algorithms, fuel injection tables and parameters found in diesel engine controllers, spark timing tables and parameters found in natural gas and gasoline engine controllers, and EGR. Furthermore, the combined usage of present day engine control system technology and advanced control algorithms are intelligent enough to distinguish sensor and actuator anomalies, including anomalies in a NO_x sensor. A NO_x sensor can be dually utilized to monitor engine health in the form of injector and ignition system functionality.

The primary objective of research focused on the development and implementation of control algorithms utilizing NO_x sensor input would be to answer the question of whether or not the NO_x sensor could be used as a primary control sensor, rather than a secondary, or "trim" sensor, primarily during transient conditions. This concern arises out of the results gathered from the transient tests, leading one to question if the response of the NO_x component in the sensor is fast enough. As a means of comparison, present day UEGO sensors respond in approximately 50 msec, making them suitable for closed loop control for either air or fuel to maintain a desired air to fuel ratio. Present day engine controllers have loop times less than 5 msec. During each loop, adjustments are made to most, if not all, parameters and devices that control the engine and combustion behavior. Therefore, it is easy to deduce that 40 control system loops can occur before the NO_x component of the NGK sensor responds *after* the O_2 component responds. Hence, how fast and aggressive could a control loop be for suitable control of NO_x during transients and steady-state operation? What kind of transport delay and sensor delay algorithms must be developed? Additional application research is required to answer these and other questions before a decision can be made regarding a NO_x sensor's placement and authority in the structure of present day engine control algorithms.

5.0 RECOMMENDATIONS

In general, the NGK combined NO_x/O_2 sensors functioned within the NGK published accuracy limits. However, the data scatter observed in the post-field demonstration tests in sensors NGK2 and NGK3 lead one to question the reliability and durability. Most of NGK's development efforts have been focused on smaller diesel engines typical of passenger cars. Therefore, SwRI recommends that the NGK NO_x sensor be evaluated in a long-term field demonstration (e.g. 1 or 2 years) on a diesel powered vehicle. A modified sensor may be in order for such an evaluation. The effect of sensor installation orientation should also be investigated to determine the most durable and accurate sensor position. Fundamental response tests should also be conducted with NO_x test gas. Tests of this nature would provide data to accurately quantify the true time response time of the sensor and could be performed relatively easy. The "burn-in" period theory should also be evaluated on a test bench apparatus.

SwRI additionally recommends that feedback from the NO_x sensor be evaluated in a rapid prototyping engine control system, to fully expose the applicability of the sensor in advanced control algorithms for emissions compliance. This could be expanded to include direct one to one comparison with a present day UEGO sensor. In this context, the UEGO sensor would initially be the primary sensor for air-to-fuel ratio control. This would allow one to compare the O_2 output of the UEGO and combined NO_x/O_2 sensors directly, and predict how the O_2 component of the NO_x sensor would respond. The second phase would be to implement the combined NO_x/O_2 sensor in the air-to-fuel ratio control loop. Here, the output of the O_2 component of the combined NO_x/O_2 sensor would be the primary control sensor. NO_x sensor feedback could then be brought in to trim the algorithm and determine its stability. The last phase would be to utilize only the NO_x sensor feedback for air-to-fuel ratio control.

In addition, CARB and the South Coast Air Quality Management District (SCAQMD) may find it beneficial to conduct a long term field demonstration on a stationary engine, either natural gas or diesel fueled, for real time, long term emissions monitoring. The interference effect of NH_3 on the sensor could be tested during a field demonstration on a SCR system.

6.0 REFERENCES

[1] Kato, Nobuhide, Nakagaki, Kunihiko, and Ina, Noriyuki, "Thick Film ZrO2 NOx Sensor, SAE Paper No. 960334, February 1996.

[2] Kato, Nobuhide, Hamada, Yasuhiko, and Kurachi, Hiroshi, "Performance of Thick Film NOx Sensor on Diesel and Gasoline engines, SAE Paper No. 970858, February 1997.

[3] Kato, Nobuhide, Kurachi, Hiroshi, and Hamada, Yasuhiko, "thick Film ZrOx NOx Sensor for the Measurement of Low NOx Concentration", SAE Paper No. 980170, February 1998.

[4] Kato, Nobuhide, Kokune, Nobuyuki, Lemire, Bertrand and Walde, Tim, "Long Term Stable NOx Sensor with Integrated In-Connector Control Electronics", SAE Paper No. 199-01-0202, March 1999.

[5] Telephone discussions with NGK-Locke representatives in March, 1999.

[6] Inagaki, Hiroshi, Oshima, Takafumi, Miyata, Shigeru, and Kondo, Noriaki, "NOx Meter Utilizing ZrO2 Pumping Cell", SAE Paper No. 980266, 1998.

[7] Kondo, Mr. N., Oshima, Mr. T., Miyata, Mr. S., NOx Meter Utilizing ZrO^2 Pumping Cell", Abstract, 97AE022.

[8] Shigaru, Miyata, Kondo, Noriald, Hiroshi, Inagaki, European Patent Application, No. EP 0 841 562 A2.

[9] Miyata, Shigaru, Ando, Masashi, Inagaki, Hiroshi, Ishida, Noboru, Oshima, Takafumi, European Patent Application, No. EP 0 869 356 A2.

[10] Phone discussions with EMC representative on March 19, 1999.

[11] EMC NO_x Sensor brochures.

[12] Fax communication from Peter Kolb of Robert Bosch Corporation on March 11, 1999.

[13] Kunimoto, Akira, Hasei, Masaharu, Yan, Yongtie, Gao, Yunzhi, Ono, Takashi, and Nakanouchi, Yukio, "New Total-NOx Sensor Based on Mixed Potential for Automobiles", SAE Paper No. 199-01-1280, March, 1999.

[14] E-mail correspondence from Akira Kunimoto, referencing Riken's NOx Sensor, March 14, 1999.

[15] Correspondence from Professor Eric D. Wachsman, University of Florida, referencing SRI NO_x Sensor, dated February 26, 1999.

[16] Popp, Peter J., Bishop, Gary A., and Stedman, Donald H., "Development of a High-Speed Ultraviolet Spectrophotometer Capable of Real-time NO and Aromatic Hydrocarbon Detection in Vehicle Exhaust, prepared for the Proceedings for the 7^{th} CRC On-Road Vehicle Emissions Workshop in April, 1997.

[17] Fax communications from Don Stedman on March 3, 1999.

[18] E-mail correspondence from Abdel Essalik on March 17, 1999.

[19] E-mail correspondence from ECOM America Ltd., on March 11, 1999.

[20] E-mail correspondence from Patrick J. Iannotta, referencing Enerac Sensors, on April 12, 1999.

[21] SwRI Draft Final Report No. 03-2610, Prepared by Jack Smith, "Evaluation of ODEGA NO_x Sensor: Phase 0", Prepared for Engelhard Corporation, April 1999.

7.0 GLOSSARY OF TERMS, ABBREVIATIONS, AND SYMBOLS

7.1 General

- EGR = Exhaust Gas Recirculation
- IGE1 = Interference gas test number 1
- IGE2 = Interference gas test number 2
- IGE2 = Interference gas test number 3
- NGK = Reference to the TNS-1010-3Z NO_x sensor developed by the NGK company (NGK Insulators, Ltd.)
- NGK1 = NGK sensor number 1, serial number 9E10B-1038
- NGK2 = NGK sensor number 2, serial number 9E10B-1044
- NGK3 = NGK sensor number 3, serial number 9F14A-1018
- NGK4 = NGK sensor number 4, serial number 9F14A-1022
- ppm = Parts per million
- SCR = Selective Catalytic Reduction
- SS1 = Steady state test number 1
- SS2 = Steady state test number 2
- SS3 = Steady state test number 3
- SS4 = Steady state test number 4
- SS5 = Steady state test number 5
- SwRI = Southwest Research Institute

7.2 Gases

- C_3H_6 = Propylene
- CO = Carbon monoxide
- CO_2 = Carbon dioxide
- HC = unburned hydrocarbons
- NH_3 = ammonia
- NO_x = Oxides of nitrogen
- O_2 = Oxygen

APPENDIX A

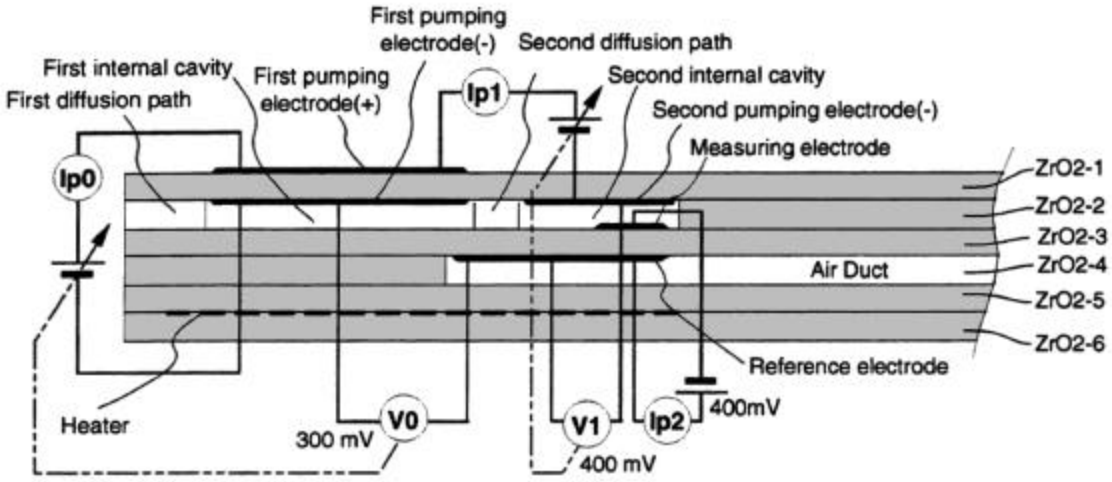

Cutaway Schematic of NGK-Insulators, Ltd. Combined NO_x/O_2 Sensor